Conceptual Design of Lightweight Automotive Body-In-White Structures for Crashworthiness

Submitted in partial fulfilment of the requirements
for the award of the degree of
Doctor of Philosophy

by

KIRAN KUMAR DAMA
Roll No. 701418

Supervisors:

Dr. V Suresh Babu
and
Dr. R Narasimha Rao

DEPARTMENT OF MECHANICAL ENGINEERING
NATIONAL INSTITUTE OF TECHNOLOGY
WARANGAL
2017

NATIONALINSTITUTEOFTECHNOLOGY

WARANGAL– 506 004, Telangana State, INDIA

CERTIFICATE

This is to certify that the work presented in the thesis entitled **"Conceptual Design of Lightweight Automotive Body-In-White Structures for Crashworthiness"** submitted by **Mr. Kiran Kumar Dama** (Roll No. 701418), to **National Institute of Technology, Warangal** in partial fulfilment of the requirements for the award of the degree of **Doctor of Philosophy in Mechanical Engineering** is a bonafide research work carried out by him under our supervision and guidance. This work has not been submitted elsewhere for the award of any degree.

Dr. V Suresh Babu
(Supervisor)
Associate Professor
Department of Mechanical Engineering
National Institute of Technology
Warangal, Telangana State – INDIA.

Dr. R Narasimha Rao
(Co-Supervisor)
Associate Professor
Department of Mechanical Engineering
National Institute of Technology
Warangal, Telangana State – INDIA.

Dr. P Bangaru Babu
(Chairman, DSC)
Professor and Head
Department of Mechanical Engineering
National Institute of Technology
Warangal, Telangana State – INDIA.

THESIS APPROVAL FOR Ph.D.

This thesis entitled **"Conceptual Design of Lightweight Automotive Body-In-White Structures for Crashworthiness"** by **Mr. Kiran Kumar Dama** is approved for the degree of Doctor of Philosophy.

_____

_____

_____

Examiner

Dr. V Suresh Babu
(Supervisor)
Associate Professor
Department of Mechanical Engineering
National Institute of Technology
Warangal, Telangana State – INDIA.

Dr. R Narasimha Rao
(Co-Supervisor)
Associate Professor
Department of Mechanical Engineering
National Institute of Technology
Warangal, Telangana State – INDIA.

Dr. P Bangaru Babu
(Chairman, DSC)
Professor and Head
Department of Mechanical Engineering
National Institute of Technology
Warangal, Telangana State – INDIA.

DECLARATION

This is to certify that the work presented in the thesis entitled **"Conceptual Design of Lightweight Automotive Body-In-White Structures for Crashworthiness"**, is a bonafide work done by me under the supervision of **Dr. V Suresh Babu**, Associate Professor, Department of Mechanical Engineering, NIT Warangal, INDIA, and **Dr. R Narasimha Rao**, Associate Professor, Department of Mechanical Engineering, NIT Warangal, INDIA, and was not submitted elsewhere for the award of any degree.

I declare that this written submission represents my ideas in my own words and where ever others ideas or words are included have been adequately cited and referenced with the original sources. I also declare that I have adhered to all principles of academic honesty and integrity and have not misrepresented or fabricated or falsified any idea/data/fact/source in my submission. I understand that any violation of the above will cause for disciplinary action by the institute and can also evoke penal action from the sources which have thus not been properly cited or from whom proper permission has not been taken when needed.

Place: Warangal.
Date: 30 October, 2017

KIRAN KUMAR DAMA
Roll No. 701418

Dedicated to

my Parents, Wife, & Son

Abstract

Computer Aided Engineering (CAE) techniques are extensively used for designing car body structures. However, their success depends on the accuracy of input data used in the analysis. This poses restrictions on their use in concept design phase of the car body, as the accuracy and availability of input data is limited during this phase. This thesis develops a knowledge-based design approach to address these challenges. It also demonstrates the application of this approach for conceptual design of a profile based car body structure designed for crashworthiness.

The knowledge-base for the presented design approach is developed by analysing the results from two sets of numerical experiments carried out during this work. The first set of Finite Element (FE) simulations is performed on two benchmark vehicles, which are constructed using the classical construction concept for various crash scenarios. The behavioural trends observed from this set of simulations are used as basis for defining crash design targets for a new profile based car body structure. The second set of FE simulations is performed on the components of a profile based car body structure. The data obtained from this set of simulations are used to evaluate different analytical methods available for predicting the behaviour of car body components under crash loads. Regression analysis is performed on these simulation results to formulate equations, and those equations are used for designing components of the new car body structure. Application of this design approach is demonstrated by generating a concept design of a micro-sized coupe vehicle and validated by FMVSS 208 crash scenario by using CAE techniques.

Acknowledgements

I wish to express my sincere gratitude to my thesis convenor, Dr. V Suresh Babu, Associate Professor, MED, for his priceless advice, encouragement and patience in guiding my research life. All his help benefit my PhD work a lot.

I would like to thank my co-supervisor Dr. R Narasimha Rao, Associate Professor, MED. In this journey I have had so many invaluable lessons from him which would help me in my future.

I would like to express my deepest gratitude to Dr. P. Bangaru Babu, Professor, MED., my Doctoral Scrutiny Committee (DSC) chairman, for his guidance, reviews and critical suggestions and constant supervision for the entire course of the research work.

I am grateful to my Doctoral Scrutiny Committee (DSC) members Dr. P. Bangaru Babu, Professor, MED., Dr. B. Satish Ben, Asst. Professor, MED., and Dr. N. Narasaiah, Associate Professor, MMED. I also extend my sincere thanks to Prof. R. V. Chalam, Head, Design section, and Prof. C. S. P. Rao, former chairman, DSC, for their kind support and motivation.

I would like to thank each and every faculty members of MED, for their kind support and motivation.

I gratefully acknowledge Ritza Technologies, India, and DEP India Pvt. Ltd., India, for their valuable guidance, technical support and help throughout the work.

Last, but certainly not the least, I want to express the sincerest gratitude to my family for all their love and encouragement. Especially my wife, Mrs. SivaKumari, accompanied me in the alien land and shared with me all the good and bad moments. I should also be grateful to my son, Trivikrama Shiva Karthikeya who raised me with a love of science.

Kiran Kumar Dama

October 30, 2017

Table of Contents

List of Figures

List of Tables

Abbreviations

Abt	about
Acc.	According
AHSS	Advanced high strength steel
Bet	between
Bench.	Benchmark
CAD	Computer Aided Design
CAE	Computer Aided Engineering
Con	Connection
Crs.	Cross member
Def.	Deformation
Defo ele	Deformation element
DoE	Design of experiments
DOF	Degree of freedom
FE	Finite element
HSS	High strength steel
Lft.	Left
LMS	Lumped mass spring
Long.	Longitudinal member
LSTC	Livermore Software Technology Corporation
Mem.	Member
NA	Not applicable
NVH	Noise, vibration, harshness
Rt.	Right
Sup	Support
SUV	Sport utility vehicle
VDI	Verein Deutscher Ingenieure
Wrt.	With respect to

1 Introduction

Design of a vehicle body structure affects the performance of the vehicle in almost all aspects such as safety, comfort and fuel consumption. Therefore, various criteria in the fields of structural mechanics and aerodynamics are used while generating the design of the body structure. This makes the design process highly complex, iterative, costly, and time consuming.

As an aid for this design process, computer aided methods (CAD and CAE) are extensively used in the present-day automotive industry. With the help of CAD techniques car body structure can be constructed and modified easily. Ability of the CAD systems to create parametric designs helps in increasing the productivity of the design process. Using the CAE techniques, the constructed structure can be virtually analysed and optimised for various loading scenarios. This helps in reducing the costs incurred by the physical tests. A typical computer aided design process of a car body structure can be divided into two phases, namely concept design phase and detailed design phase. The concept design phase is characterised by frequent changes in the design of the body structure. In this phase, an initial design is generated considering customer and legal requirements. Using CAE techniques, the initial design is analysed and optimised through number of iterations until the requirements are satisfied within acceptable limits. The concept design thus created is then handed over to the detailed design phase for fine tuning. In the detailed design phase components of the vehicle body structure are further optimised and production drawings are created [1], [2].

Since the decisions taken in the concept design phase influence all further design stages as well as the performance of the vehicle, this phase is considered to be very crucial in the whole design process. The quality of the concept design generated can decrease or increase the amount of optimisation required in further design stages, and thereby reduce or extend the duration of the design process.

Although the integration of CAE techniques in the design process has made considerable improvements, these techniques have certain limitations. Firstly, the usefulness of CAE analysis results depends on the accuracy of the input data used for building the numerical models. Therefore, availability of detailed and accurate input data at the beginning of the design process is desirable for creating an optimum concept design in least possible time. Secondly, the amount of efforts and time required for building these models increases with increasing complexity of the model, thereby prolonging the construction and analysis period.

These limitations are especially problematic for small series vehicle manufacturers. The limited amount of information and guidelines available to the design engineers may require longer optimisation cycles during the concept design phase. The restricted amount of resources available, further decelerates the design process, thereby increasing time as well as costs for vehicle development. Rapidly changing automotive market and ever-increasing market competition, however, compel the small series manufactures to accelerate the design process. It is, therefore, highly desirable for the small series design engineers to possess a tool that can create an optimised concept design in time efficient manner. Simple to use methods may be employed by such a tool to cleverly plan and execute the concept design phase.

1.1 Objectives

The objective of this work is to develop and demonstrate an approach for generating an optimum concept design of vehicle body structures for crashworthiness. This new approach, named the Multi Objective Knowledge-based (MOK) approach, addresses the difficulties faced by the small series vehicle manufacturers during the concept design phase of the vehicle. It provides a guideline for creating a crashworthy and lightweight design of the car body structures in a time efficient manner.

The MOK design approach proposed in this work divides the process of concept design of a vehicle body structure into seven definite steps, namely, vehicle base information, attribute configuration, topology configuration, deformation configuration, section configuration, joint configuration and virtual validation. Goals, input and output of each step are clearly defined to satisfy the design criteria for crashworthiness. This work focuses on developing time efficient and simplified methods to perform the steps attribute configuration, deformation configuration and section configuration. These methods help in identification and definition of design targets for generating a crashworthy car body and selection of suitable dimensions and materials for the car body components to match the defined targets. In a typical concept design phase, the design targets are approximately defined for the full vehicle and not for individual car body components. Also, the geometry and materials of the car body components are generally chosen using previous experience. This work proposes and demonstrates methods for determining the full vehicle design targets with more precision. Moreover, it also gives a method for breaking down these targets to the level of individual car body components in the concept design phase. In order to define the initial dimensions and materials for individual components, this work proposes a knowledge-based approach. These improvements lead to better conceptual design,

which in turn, needs less number of optimisation iterations.

1.2 Organisation of the thesis

The remaining of this thesis is organised as follows. **Chapter 2** gives basic introduction to car body structure, its functions and its construction concepts. Analytical methods available for crashworthy design of the car body structures are also summarised in this chapter.

Chapter 3 introduces the Multi Objective Knowledge-based (MOK) approach and explains various steps involved in it. It also talks about the structural knowledge-base, an integral part of the MOK approach.

Chapter 4 explains the development of the structural knowledge-base, which comprises of three configurations: attribute configuration, deformation configuration and section configuration. This chapter also elaborates various tasks conducted during this work while developing the structural knowledge-base. Development of the time efficient methodologies suggested in the MOK approach involves application of Computer Aided Engineering (CAE) techniques and regression techniques. In order to determine the design targets for a car body structure under consideration, benchmark data are obtained by performing finite element analysis of full vehicles and are used as basis. In this work, various analytical and experimental methods are studied, which can be used for predicting the behaviour of car body components under different types of crash loads. In order to find the most appropriate method, another set of finite element simulations is performed on a set of car body components. The results obtained from these simulations are taken as reference for assessing the analytical methods. When applied in their simplest form, the analytical methods are found to be incompetent for predicting performance of the car body components realistically. Regression analysis is therefore performed on the results obtained from the simulations and regression equations are derived for predicting the performance of the components. These regression equations are used for selecting the initial dimensions and materials for the car body components satisfying the previously defined design targets within acceptable limits.

Chapter 5 demonstrates the application of the structural knowledge-base for creating a concept design of a car body front end structure considering its crashworthiness. The application of the design approach developed in this work is demonstrated for a micro sized coupe passenger vehicle, a representative of a small series vehicle. The simplified methods formulated in this work are used for creating the concept design of the front-end structure of this passenger vehicle. This concept design is validated by analysing the structure using finite

element method. The scope of this work is limited to formulating a new design approach and demonstrating its application in a research domain.

Chapter 6 explains the summary and conclusions of this work followed by the future work of this research.

2 Review of Literature

2.1 Car body structure

The body structure of a passenger vehicle is one of the important functional groups of a vehicle. The functions performed by the car body structure and its requirements are summarised in Section 2.1.1. In order to satisfy these requirements, various construction concepts have been gradually developed and applied for the car body design over the years. Section 2.1.2 briefly describes some of the most commonly used construction concepts. Construction of lightweight car body structures is an important trend in the present automotive industry [3]. Section 2.1.3 summarises the importance of lightweight construction and common design principles applied for realising the lightweight construction.

2.1.1 Functions of car body structure

According to the "absolute automotive theory" [4], a car body structure is designed considering following requisites:

- Maximising design and performance attributes
- Maximising space available for passengers, luggage and package components
- Minimising weight of the car body structure
- Minimising initial investment and production costs

It is necessary for the car body structure to possess necessary structural performance under different types of loads and thereby provide the passengers comfort and safety during the entire life-span of the vehicle. The car body should be light in weight. However, its lightweight characteristics should not impose adverse effects on its structural performance. The car body structure should provide sufficient space for the passengers and the luggage. The package components should also be appropriately supported by the car body. The design of the car body structure should be cost effective considering initial investments and production aspects [4].

By taking appropriate measures during the structural design of the car body, safety and comfort of the passengers can be improved considerably. The structural design of a car body is realised considering following performance attributes, illustrated in Figure 2.1.

- Crashworthiness or passive safety
- Noise, vibrations and harshness (NVH)
- Durability or endurance strength

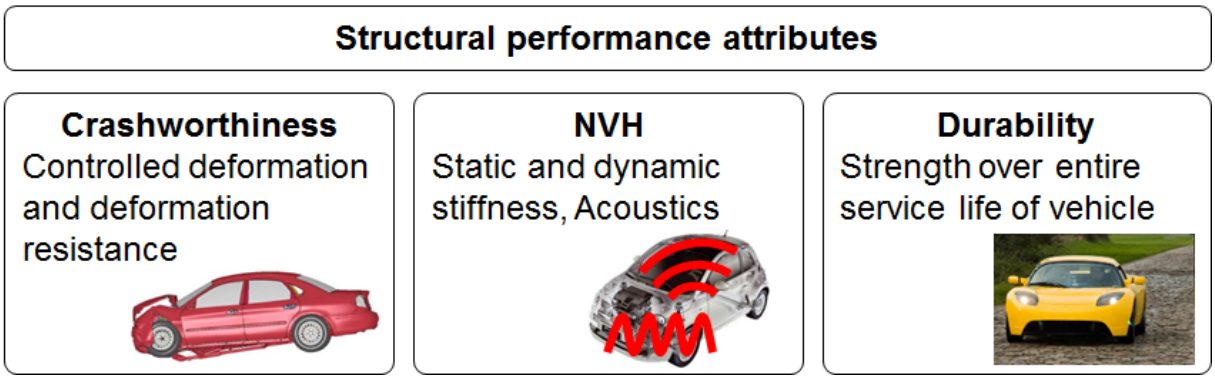

Figure 2.1: Performance attributes for structural design of a car body

2.1.1.1 Crashworthiness or passive safety

Crashworthiness of a car body structure accounts for the safety of the vehicle, its occupants and other participants in the event of an accident. In such an event, high dynamic loads are generated that last for few milliseconds. The car body structure should be able to react to these loads in this very short duration and provide survivable conditions for the occupants. As this work deals with design methodology for crashworthy car body structures, this topic is discussed in detail in Section 2.3.

2.1.1.2 Noise, vibrations and harshness (NVH)

NVH deals with the static and dynamic stiffness of the car body structure and its sound damping properties. Various static and dynamic loads are imposed on the car body structure during its operation [1]. Static loads are mainly of two types: bending loads and torsional loads. Bending loads are exerted, for example, from the self-weight of the vehicle and the weight of the passengers and luggage. The car body is subjected to torsional loads, for example, while moving on an uneven road, when all tires are not on the same level. In order to sustain these loads, the car body structure should possess sufficient bending and torsional stiffness.

In addition to the static loads, dynamic vibrations are induced in a car body through the engine, the drive train and movements of the axle. The car body and other vehicle subsystems are needed to be designed in such a way that their natural frequencies of vibration are not coincident with each other, and are not in the range of the first natural torsional and bending frequencies of the vehicle. If the car body has a natural frequency in these ranges, it may resonate and shake during the operation generating discomfort [1]. Therefore, the car body structure should be appropriately designed to possess high dynamic stiffness.

The dynamic vibrations generated by the engine, the drive train and the axle movements are transferred to the flexible outer panels of the vehicle through their mounting points by means of structure borne sound transfer. Vibrations of these outer panels create sound that is conveyed to the passenger compartment. Also, the sound emitted by the engine during its operation is transferred to the passenger compartment, causing discomfort to the passengers. In order to minimise the structure borne sound transfer, the mounting points of the engine, the drive train and axles should possess appropriate damping characteristics [1].

2.1.1.3 Durability or endurance strength

Durability is another important attribute of the car body structure considered during its design. Passenger vehicles are subjected to different types of loads during their service life. These loads can vary from constant loads, such as curb weight or residual stresses in the components, to random vibrational loads imposed due to uneven road surfaces. Such loads induce dynamic stresses in the car body structure over its entire service life. Durability or endurance strength of a body structure is its strength to withstand these accumulated dynamic stresses over its life span [1].

2.1.2 Construction concepts of car body structure

As illustrated in Figure 2.2, a car body structure consists of load bearing structures, closing structures and outer skin. Load bearing structures can be further divided into profile structures and joints. The closing structures essentially fill the gap between the load bearing structures and carry the shear loads. The outer skin acts as a covering of the car body. Depending on the construction concept, it may or may not carry the loads [4].

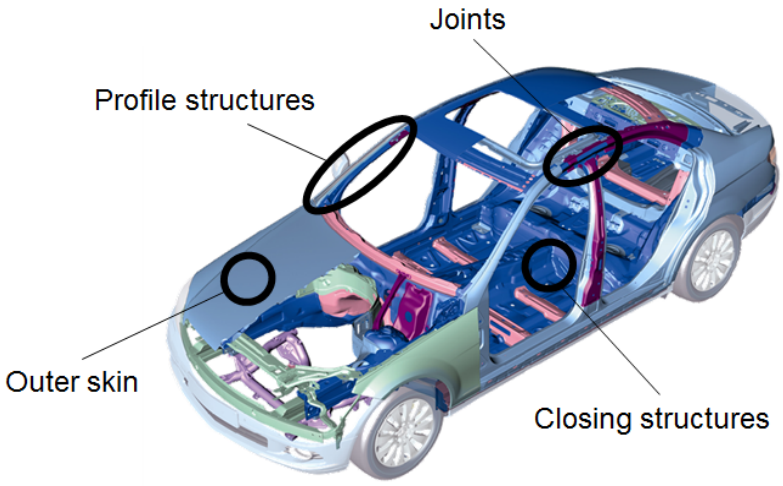

Figure 2.2: Components of the car body structure [5]

Using different material, structural and manufacturing concepts for constructing these car body components, various construction and design concepts have been developed over the years. This section presents a brief historical background of the car body design concepts and describes the main concepts used in the present-day automotive industry.

In the initial years, the car body structures were mainly constructed using wood. In order to increase the load carrying capacity to the car body structures, steel was mostly used as a supplementary material for their construction. Evolution of the ladder frame construction concept in the initial years of 20th century was an important next milestone in the development of car body structures. The ladder frame structure mainly consisted of U-profiles made of steel as longitudinal members, which were connected to each other using lateral members at the front and rear side of the frame. In the year 1923, the central tube structure was introduced as another construction concept through Tatra 11, developed by Austrian designer Hans Ledwinka. A stiff tube placed centrally under the floor panels built the basic structure of this car body. Other vehicle components, including engine, drive train and the body shell were mounted on this central tube. Another construction concept, the tube frame structure, was introduced in mid 1950s, which mainly found application in construction of sports cars and small series vehicles. This structure was constructed using metal tubes, which were placed in such a way that they were loaded only in tension and compression. The frame, thus constructed using these metal tubes, constituted the main load carrying structure of the vehicle. Although, historically, steel dominated the construction of the car body structures, other materials, such as aluminium and magnesium, were also explored as car body construction materials by the designers [4].

The modern types of car bodies can be differentiated considering the combinations of the structural, material and production concepts employed for constructing the body structures. Depending on the vehicle batch size, the performance and weight targets and the costs, appropriate structural, material and production concepts are chosen for a particular car body structure [4], [6]. The types of the car body structures found in the present-day vehicles are described briefly in the following sections.

2.1.2.1 Self-supporting body structure

The self-supporting body structure is the most popularly used construction concept in the passenger vehicles. This type of structure was initially employed in passenger vehicles Lancia Lambda in 1922 and Opel Olympia in 1935. This structure is mainly constructed using deep drawn steel or aluminium sheets. These metal sheets build the profile structures, the closing

structures and the outer skin of the car body, which together carry the loads acting in the body structure. The metal sheets are essentially joined using spot welding, laser welding and adhesives. The self-supporting body structure is very advantageous in constructing lightweight structures. When produced in large volumes, this design offers an opportunity for a high degree of automation during production and thereby reduces the production costs. However, high investments in the initial tooling and low flexibility in terms of manufacturing of vehicle design variants, limit its use in the small and medium sized vehicle batch production [1], [4]. An example of a self-supporting body of Golf VII is illustrated in Figure 2.3.

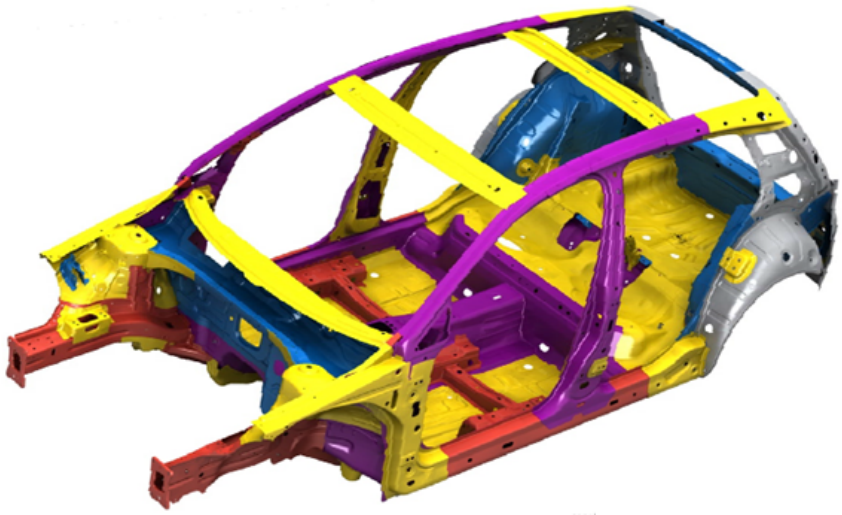

Figure 2.3: Example of a self-supporting body structure [7]

2.1.2.2 Ladder frame structure

A ladder frame structure, as presented in Figure 2.4, is predominantly used in off-road vehicles and commercial vehicles. In this concept, the floor structure is constructed using two longitudinal profiles running along the full length of the vehicle and connected using adequate number of lateral members. The upper body structure is essentially bolted to this frame structure. This type of ladder frame construction is called a “body on frame” construction. Steel is predominantly used as the construction material for the frame structures. Alternately, aluminium profiles can be also used as construction material. In a so called “body integrated frame”, the ladder frame structure is employed in combination with the self-supporting structure [4]. Car bodies of SUVs, such as Audi Qx, Porsche Cayenne and VW Touareg, are built as body integrated frame.

Body on frame of Mercedes G [4]

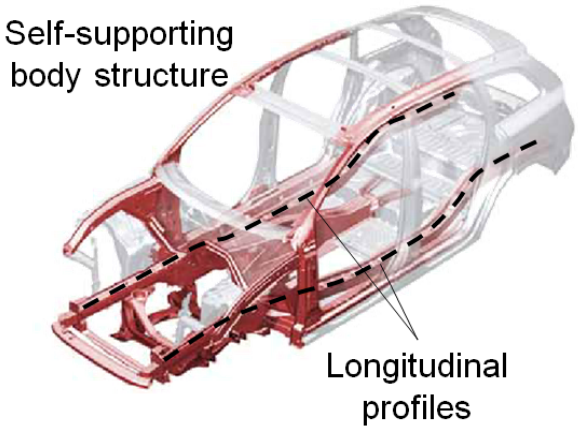

Body integrated frame - Audi Q7 [8]

Figure 2.4: Examples of ladder frame structure

2.1.2.3 Monocoque structure

In a monocoque construction concept, the passenger compartment is essentially constructed as a single shell. This type of car body structure supports the loads through its outer skin. For small vehicle batch sizes, the monocoque structure is mainly constructed using carbon fibre reinforced plastics (CFRP) and glass fibre reinforced plastics (GFRP). The main load bearing members, such as A-pillar, roof post etc., can be filled with foam or honeycomb structure, in order to increase their load carrying capacity. RTM technique and hand lamination technique are used for manufacturing the monocoque structures. For mass vehicle production, the complete monocoque structure can be constructed using aluminium sheets or a CFRP passenger compartment can be attached with front and rear end modules constructed using aluminium profiles [4]. Figure 2.5 illustrates a monocoque structure of Porsche 918 Spyder.

Figure 2.5: Example of a monocoque structure [9]

2.1.2.4 Profile based structure

In the profile based car body structures, which may also be generally called as space-frame structures, the load carrying structure comprises of tubes or profile structures of different cross sections. The cross-sectional geometries of the profile structures range from regular square or rectangular shapes to irregular complex shapes. The profiles intersecting with other profiles at the junctions are connected with each other by welding or through casted joints. These car bodies are mainly constructed using aluminium profiles. However, steel profiles manufactured from different variants of steel also find application in the profile based structures. Steel profiles can be either used for constructing the whole body structure or can be used at strategic positions in the car body together with the aluminium profiles. The closing structures are generally constructed from metal sheets or CFRP and help in carrying the shear forces acting on the body structure. The outer skin of the profile based car body is generally manufactured using plastics or aluminium stampings. Various manufacturing techniques, such as deep drawing, extrusion, casting, hydroforming etc. are employed for the profile based car body structures. The choice of the manufacturing techniques highly depends on the vehicle batch size and the initial investment required [4]. Depending on the material and the manufacturing techniques used, different joining techniques, such as spot welding, MIG welding, laser welding, riveting and adhesives, find application in the profile based structures.
Over the years the profile based construction concept has been employed in different vehicles by different vehicle manufacturers. The aluminium space frame concept introduced by Audi AG [10] and the FlexBody construction concept introduced by Imperia GmbH [11] can be classified under the profile based structures. Figure 2.6 illustrates car body structures of Audi R8 and Audi A8 as examples of the profile based structures. Audi R8 is produced in small batch sizes whereas Audi A8 is a produced in mass volumes. The difference between both the car bodies lies in the amount of cast structures used, presented as pink coloured structures in Figure 2.6. As casting is a costly process, the amount of cast structures applied in a profile based car body reduces with increasing production volume of the vehicle.
Since the design approach developed in this work for the profile based structures is applied and validated using the FlexBody concept, Section 2.2 is dedicated to a more detailed explanation of the FlexBody construction concept.

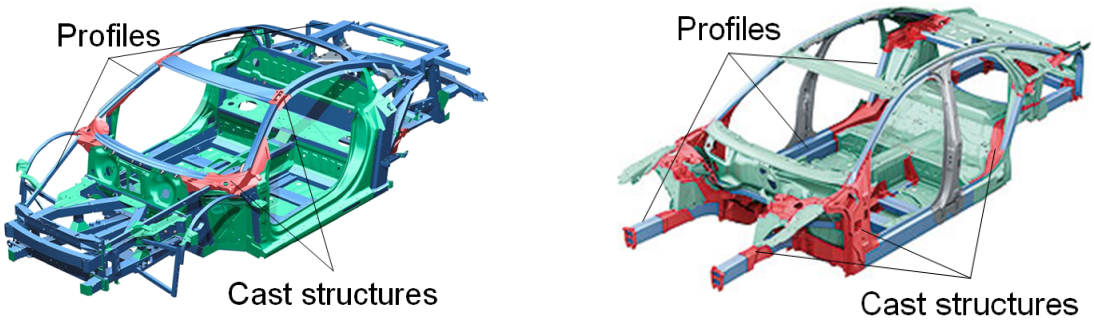

Space frame structure of Audi R8 Space frame structure of Audi A8

Figure 2.6: Example of profile based structures [12]

2.1.2.5 Mixed construction concept

A car body structure with mixed construction concept can be generated by combing three aspects of construction, namely, material, type of structure and manufacturing technique. A car body structure can be constructed using different materials, such as common steels, high strength steels, aluminium, plastics etc. A car body constructed using different structural concepts, for example by mixing the self-supporting body type and a tube frame body type, is classified under structural mixed construction. Combination of different manufacturing and joining techniques in a car body structure is classified under manufacturing mixed construction. Using the mixed construction concepts, advantages of different construction concepts can be combined in one car body structure. In the present-day automotive industry, the type of the vehicle and the vehicle batch size are the determining factors for the extent of mixed construction concepts employed in a particular car body structure. An example of mixed construction concept employing different materials and manufacturing techniques is presented in Figure 2.7 for Porsche 911 Carrera Cabriolet.

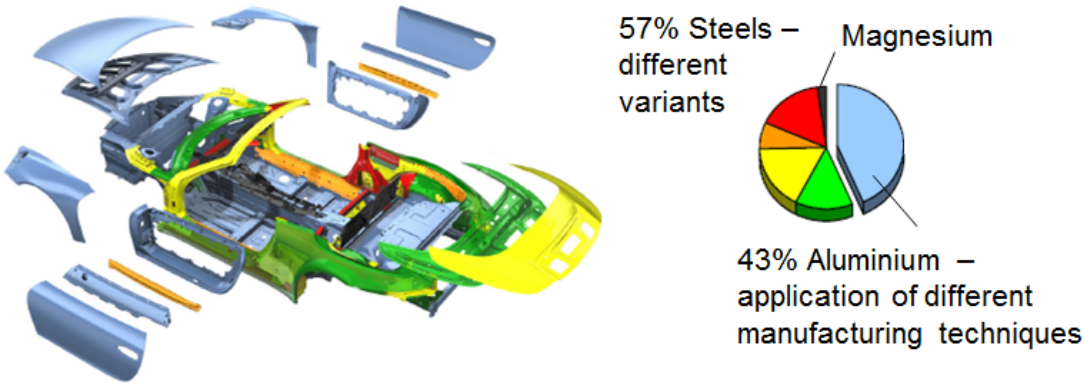

Figure 2.7: Example of material and manufacturing mixed construction [13]

2.1.3 Lightweight body design

2.1.3.1 Importance of lightweight design

Continuously increasing concerns about depleting non-renewable energy resources and high pressure for reducing the vehicle emissions in the form of greenhouse gases, have driven the application of renewable energy resources in the automotive field. For the same reasons, improving the fuel efficiency of vehicles, is also given high importance. Development and application of efficient drive train concepts and reducing the driving resistance are, therefore, highly emphasised issues in the present-day automotive industry. One of the main factors affecting these issue is the weight of the vehicles. Almost 40% of the vehicle weight is accounted by the car body structure. Additionally, handling and agility of the vehicles are also considerably influenced by their weight. Application of the strategies of lightweight design for the car body structure is consequently gaining increasing importance [3].

A vehicle has to overcome various resistances during the motion. The power required to drive the vehicle, can be represented by the following Eq. 2.1.

$$P_{total} = P_{roll} + P_a + P_{as} + P_{air} \qquad \textit{Eq. 2.1 [1]}$$

Where,

P_{total} is the total power required to drive the vehicle.

$P_{roll} = (m_v + m_l) \cdot g \cdot \cos(\alpha_{as}) \cdot f_R \cdot v$ accounts for the rolling resistance.

$P_a = (e_i \cdot m_v + m_l) \cdot a \cdot v$ accounts for the acceleration resistance.

$P_{as} = (m_v + m_l) \cdot g \cdot \sin(\alpha_{as}) \cdot v$ accounts for the gradient resistance.

$P_{air} = \frac{\rho_{air}}{2} \cdot c_d \cdot A \cdot (v - v_w)^2 \cdot v$ accounts for the aerodynamic resistance.

And

m_v : Mass of vehicle

m_l : Payload

g : Gravitational acceleration

α_{as} : Gradient of the road

f_R : Coefficient of rolling resistance

v : Velocity of vehicle

e_i : Inertia coefficient for i-th gear

a : Acceleration of vehicle

ρ_{air} : Density of air

c_d : Coefficient of drag

A : Cross-sectional area of vehicle

v_w : Velocity of wind

As can be seen from the above equation, apart from the aerodynamic resistance, the power required to overcome all the driving resistances is directly proportional to the mass of the vehicle [3].

The reduction in the driving resistance due to reduced vehicle mass also reduces the fuel consumption and emissions of a vehicle. The factor "Fuel Reduction Value" (FRV) [3] represents the effect of reduction of vehicle mass on the fuel consumption. Reduction in the fuel consumption of a vehicle derivative compared to its reference vehicle, due to the application of lightweight strategies for the design of the vehicle components, can be represented by Eq. 2.2 and Eq. 2.3.

$$C_{comp,i} = \left(m_{comp,i} - m_{comp,ref}\right) \cdot FRV \times 0.01 \qquad \textit{Eq. 2.2 [3]}$$

$$C_{veh,j} = C_{veh,ref} + \sum_{i=1}^{n} C_{comp,i} \qquad \textit{Eq. 2.3 [3]}$$

Where,

$C_{comp,i}$: Fuel saved due to reduction of mass of component i

$m_{comp,i}$: Reduced mass of component i

$m_{comp,ref}$: Original (or reference) mass of component i

FRV : Fuel reduction value

$C_{veh,j}$: Fuel consumption of vehicle design j with reduced mass

$C_{veh,ref}$: Fuel consumption of original (or reference) vehicle

n : Number of lightweight design measures

Weight of the vehicle also affects its handling, in terms of stability during the motion, the motion of the vehicle on a curve and braking distance of the vehicle. Lighter vehicles help in reducing the rolling motion of the vehicle, thereby maintain uniform frictional connection between the tyres and the road surface, and consequently help in achieving a stable motion. Due to reduced centrifugal force acting on the lighter vehicles, these vehicles exhibit a better motion on a curve. Additionally, lighter vehicles have a shorter braking distance and thereby help in improving the vehicle safety.

Application of lightweight design methods is therefore gaining increasing importance and is becoming an integral part of the vehicle and car body design process.

2.1.3.2 Lightweight design methods

Lightweight design methods can be classified into three categories depending on the perspective followed; namely, strategic, constructive and principle lightweight design. The strategic lightweight design represents various strategies, such as use of lightweight materials, application of optimum geometry etc., which can be employed for constructing lightweight structures. The constructive lightweight design suggests various construction approaches to resolve the weight related issues of vehicles and their components. The principle lightweight design gives priority to the functional aspects of the components. A suitable lightweight approach is chosen in such a way that, none of the functions of the components are compromised due to the reduction in its weight.

Although a basic distinction exists in these three categories, a particular lightweight design method can often be classified under more than one of the above categories [3]. Different methods applied for lightweight design of vehicles are briefly explained in the following paragraphs.

Material lightweight design

Using lighter material variants, the weight of a component can be reduced. The alternative material to be employed, is chosen considering the material costs, the production costs and the manufacturing possibilities. Additionally, care is taken that the functional characteristics of the component are not adversely affected. Generally, changes in materials are accompanied by the change in the geometry and the construction concepts [3].

Conventionally, mild steel was the most popular construction material used for a car body structure. Alternative lighter materials, increasingly being used in the car body structures

include, high strength steel (HSS), advanced high strength steels (AHSS), aluminium alloys, magnesium alloys and plastics [3]. Due to considerable high strength of HSS & AHSS, the thickness of the car body components can be reduced without compromising their strength. Aluminium is another light weight material popularly being used now-a-days. It has significantly lower specific mass compared to the conventional mild steel. The comparatively lower strength of aluminium can be compensated by thicker body components without increasing much of the weight of the car body structure. Suitable material properties of aluminium for manufacturing extruded sections, permit the use of aluminium for construction of lightweight space frame body structures. Fibre-reinforced plastics, such as CFRP and GFRP, also offer high potentials for reducing the vehicle weight. Typical examples of components made of plastics are the outer skin components and wheel rims. In monocoque car body construction concept, the fibre-reinforced plastics can also be used to construct the complete passenger compartment.

Production lightweight design

Application of special manufacturing processes can be helpful in reducing the component weight. Use of manufacturing techniques, such as tailored blanks, tailored tubes can be classified under production lightweight design. Using the technique of tailored blanks, metal sheets with variable wall thickness can be produced. Consequently, areas of the component requiring high strength can be selectively made of higher thickness and oversizing of the component can be avoided. Weight of the vehicle can also be reduced by changing the joining techniques. Application of adhesives, soldering, laser welding techniques can be useful in reducing the vehicle weight [3].

Use of lightweight materials for the construction of vehicle components, often alters the manufacturing processes employed. For example, aluminium extruded profiles can be used instead of deep drawn steel sheets, in order to reduce the weight of the components.

Shape-based lightweight design

Optimum distribution of material in a component, is another method used for reducing the vehicle weight, which can be classified under shaped-based lightweight design. The basic principle followed here is, using the material where it is necessary, by considering the load distribution in the component and the manufacturing restrictions. Accordingly, the areas which are highly loaded are reinforced and the regions with lower loads are designed to possess lower strength, thereby reducing the weight of the component. Integration of beads, ridges and ribs in

the sheets, are examples of constructive shape-based lightweight design. Using these techniques, the thickness of the metal sheets can be reduced. Computerised optimisation techniques, such as topology optimisation, are increasingly applied for the shape-based lightweight design. According to the load distribution in the component, topology optimisation technique optimises the distribution of the material. Designing the topology of car bodies using this method is now-a-days becoming a common practice [3].

Conceptual lightweight design

The basic principle of conceptual lightweight design methods is to choose an appropriate construction concept for the vehicle or its components by considering their functional requirements and production costs, so as to reduce their weight. Two basic concepts used in the conceptual lightweight design are, differential and integral construction concepts. For these concepts, the distinction lies in the number of functions performed by a single component [3].

According to the integral construction concept, a component is designed to perform more than one functions. Thereby the number of components in a system are reduced. Since no extra elements are required for assembling the components, lightweight systems can be designed and produced at lower costs. However, repairing costs can be considerably high for the integral construction concept, as the whole component has to be replaced in case of damage. Self-supporting body structure is an example of the integral construction concept. The metal sheet components of this body structure perform both the functions of carrying the load and acting as an outer layer of the body structure.

On the other hand, according to the differential construction concept, a single function is assigned to each component, and thereby increasing the number of components in a system. The components can be constructed using different materials and different wall thicknesses, and thereby the weight of the system can be minimised. Reduced repairing costs is an advantage of this concept, whereas high assembling costs and efforts are disadvantages [3]. Profile based car body structure is an example of the differential construction concept. The profiles of the car body structure carry the loads, whereas the function of covering the body is performed by the outer skin, which can be made of lightweight materials.

Different layouts of the drive train, such as front engine front drive, front engine rear drive etc., can also be considered as conceptual lightweight design. Depending on the positioning of the drive train components, the number of components required may increase or decrease, and thereby contribute in creating light or heavy systems [3].

Conditional lightweight design

Investigating the influence of external factors on the vehicle, such as road conditions, misuse conditions, legal safety requirements etc., and optimising the design concept accordingly to minimise the vehicle weight, is classified under conditional lightweight design. Generally, all the vehicle components do not have the same life-span. Some of the components are over dimensioned. By designing all the components to serve for the same duration, lightweight components can be constructed. Different automotive market segments have different requirements for the vehicles. Difference in the performance requirements of off-road vehicles and city vehicles, is such an example. By considering appropriate requirements, city vehicles can be designed to possess lower strength and, consequently, lower weight compared to the off-road vehicles. Similarly, considering only those misuse conditions applicable for a particular vehicle, can help in designing lighter systems. However, it is not always possible to use conditional lightweight design, as it is generally difficult to define the exact conditions that may arise during the operation of the vehicle [3].

2.1.3.3 Limitations of lightweight design

Although, lightweight design of the vehicles and the car body structures proves to be advantageous in many ways, as summarised in Section 2.1.3.1, it also has some limitations.

- Reducing the weight of the car body may have adverse effects on the strength, stiffness and safety performance characteristics of the body structure.
- Using alternative materials for lightweight design, increases the costs of manufacturing. If these increased costs are not compensated by the reduction in the fuel consumption or by increased vehicle performance, the overall cost of the vehicle may considerably increase.
- In order to make optimum and efficient use of alternative materials, suitable and cost-effective manufacturing and joining techniques should be available.
- Recycling of the car body structures constructed using mix of materials may show undesirable effects on the environment.

In order to use the lightweight design methods efficiently, without any adverse effects on the performance of the vehicle and on the environment, conducting a thorough risk analysis is always recommended. Assessing the performance and customer requirements, can help in identifying weight reduction potentials and in choosing suitable design strategies for the body structure and other vehicle systems.

2.2 The FlexBody lightweight construction concept

As summarised in Section 2.1.2, different car body construction concepts have been developed over the years. Owing to the trends of lightweight design, an innovative, modular and multi-material construction concept, FlexBody®, has been developed by Imperia GmbH, Aachen, Germany, University of Applied Sciences Aachen, Germany and number of other industrial and university partners, such as TU Braunschweig, Germany, Grunewald GmbH, Germany, Brökelmann Aluminiumwerk GmbH & Co. KG, Germany, ThyssenKrupp System Engineering GmbH, Essen, Germany etc [11].

The FlexBody construction concept can be classified under the profile based structures. As mentioned before, the FlexBody concept is used for the application and validation of the design approach developed in this work. Therefore the FlexBody concept is explained in more details in this section. Section 2.2.1 explains the basic construction concept employed in the FlexBody. A brief overview of the manufacturing concepts of FlexBody structures is given in Section 2.2.2. Section 2.2.3 presents some application examples of the FlexBody lightweight construction concept.

2.2.1 Basic construction concept

The FlexBody construction concept follows the principle of profile based structures. According to this concept, a car body structure is constructed using profile structures and standardised joints, called as *building blocks* of the FlexBody structure, as illustrated in Figure 2.8.

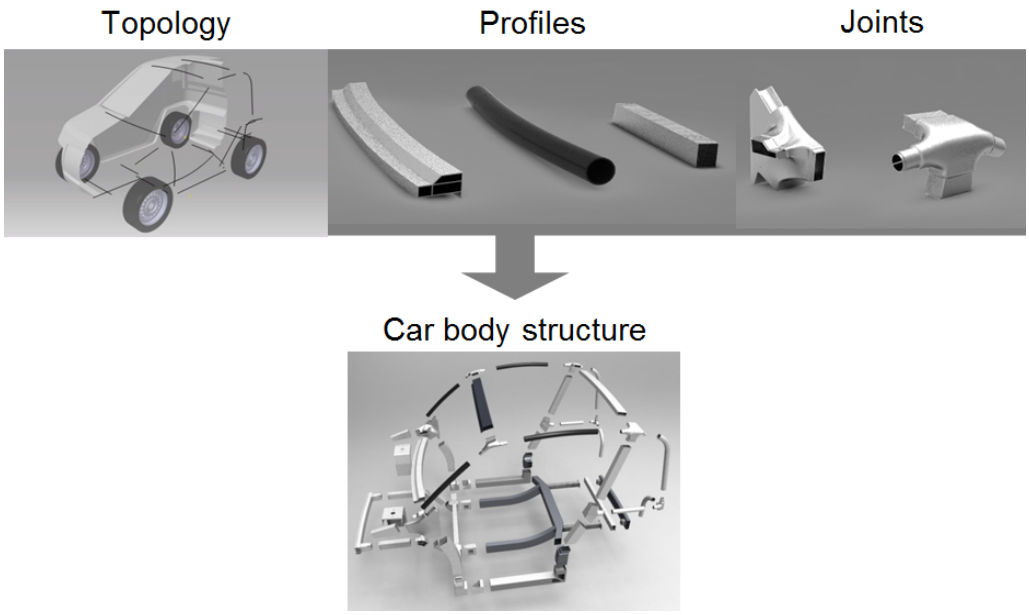

Figure 2.8: Construction concept of FlexBody [11]

The FlexBody components are manufactured using various materials, ranging from conventional materials used for the car body construction, such as different variants of steel, to non-conventional materials, such as aluminium alloys, fibre-reinforced plastics etc. The aim here is to employ an optimum mix of materials for the car body, while considering following aspects for its components:

- The load carrying capacity required
- Potentials for lightweight design
- Number of components to be manufactured and manufacturing costs
- Initial investment required for manufacturing
- Costs of materials

The optimum use of materials in the FlexBody concept allows the construction of a car body structure possessing high load carrying capacity in spite of its light weight. Figure 2.9 shows an example of a FlexBody structure constructed using a mixture of materials and manufacturing processes.

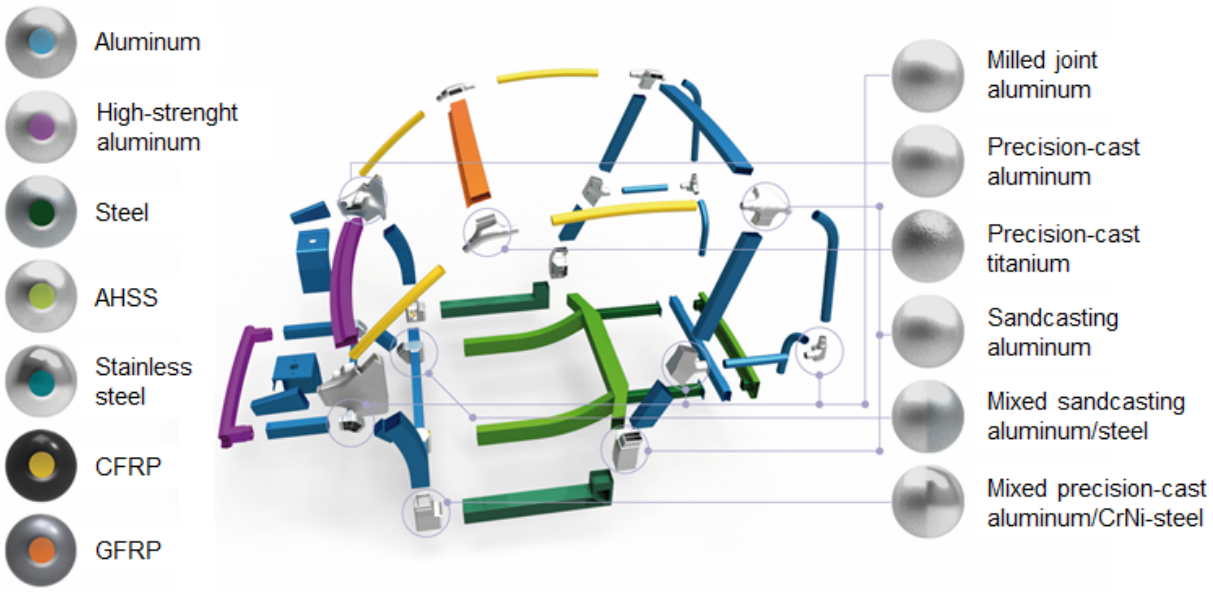

Figure 2.9: Example: mix of materials and manufacturing techniques in FlexBody [11]

Following the principle of the profile based structure, the building blocks of FlexBody - profile structures and joints - carry all the structural loads imposed on the vehicle. Mainly, two functions are assigned to the profiles structures, first, carrying the structural loads and second, deforming in controlled manner and absorbing energy whenever necessary. Joints, on the other hand, owing to their complex geometries, are generally conceptualised stronger than profiles. Thereby the joints undergo minimum deformation. In exceptional situations, when their deformation is unavoidable, joints can be constructed as deformable components. The main

function of the joints is to connect three or four profiles at their intersection and transfer the structural loads from one profile to another.

The closing structures in the FlexBody car body have limited contribution in carrying these structural loads, whereas the outer skin of the vehicle does not contribute at all. Owing to this design philosophy, the outer skin of the vehicle can be manufactured using lightweight materials, such as thermoplastics, and thereby the total weight of the vehicle can be further reduced.

2.2.2 Manufacturing concepts

Profile structures used in the FlexBody concept are normally thin walled closed sections and are made of different variants of steel, aluminium and composite materials. Depending on the material, they can be manufactured using techniques such as extrusion, edging and welding, laser cutting and welding (tailored profiles), or hand lamination in case of composite materials. Depending on the cross-sectional shape and the manufacturing technique applied, the FlexBody profile structures are classified into four categories. The description, advantages and disadvantages of each category are presented in Table 2.1. Considering the materials, geometrical dimensions and cost restrictions, suitable profiles are chosen for the target car body structure from one of these categories.

Table 2.1: Manufacturing techniques and categories of profile structures [11], [14]

Level	**1**	**2**	**3**	**4**
Shape of profile	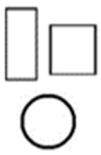	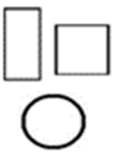	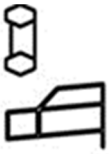	
Manufacturing	at dealer	To be manufactured	Manufactured to drawing	Shells to drawing
Steel	Yes	Yes	No	Yes
Aluminium	Yes	Yes	Yes	Yes
Material range	Very low	Low	Wide	Wide
Vehicle batch size	Very low	Low	Low – medium	Low – medium
Investment	No	No	Low	Low
Price / piece	Low	Medium	Medium	Medium
Integration in car body structure	Very low	Very low	Medium	Medium

As mentioned in the previous section, joints are generally constructed stronger than the profiles attached to them and thus use stronger variants of steel, aluminium and titanium alloys. Joints are normally manufactured using precision casting, sand casting or milling techniques. Depending on the number of joints to be manufactured and initial investments required for the manufacturing tools, suitable manufacturing technique is chosen. Similar to the profiles, the joints are also classified into four categories depending on the manufacturing technique used. Essential features of each category are summarised in Table 2.2.

Table 2.2: Manufacturing techniques and categories of joints [11], [14]

Level	**1**	**2**	**3**	**4**
Example	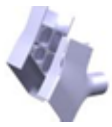			
Manufacturing technology	Milling	Precision casting	Sand casting	Chill casting
Steel	Yes	Yes	Yes	No
Aluminium	Yes	Yes	Yes	Yes
Closed joint possible	With 2 parts	Yes	Yes	With 2 parts
Material range	Medium	Wide	Wide	Medium
Vehicle batch size	Very low	Very low – medium	Low – high	High
Investment	No	Low	Low – medium	No – low
Price / piece	High	High	Medium	Low
Integration in car body structure	Medium	High	High	Low

A special type of joint, the hybrid joint, illustrated in Figure 2.10, can also be used in the FlexBody concept. In this type, a steel sheet is cast along with the material of the joint. This technique is useful to strengthen the joint locally. Another advantage of the hybrid joint is its capacity to realise a pair of same materials at the connection of the joint and the profile, and thereby offer the possibility to use conventional joining techniques.

Profiles and joints are preferably connected using injection bonding techniques. These techniques have been developed in co-operation with Institut für Füge- und Schweißtechnik (isf), TU Braunschweig, Germany and ThyssenKrupp System Engineering GmbH, Essen, Germany. Conventional joining techniques, such as welding, can also be used for connecting profiles and joints made from same materials.

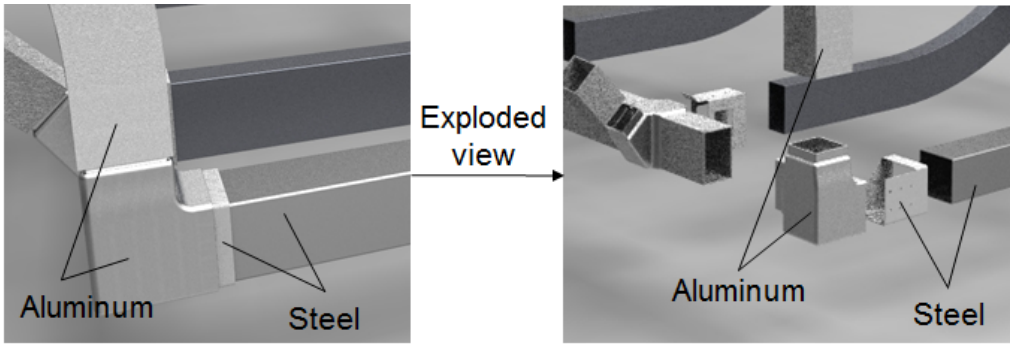

Figure 2.10: Example of a hybrid joint [11], [15]

2.2.3 Application examples

The FlexBody construction concept is conceptualised so as to be freely adaptable to different vehicle designs and package layouts. This concept has been employed in three concept designs till date, for micro electric vehicles “urb-e” [16] and “ecgo” [17] and a sports car “Lampo3” [18]. Figure 2.11 presents the FlexBody car body structures of the urb-e and the Lampo3 as example.

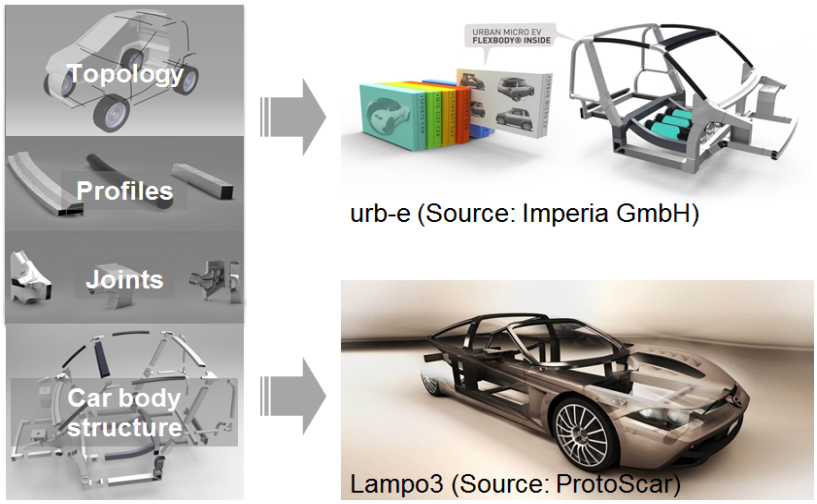

Figure 2.11: Application examples of FlexBody [11], [16], [18]

2.3 Design for crashworthiness

Crashworthiness of a vehicle can be defined as its ability to protect its passengers and other participants, like pedestrians and other vehicles, involved in an event of impact. The car body structure is one of the important vehicle systems that helps in mitigating the impact loads. Therefore, appropriate design measures should be taken while designing the car body structure. Basic principles of design for crashworthiness are briefly explained in Sections 2.3.1 and 2.3.2

summarises conventional approaches used for analysing crashworthiness.

2.3.1 Principles of crashworthiness

A crashworthy car body structure is so conceptualised as to absorb considerable amount of the impact energy by deforming in definite areas, and thereby reduce the deceleration experienced by its passengers to survivable levels. The non-deforming areas of the car body structure are designed as stiff survivable space for the passengers. Various criteria, such as deformation pattern, deceleration pulse of the vehicle, different bio-mechanical criteria defined for the passengers etc., can be used for assessing the crashworthiness of vehicles.

The foundations of crashworthy design for a vehicle were laid by the engineer Bela Barenyi during 1940s at the Daimler-Benz company in Germany, independent of the developments in the USA. He developed various concepts for achieving passenger safety, one of the main concepts being that of the crumple zones [19]. This basic principle is still followed today for designing a crashworthy vehicle structure. A stiff passenger compartment is constructed and it is surrounded by pre-defined energy absorbing zones, called crumple zones or deformation zones. These zones are situated at the front and rear ends, on both sides, and in the top region of the passenger compartment. Figure 2.12 schematically displays various deformation zones situated in a passenger vehicle.

A deformation zone can be divided into primary and secondary deformation zones. The primary zone consists of the main energy absorbing structures, whereas the secondary zone is a structural interface between the primary zone and the stiff passenger compartment. The secondary zone acts as a stable platform for the progressively deforming primary zone and transmits the loads to the passenger compartment [21]. The secondary zone can also be designed to deform in controlled manner, in order to reduce the energy flowing into the passenger compartment. However, the load levels sustained by the secondary zone are kept higher than those sustained by the primary zone, thereby ensuring that the components in the primary zone deform before the components in the secondary zone.

Figure 2.13 illustrates the concept of primary and secondary deformation zones schematically for the frontal, rear and side zones.

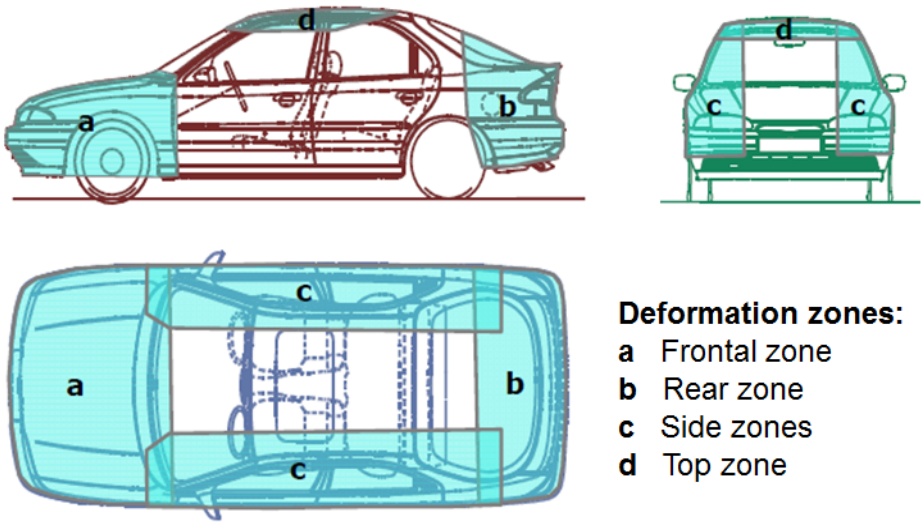

Figure 2.12: Deformation zones in a passenger vehicle [20]

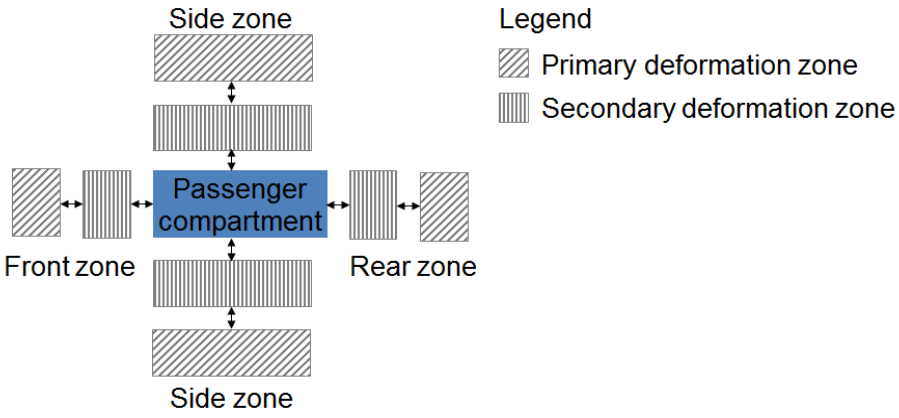

Figure 2.13: Schematic representation of primary and secondary deformation zones [21]

The passenger compartment supports the deformation zones and provides survival space for the passengers. The deformation zones, together with the passive safety systems, such as seat belts and airbags, help in reducing the deceleration experienced by the passengers. The survivable levels of the decelerations, the forces and the deflections of different regions of the passenger's body are defined by various biomechanical criteria, such as Head Injury Criterion (HIC), Neck Injury Criterion (NIC), chest deflection etc. The deformation zones and the passive safety systems are, therefore, designed considering these criteria and their limiting values in different crash scenarios.

The HIC value, describing the deceleration limit of the human brain, is calculated using following Eq. 2.4 [22].

$$HIC = \Delta t \cdot \left[\frac{1}{\Delta t} \int_{t_1}^{t_2} \left(\frac{-a_k(t)}{g} \right) \cdot dt \right]^{2.5} \qquad \textit{Eq. 2.4}$$

Where,

Δt : Time interval for which HIC value is measured = $(t_2 - t_1)$

a_k : Deceleration of occupant's head

The limiting values of the HIC value set in the crash regulations can be used for estimating the allowable value of average decelerations that a vehicle can undergo in a particular crash scenario. These average deceleration values can then be used for designing the crumple zones of the car body structure.

2.3.2 Available methods of designing for crashworthiness

Various methods have been developed and used over the years to analyse and optimise the crashworthiness of vehicles [1], [21]. This section summarises some of the most popular methods and presents their advantages and disadvantages.

2.3.2.1 Finite element method

The most popular method in use today for analysing the crashworthiness of vehicles is the computer aided non-linear finite element (FE) method. According to this method, a continuum is divided into finite number of sub-structures, called finite elements. The state of the whole continuum can thus be described using a finite number of parameters, such as displacement, forces etc. at each node of the FE, resulting in a set of equations of motion. These equations are solved using numerical techniques and thereby an approximate behaviour of the continuum under the given loading conditions is studied [23], [24]. Owing to the continuous improvements in computer hardware and software as well as in the numerical structural mechanics, the FE method has become more efficient and accurate since its introduction. Various software, such as Radioss by Altair Engineering, LS-Dyna established by Livermore Software Technology Corporation (LSTC), PAM-Crash by ESI Group etc. are used in today's automotive industry to analyse the highly non-linear and dynamic problem of the vehicle crashworthiness. Depending on the phase of the design, the complexity and size of the FE model varies considerably.

However, the FE method has some limitations. It gives an approximate solution of a problem and, therefore, may not always represent the reality. Certain amount of expertise is needed for using this method efficiently [23]. Due to advances in computer technologies, the speed and accuracy of generating FE models and simulating them has increased. In spite of these advances, modelling of complex structures, building a numerically stable model and getting realistic results is still a time-consuming task for the analysts. Moreover, due to the detailed input data needed for building an FE model, such as material and geometry data, these models prove to be less useful in the concept design stage of a vehicle. In this stage, the design concept changes quite often and different design concepts are evaluated against each other for their crashworthiness. Therefore, considering the efforts needed to build a single FE model, this method is not always suitable for the concept design phase.

2.3.2.2 Lumped mass spring method

Another analysis method that was primarily used for analysing vehicle crashworthiness before the advance of FE method is the lumped mass spring (LMS) method. LMS models are simple models that approximate a vehicle as a one-dimensional model consisting of a system of springs and lumped masses. The springs mainly represent the deformable structures of the vehicle, whereas lumped masses represent non-deformable components of the vehicle. The load deflection characteristics of the springs are determined either from tests of the respective deformable structures or from their validated FE models. LMS models prove to be very useful in designing vehicle derivatives or upgrading the body structure, where the crash performance results of the basic model are available either in the form of tests or FE simulations.

However, for designing a completely new vehicle structure, the LMS models are not beneficial, since in this case the spring characteristics are unknown. The accuracy and reliability of the LMS models highly depends on the experience, knowledge and understanding of vehicle crashworthiness of the design engineer [21].

2.3.2.3 Hybrid approach

The simplicity of LMS models and the flexibility of FE models is combined into so called hybrid models by researchers, in an attempt to overcome the limitations of both the methods. The most common approach followed by various researchers is developing a collapsible beam finite element and integrating it into FE software. Different concepts and formulations are developed and used by different researchers, such as elastic-plastic beam, Super-collapsible

beam element [21], Superfolding elements and Superbeam elements [25], [26] etc. The formulations of these elements follow various simplified approaches, ranging from purely analytical to purely experimental. Some of the approaches relevant to and studied in this work are summarised in the next Section 2.4.

2.4 Simplified approaches for crashworthy design of car body components

This section presents an overview of simplified design approaches for analysing car body components for their behaviour in crash events. These components are observed to deform in various collapse modes. Section 2.4.1 gives a brief summary of these collapse modes. Main characteristics of the axial and bending collapse modes and simplified design approaches available for these modes, relevant for this work, are presented in Sections 2.4.2 and 2.4.3, respectively. A brief introduction to the tools available for accelerating concept design phase based on these approaches is presented in Section 2.4.4. The limitations of the available simplified approaches are presented in Section 2.4.5.

2.4.1 Collapse modes of car body components

The car body structure mainly consists of thin walled components, which act as energy absorbers as well as the structures maintaining integrity of the passenger compartment during an event of impact. Two basic collapse modes are mainly observed in these thin walled structures: axial and bending collapse, bending being the predominantly observed mode [1], [21]. In their pure form, these modes are observed only in some specific structures, where the loading conditions are ideal for occurrence of the respective modes and due care is taken in designing these structures. All other structures are generally subjected to mixed collapse modes. Various analytical models have been developed for describing these basic collapse modes. Torsional mode of collapse is generally encountered in the thin walled structures of the passenger compartment. Due to the complexity involved in this mode, it is not yet clearly understood and therefore no specific analytical models exist for analysing this mode. However, in most cases, the effects of torsion are negligible, and can be considered only in the detailed design stage using FE method [21].

2.4.2 Axial collapse

2.4.2.1 Main features

The axial mode of collapse is the most effective collapse mode for absorbing impact

energy. This collapse mode is generally observed in front and rear body structures when subjected to frontal and rear impacts. Depending on the following factors, different modes of axial collapse can be observed in the thin walled car body structures [1], [27], [28].

- Angle of impact
- End constraints
- Attachments to the structure
- Material of the structure
- Cross-sectional geometry of the structure

Figure 2.14 illustrates these modes, along with the corresponding force-deflection curves. The first two modes, regular and irregular folding, absorb the highest amount of energy and are, therefore, always preferred. In the global bending mode, the component deforms only in a narrow region and the rest of the component is practically not deformed. Thus, this mode absorbs the least amount of energy and therefore, is not preferred for the energy absorbing structures. Some components may initially develop some folds and later deform in the global bending mode, representing a transition from axial folding to global bending collapse.

The regular and irregular axial folding modes are difficult to achieve in the car body structures. These mode can be achieved only when the axial load is applied at a particular angle (0 – 10 degrees [21]). Even in the most favourable conditions the components may not deform in the axial folding mode, unless they are carefully designed for this purpose. The end constraints and attachments to the component also play an important role in determining the mode of collapse of the components under axial impact, as they can restrict the deformation process. The material, cross-sectional shape and dimensions of the component also have a considerable influence on the axial deformation mode.

A typical force – deformation curve observed for a box column with square or rectangular cross-section, loaded axially and deforming by folding, is illustrated in Figure 2.15.

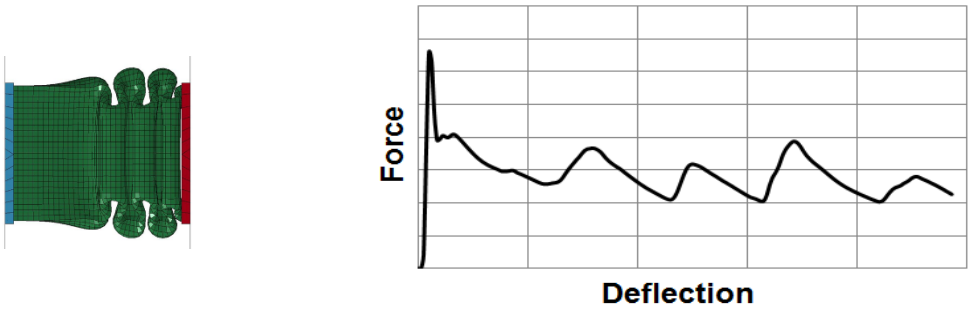

a) Regular folding

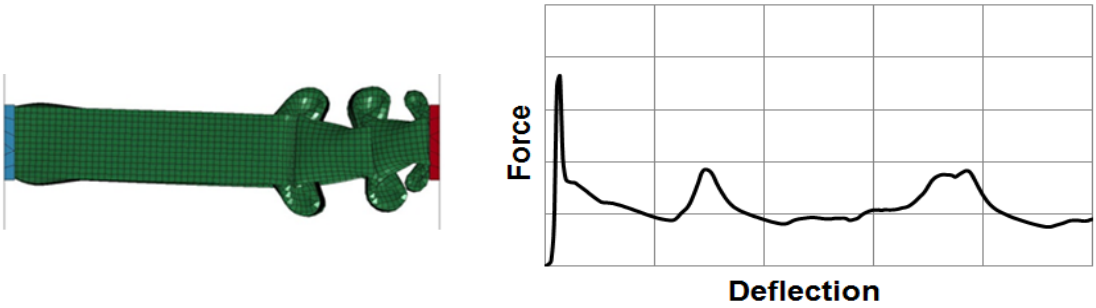

b) Irregular folding

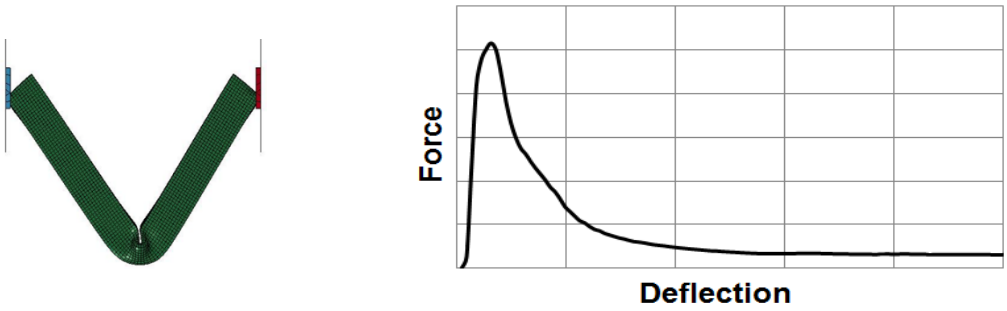

c) Global bending

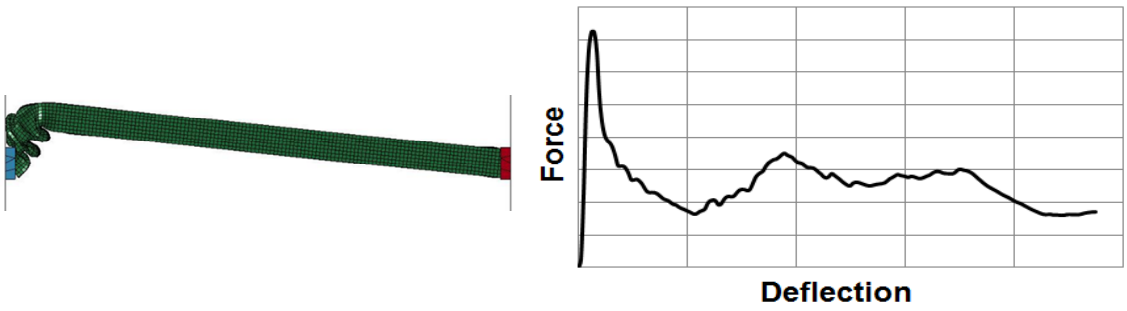

d) Transition: folding to bending

Figure 2.14: Modes of axial collapse

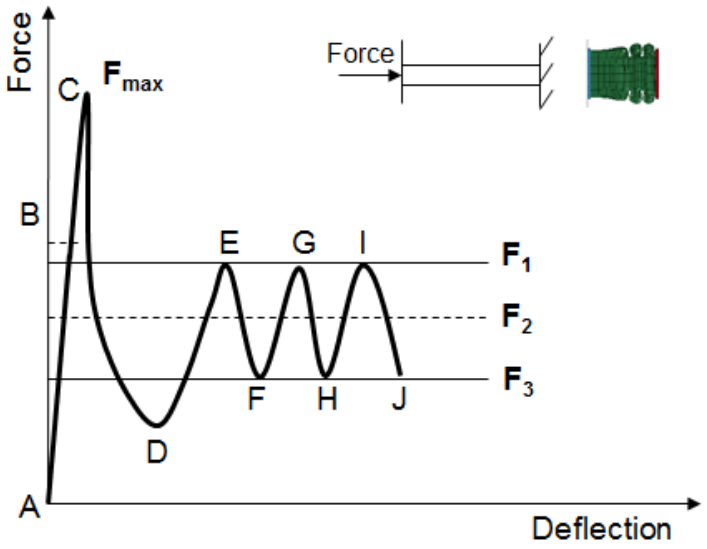

Figure 2.15: Typical force – deformation curve of an axially folding column [29]

Where the alphabets represent,

B : Critical buckling load

C : Crippling or maximum load F_{max}

D : First fold is formed

E : Corner crush load or 2nd crippling load

F : Minimum crush load

And force levels F_1, F_2 and F_3 represent,

F_1 : Corner crush load

F_2 : Mean crush load

F_3 : Minimum crush load

The critical buckling load at point B, is the force at which the column starts to buckle locally. This *local buckling* can eventually lead to progressive collapse or folding of the column. Euler type of buckling of the columns [30] is understood as *global buckling* or *global bending* in this sense [29]. Thin walled box structures loaded axially can buckle locally in two types of modes depending on their side to thickness (b/t) ratio, namely elastic buckling mode and inelastic or plastic buckling mode. Thick structures, called *stocky* columns, buckle in inelastic or plastic mode whereas thin structures, called *slender* columns, buckle in elastic mode. The difference between the behaviour of slender and stocky columns can be seen in the different

forms of force – deformation curves during the initial phase of the axial collapse (curve A-B-C-D in Figure 2.15). Typical forms of the initial phase of force – deformation curves of axially collapsing stocky and slender columns are illustrated schematically in Figure 2.16.

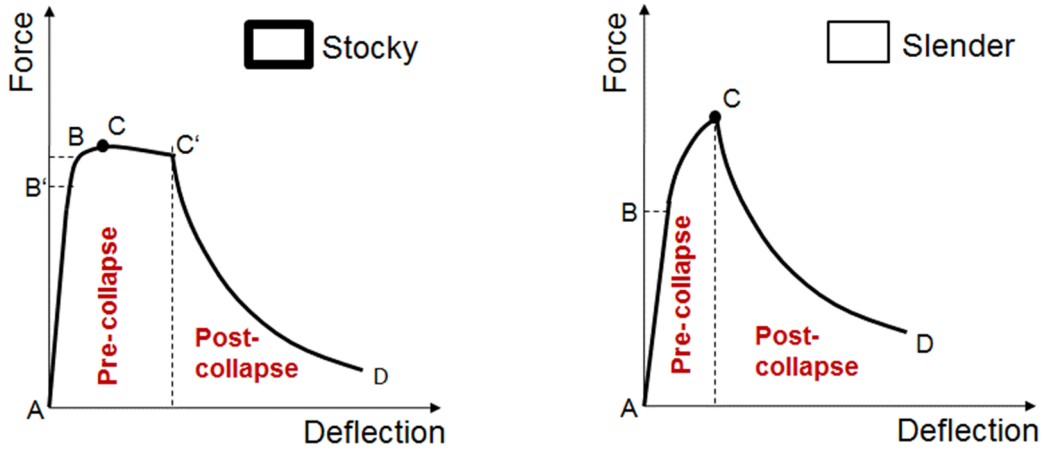

AB‘	: Uniform elastic compression	AB	: Uniform elastic compression
B‘B	: Elastic plastic compression	B	: Local buckling
B	: Local buckling	BC	: Elastic plastic compression
C	: Maximum load	C	: Maximum load
BC‘	: Transition zone	CD	: Post collapse phase
C‘	: Onset of local collapse		
C‘D	: Post collapse phase		

Figure 2.16: Local buckling of slender and stocky columns [28]

Crippling or maximum strength of a column at point C is dependent on the plasticity effects of the material. After the maximum load is reached the column starts losing its strength and thereby the load decreases up to point D. During this process, first fold is formed. When no more deformation can be incorporated in the first fold, the column starts to deform locally at another place, thereby initiating the formation of a second fold and increasing the load supported by the deforming column up to point E in Figure 2.15. Since the column has already undergone deformation, the maximum load reached during the formation of the second fold at E is at a lower level than that of the first fold, at C. As the second fold nears its completion, the load carrying capacity of the column again decreases to F. This trend continues for next folds and each pair of crest and trough is attributed to the formation of one-fold. It is observed from experiments that the load at D is equal to or less than the loads at F, H and J [29]. The peak load

during development of further folds is observed to remain approximately at the same level (points E, G, I in Figure 2.15). This load level is called corner crush load F_1, as illustrated in Figure 2.15. Similarly, the lowest load during formation of each fold is also approximately at same level. This load level is called minimum crush load F_3, shown in Figure 2.15. The mean crush resistance of the thin walled structure F_2 in Figure 2.15 represents the average of load levels F_1 and F_3. For the axially deforming car body components in front end of a vehicle during a front crash, for example, this load influences the deceleration of the vehicle [1], [29].

2.4.2.2 Summary of analytical approaches

Various researchers have developed analytical analysis methods for calculating the important crush characteristics of thin walled columns collapsing axially. As this work deals with the design of thin walled profile structures with a square or rectangular cross-sectional shape, relevant analytical methods are summarised in this section.

Theory by Mahmood and Paluszny

Mahmood and Paluszny [29] presented a semi-empirical approach for calculating the crush characteristics of box columns collapsing in the axial folding mode. Along with the fundamentals of plate theory, their approach uses certain experimentally determined factors for calculating the crush characteristics. The experimental factors used, vary depending on the cross sectional dimensions of the columns and their material properties. Mahmood and Paluszny presented results of experiments carried out on thin walled steel box columns as a validation for their equations. Following equations are presented in [29] for calculating the maximum load (F_{max}), mean crush load (F_2), corner crush load (F_1) and minimum crush load (F_3) supported by a thin walled box column.

$$\sigma_{\max} = \left[\frac{k_p E (t/b)^2}{(1-\nu^2)\beta\sigma_y} \right]^{0.43} \cdot \sigma_y \qquad \textit{Eq. 2.5}$$

$$F_{\max} = \sigma_{\max} \cdot A$$

Maximum load considering length effect:

$$\sigma'_{max} = \sigma_{max} - \frac{\sigma^2_{max}}{4\pi^2 E} \cdot \left(\frac{l_{eff}}{\rho} \right)^2$$

$$F_{max} = \sigma'_{max} \cdot A$$

Eq. 2.6

Where,

$$\rho = \left[\frac{\alpha^2 (3+\alpha)}{12(1+\alpha)} \cdot b^2 \right]^{0.5}$$

The post collapse loads are given by:

$$\sigma_i = \left[\frac{k_i E (t/b)^2}{(1-\nu^2)\beta\sigma_y} \right]^{0.43} \cdot \sigma_y$$

$$i = 1,2,3$$

$$F_i = \sigma_i \cdot A$$

Eq. 2.7

Where,

k_p : Crippling plate coefficient, depends on the section aspect ratio α = d/b

k_i : Plate coefficient, depends on the section aspect ratio α = d/b

ν : Poisson's ratio of material of the column

β : Is a function of aspect ratio t/b and material strength

t : Wall thickness

b : Width of buckling plate (longer side of the cross section of column)

d : Width of restraining plate (shorter side of the cross section of column)

E : Young's modulus of material of the column

σ_y : Yield stress of material of the column

A : Cross-sectional area of the column

ρ : Radius of gyration

l_{eff} : Effective length of the column (as in Euler's elastic buckling theory)

α : Section aspect ratio d/b

The values of k_p, k_i and β are determined experimentally by Mahmood and Paluszny, and the corresponding charts are presented in [29].

Mahmood and Paluszny also presented three criteria for assessing stability of the column during the axial collapse and determining whether a column will collapse in axial folding or global buckling mode [27]. These criteria depend on the geometrical and material properties of the box columns.

Theory by Jones and Abramowicz

Jones and Abramowicz [31] used two types of basic folding elements developed in [32] and [33], to theoretically assess the post collapse behaviour of box columns. They identified four modes of axial folding [34], namely, symmetric mode, asymmetric mode of type A, asymmetric mode of type B and extensional mode, occurring in box columns loaded axially. Figure 2.17 schematically illustrates these four modes. Each of these modes is differentiated from another mode in the manner in which the individual sides of the box column in one layer of the axial fold deform. Asymmetric modes are characterised by formation of a symmetric fold in one layer and formation of an asymmetric fold in the successive layer. This sequence is repeated throughout the deformation. Due to formation of the asymmetric layer, inclination can be observed between the undeformed and deformed part of the column. Subsequently, transition from axial folding to global buckling can occur in an asymmetrically deformed column. Symmetrically deforming columns can also undergo global buckling due to introduction of imperfections in the undeformed part during the deformation [34].

<table>
<tr><td rowspan="4"> 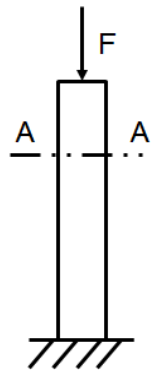
</td><td>  </td><td>  </td></tr>
<tr><td>a) Symmetric mode</td><td>b) Asymmetric mode (A)</td></tr>
<tr><td>  </td><td> 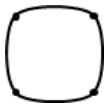 </td></tr>
<tr><td>c) Asymmetric mode (B)</td><td>d) Extensional mode</td></tr>
<tr><td>Axially loaded box column</td><td colspan="2">Deformed cross-section A-A</td></tr>
</table>

Figure 2.17: Axial folding modes of box columns according to Jones and Abramowicz [34], [35]

Depending on contribution of each type of the basic folding element in each of the above modes, the energy absorbed in each mode is found. Equating this energy to the external energy,

analytical equations for static and dynamic mean crushing load for each axial folding mode are derived by Jones and Abramowicz. They have also included the influence of the effective crushing distance and the material strain rate sensitivity in the analytical equations. They presented a comparison of experimental results conducted on square columns and the analytical results for validating their theory.

Depending on the analytical predictions, it is observed by Jones and Abramowicz, that a particular axial folding mode occurs in a particular range of the C/t ratio, where,

$$C = \frac{b + d}{2} \qquad \textit{Eq. 2.8}$$

With,

b and d : Lengths of sides of cross section of box column

t : Wall thickness

The ranges of the C/t ratio and the corresponding mode of axial folding are summarised below [31].

- Symmetric mode for thin sections, for $C / t \geq 40.8$
- Asymmetric mode B, for $7.5 \leq C / t \leq 40.8$
- Extensional mode for thick sections, for $C / t \leq 7.5$
- Asymmetric mode A does not control the collapse of box columns in the range $0 \leq C/t \leq 40$.

The analytical equations presented in [31] are reproduced below for each mode of axial folding.

- Symmetric mode:

- Mean static crushing load considering effective crushing distance:

$$F_2' = 52.22\left(\frac{C}{t}\right)^{1/3} \cdot M_0 \qquad \textit{Eq. 2.9}$$

Where,

$$M_0 = \frac{\sigma_0 t^2}{4} \qquad \textit{Eq. 2.10}$$

With,

M_0 : Fully plastic moment per unit length

σ_0 : Flow stress of material

- Mean dynamic crushing load considering effective crushing distance and material strain rate sensitivity:

$$F_2^{d}{}' = 52.22\left[1+\left(\frac{0.33V}{CD}\right)^{1/p}\right]\left(\frac{C}{t}\right)^{1/3}\cdot M_0^{d} \qquad \textit{Eq. 2.11}$$

Where,

V : Velocity of impact

D and p : Cowper-Symonds coefficients given by D = 6844 s^{-1} and p = 3.91.

In Eq. 2.11,

$$M_0^{d} = \frac{\sigma_0^{d} t^2}{4} \qquad \textit{Eq. 2.12}$$

Where,

σ_0^{d} : Dynamic flow stress

- Asymmetric mode of type A
- Mean static crushing load considering effective crushing distance:

$$F_2' = \left[42.92\left(\frac{C}{t}\right)^{1/3} + 3.17\left(\frac{C}{t}\right)^{2/3} + 2.04\right]\cdot M_0 \qquad \textit{Eq. 2.13}$$

- Mean dynamic crushing load considering effective crushing distance and material strain rate sensitivity:

$$F_2^{d}{}' = \left[1+\left(\frac{0.44V}{CD}\right)^{1/p}\right]\cdot\left[42.92\left(\frac{C}{t}\right)^{1/3} + 3.17\left(\frac{C}{t}\right)^{2/3} + 2.04\right]\cdot M_0^{d} \qquad \textit{Eq. 2.14}$$

- Asymmetric mode of type B
- Mean static crushing load considering effective crushing distance:

$$F_2' = \left[45.9\left(\frac{C}{t}\right)^{1/3} + 1.75\left(\frac{C}{t}\right)^{2/3} + 1.02\right]\cdot M_0 \qquad \textit{Eq. 2.15}$$

- Mean dynamic crushing load considering effective crushing distance and material strain rate sensitivity:

$$F_2^d{}' = \left[1+\left(\frac{0.39V}{CD}\right)^{1/p}\right]\cdot\left[45.9\left(\frac{C}{t}\right)^{1/3}+1.75\left(\frac{C}{t}\right)^{2/3}+1.02\right]\cdot M_0^d \qquad \textit{Eq. 2.16}$$

▪ Extensional mode

- Mean static crushing load considering effective crushing distance:

$$F_2{}' = \left[32.64\left(\frac{C}{t}\right)^{1/2}+8.16\right]\cdot M_0 \qquad \textit{Eq. 2.17}$$

- Mean dynamic crushing load considering effective crushing distance and material strain rate sensitivity:

$$F_2^d{}' = \left[1+\left(\frac{0.25V}{CD}\right)^{1/p}\right]\cdot\left[32.64\left(\frac{C}{t}\right)^{1/2}+8.16\right]\cdot M_0^d \qquad \textit{Eq. 2.18}$$

Theory of superfolding element (SE) by Wierzbicki and Abramowicz

Using the basic folding elements developed previously in [32], [33] and [36], Wierzbicki and Abramowicz conceptualised a macro element, called a superfolding element (SE) or a corner element [25], [36], for theoretically analysing the axial folding of box columns in the post collapse phase. They define a superfolding element (SE) or a corner element as a "large finite element with a prescribed knowledge of the deformation process and a few degrees of freedom" [25]. It can be described as a representative element of a crushed zone, which repeats itself throughout the crushed zone. Figure 2.18 illustrates a SE with its essential dimensions.

According to this theory, the strength of one SE is calculated using a mixed folding mechanism, which combines two types of basic folding elements described earlier in [32], [33], [34] and [36], namely quasi-inextensional and extensional elements. In these elements, the energy is assumed to be absorbed in narrow zones of the structure undergoing plastic deformation. The mixed folding mechanism considers a model, in which the quasi-inextensional mode exists during the first phase of the deformation up to an intermediate configuration, and in the second phase of the deformation, the extensional mode controls the deformation of the SE.

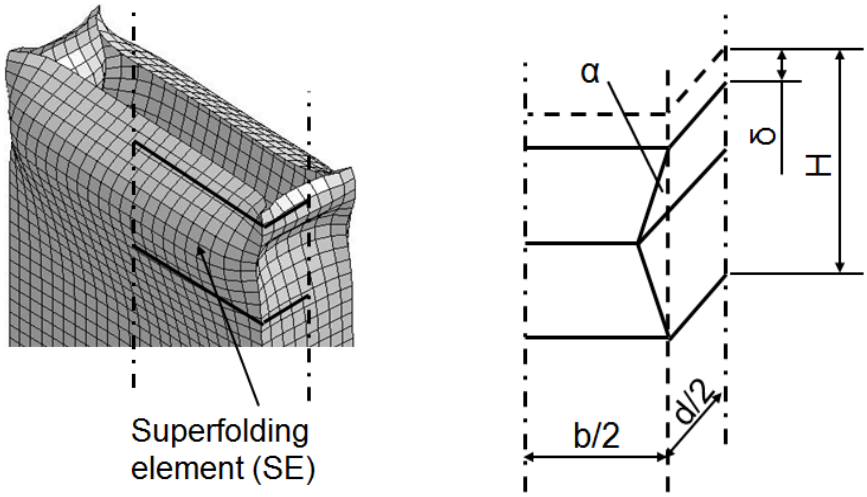

a) Position of SE in box column b) Schematic representation of SE

Figure 2.18: Representation of a superfolding element (SE) [25], [36]

Where,

H : Half the length of the folding wave

δ : Shortening of the column

α : Rotation angle of side panels

C : Half the sum of the lengths of sides of box column and is given by Eq. 2.8

For a square or rectangular column composed of four SEs, the effective mean crushing force is given by following equation in [25].

$$F_{2,eff,sq/rect} = 16\pi M_o \left(\frac{C}{t}\right)^{1/3} \qquad \textit{Eq. 2.19}$$

In [25], an approximation for calculating the instantaneous crushing force for one SE is also presented (Eq. 2.20).

$$F(\alpha) = F_2\left[0.6 + \frac{0.512}{\alpha}\right] \qquad \textit{Eq. 2.20}$$

Where,

$$\delta = 2H(1-\cos\alpha) \qquad \textit{Eq. 2.21}$$

$$H = t^{1/3}C^{2/3} \qquad \textit{Eq. 2.22}$$

2.4.3 Bending collapse

2.4.3.1 Main features

A bending collapse mode involves formation of a local hinge mechanism and energy is absorbed only in this narrow area. Thus, the energy absorption capacity of the bending collapse mode is less as compared to the axial folding mode. Bending mode is the most commonly observed mode of collapse in automotive structures. The reason can be attributed to the fact that the natural tendency of thin walled structures is to collapse in a mode that requires less amount of energy. Pure bending is observed only in side structures of the vehicles during side impacts. Generally, a mixed mode of axial compression and bending is encountered in thin walled car body structures.

As stated earlier, a thin walled structure loaded in bending forms a local plastic hinge between two plastically undeformed sections of the structure. The whole energy of deformation is absorbed in this plastic hinge. The rest of the undeformed structure does not contribute in energy absorption. Kecman [37] identified four phases in the development of the plastic hinge, observed from various experiments conducted by him. Figure 2.19 depicts these four phases exemplarily, using an FE simulation performed on a thin walled box structure during this work.

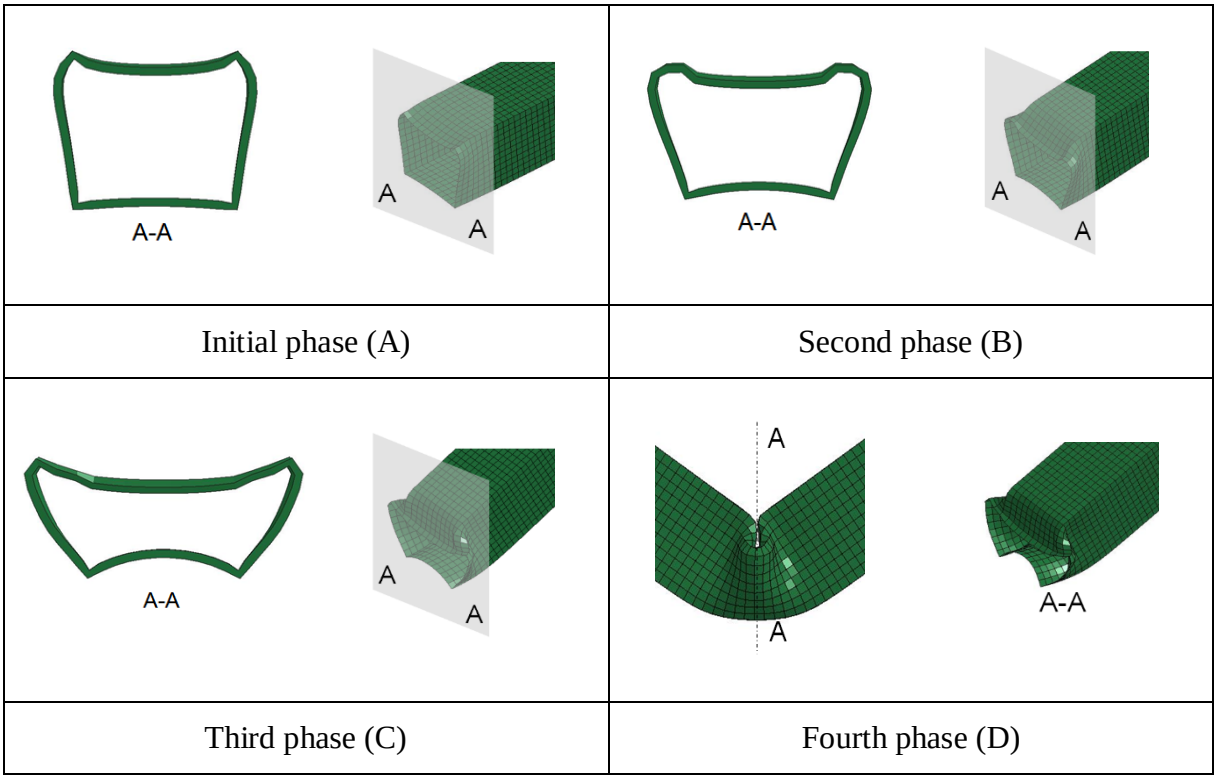

Initial phase (A)	Second phase (B)
Third phase (C)	Fourth phase (D)

Figure 2.19: Phases in development of plastic hinge during bending collapse

- Initial phase (A): In this phase a bulge is observed in the webs but without any rolling deformation in the corners.
- Second phase (B): This phase is marked by rolling deformations in the corners and the cross-section of the member attains an approximate trapezoidal shape.
- Third phase (C): The third phase starts when the rolling deformations of the corners are jammed and recognisable deformations can be observed in the web.
- Fourth phase (D): This stage is marked by jamming of the entire plastic hinge, i.e. when the two halves of the compression flange touch each other and further deformation in this hinge is completely ceased.

A typical moment – rotation curve of a plastic hinge formed in a thin walled structure without prominent material separation is illustrated in Figure 2.20. The positions A to D approximately represent four phases of the plastic hinge.

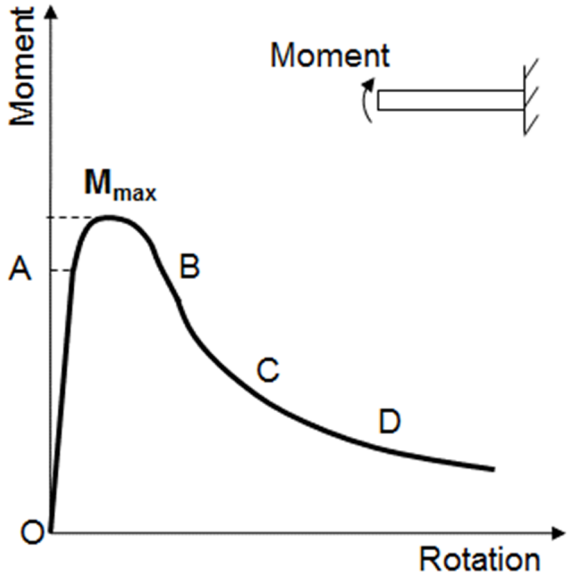

Figure 2.20: Typical moment – rotation curve of a plastic hinge [21]

2.4.3.2 Summary of analytical approaches

In spite of being the most commonly found mode of collapse, the bending mode has received less attention among researchers compared to the axial mode [21]. The theories available for analysing the deformation characteristics of box beams under bending load are summarised in this section.

Theory by Kecman

Kecman [37], [38] presented an analytical model for predicting the performance of thin walled box beams under bending loads. The analytical mechanism described by Kecman is based on the second phase of the hinge formation. It neglects the initial phase, in which mostly elastic deformations occur and thereby contribute very little to the energy dissipation. The references [37] and [38] give analytical equations for predicting the maximum bending moment of the section, the moment – rotation curve and energy absorbed during the bending collapse. Figure 2.21 and Figure 2.22 depict the essential notions in the kinematic model developed by Kecman.

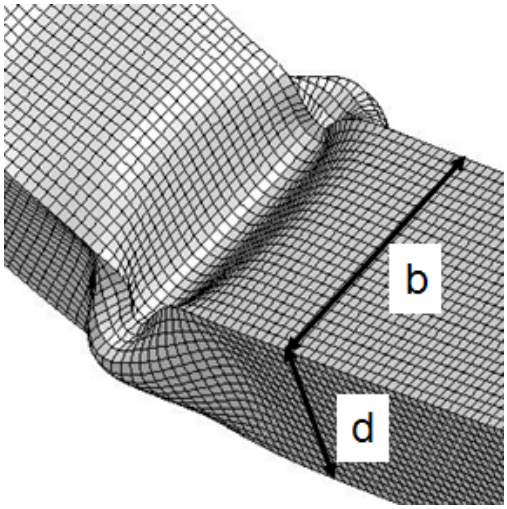

Figure 2.21: Bending deformation of a box beam with compression flange b and depth d [37], [38]

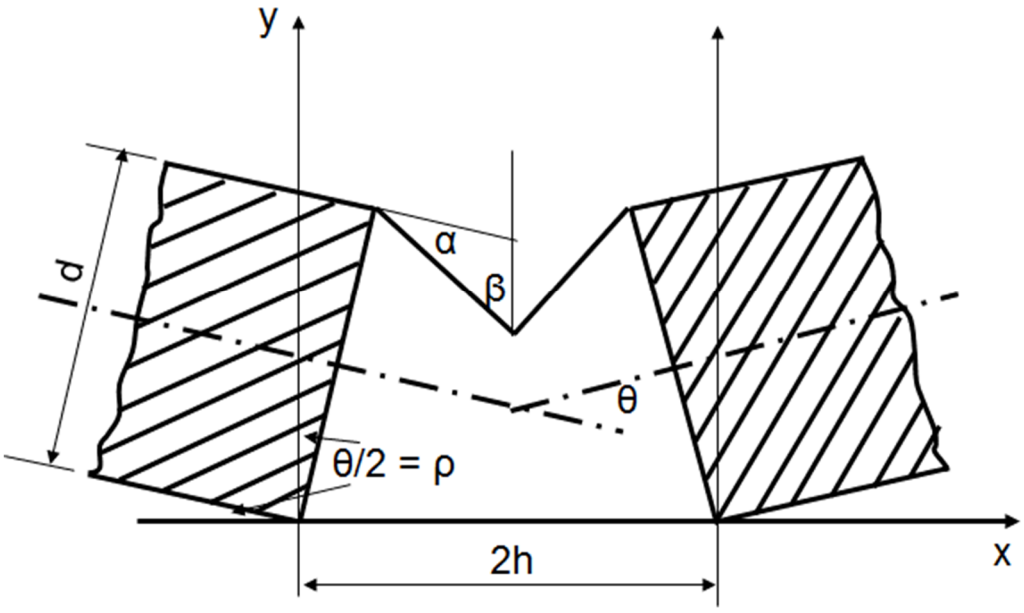

Figure 2.22: Cross section of a plastic hinge [37], [38]

The analytical equations presented in [37] and [38] are reproduced below.

Critical stress of the compression flange can be calculated by Eq. 2.23:

$$\sigma_{cr} = \frac{\pi^2 E}{12\left(1-\nu^2\right)} \cdot \left(5.23 + 0.16\,\frac{b}{d}\right) \cdot \left(\frac{t}{b}\right)^2 \qquad \textit{Eq. 2.23}$$

Where,

b : Width of compression flange

d : Depth of the box section undergoing bending deformation

If the critical stress σ_{cr} is less than the yield stress σ_y of the material, the compression flange buckles with an effective flange width given by Eq. 2.24:

$$b_e = b \cdot \left(0.7\,\frac{\sigma_{cr}}{\sigma_y} + 0.3\right) \qquad \textit{Eq. 2.24}$$

The maximum moment depends on the actual stress distribution in the compression flange when it buckles, and therefore can be calculated using following formulae (Eq. 2.25 to Eq. 2.27), depending on the values of σ_{cr} and σ_y.

If $\sigma_{cr} \leq \sigma_y$

$$M_{\max} = \sigma_y t d^2 \cdot \frac{2b + d + b_e \cdot \left(3\,\frac{b}{d} + 2\right)}{3(b+d)} \qquad \textit{Eq. 2.25}$$

If $\sigma_{cr} \geq 3\sigma_y$

$$M_{\max} = M_p = \sigma_y t\left[b(d-t) + 0.5(d-2t)^2\right] \qquad \textit{Eq. 2.26}$$

Where, M_p is fully plastic moment.

And if $\sigma_y < \sigma_{cr} < 3\sigma_y$

$$M_{\max} = M_p' + \left(M_p - M_p'\right) \cdot \frac{\sigma_{cr} - \sigma_y}{2\sigma_y}$$

$$with: M_p' = \sigma_y t d \cdot \left(b + \frac{d}{3}\right) \qquad \textit{Eq. 2.27}$$

The angle θ depicted in Figure 2.22 is the rotation angle of the hinge.

The hinge length KL = 2h is given by Eq. 2.28:

$$2h = a \text{ if } a \le b$$
$$2h = b \text{ if } a \ge b \qquad \textit{Eq. 2.28}$$

The analytical model jams when the buckled halves of the compression side touch each other. Angle of jamming is calculated using Eq. 2.29:

$$\theta_J = 2\arcsin\left(\frac{h - 0.5t}{d}\right) \qquad \textit{Eq. 2.29}$$

For $0 \le \theta \le \theta_J$, the total nominal energy absorbed in the plastic hinge is calculated by:

$$W(\theta) = 2m_p\left[(b + z_A)(\pi - 2\beta) + h\left(\pi + 2\arctan\frac{z_A}{y_A}\right)\right] +$$
$$2m_p\left[2d\arctan\left(\frac{z_A}{\sqrt{(h - x_{A''})^2 + (y_{A''} - y_B)^2}}\right)\right] + \qquad \textit{Eq. 2.30}$$
$$2m_p\left[2\frac{z_A}{r}\left(h + \frac{2}{3}\sqrt{h^2 + y_B^2 + z_A^2}\right)\right]$$

In the above equation:

$$\rho = \frac{\theta}{2}$$
$$m_p = \frac{\sigma_{pu} \cdot t^2}{4} \qquad \textit{Eq. 2.31}$$

With, σ_{pu} : maximum nominal flow stress of material in uniaxial tension, and

$$\beta = \arcsin\left(1 - \frac{d}{h}\sin\rho\right)$$

$$z_A = d\sin^2\rho - h\sin\rho + \sqrt{d\sin\rho\cdot(2h - d\sin\rho)}\cdot\cos\rho$$

$$x_{A''} = y_{A''}\tan\rho$$

$$y_{A''} = \frac{h\tan\rho + d\cos\rho - \sqrt{d\sin\rho(2h - d\sin\rho)}}{1+\tan^2\rho} \qquad \textit{Eq. 2.32}$$

$$y_B = d\cos\rho - \sqrt{d\sin\rho(2h - b\sin\rho)}$$

$$r = \left(0.07 - \frac{\theta}{70}\right)h$$

Since it is difficult to differentiate Eq. 2.30, the moment M(θ) applied to the hinge at any rotation angle θ can be calculated numerically using Eq. 2.33:

$$M(\theta) = \frac{W(\theta + \Delta\theta) - W(\theta)}{\Delta\theta} \qquad \textit{Eq. 2.33}$$

At θ = 0° the moment is at its maximum value which is given by Eq. 2.25, Eq. 2.26 or Eq. 2.27.

Theory of superbeam element (SB) by Wierzbicki and Abramowicz

Wierzbicki and Abramowicz extended the concept of the superfolding element (SE) developed in [25], [36] to a superbeam element (SB) to analyse the deformation characteristics of a thin walled box beam deforming in bending mode under bending and combined bending-compression loading [26]. They used the kinematical model developed by Kecman in [37], [38] to develop the analytical solution for a SB. A SB consists of only half of the deformed portion of a box beam. The other half of the beam undergoes symmetrical deformation. Figure 2.23 is reproduced from [26] and shows an SB element observed in an FE simulation and superimposed by Kecman's simplified model.

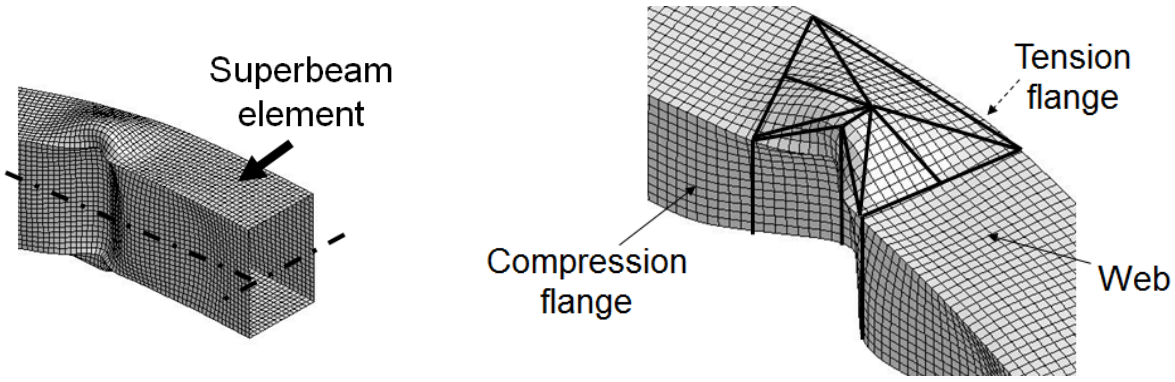

Box beam deformed in bending Superbeam element (SB)

Figure 2.23: Superbeam element [26]

This SB is further divided into two corner elements: compressed element SE1, containing compression flange and half of the web, and tensile element SE2, containing tension flange and the other half of the web. The deformation pattern of the compression flange can be compared to the deformation of a column subjected to pure axial compression. The second corner element SE2, containing the tension flange, deforms in a different way as compared to the compression flange. Due to this reason, the folding wavelength of an SB is larger compared to that of a comparable SE. In an actual bending mechanism, the neutral axis translates within the cross section of the beam during the deformation and its position is one of the unknowns in the kinematical model developed by Wierzbicki and Abramowicz. It was observed in [26], that for the most part of the deformation process the neutral axis is located in the tension flange. This assumption is used by Wierzbicki and Abramowicz to derive an approximate solution. This theory [26] uses principle of virtual work i.e. equating the rates of external and internal energy dissipation for analysing the deformation characteristics of a SB.

An approximate simplified solution given in [26] for evaluating mean crushing force for a box beam deforming in bending mode is presented below. For this solution, it is assumed that the neutral axis lies in the tension flange.

For one SB:

$$F_2^b = 1.17\left(3\pi M_o\right)\left(\frac{C}{t}\right)^{1/3} = 1.17F_2^c \qquad \textit{Eq. 2.34}$$

Since a thin walled box beam collapsing in bending mode consists of two SBs, the mean crushing force for the complete box beam is given as:

$$F_{2,sq/rect}^{b} = 2 \times 1.17 \left(3\pi M_o\right) \left(\frac{C}{t}\right)^{1/3} = 2 \times 1.17 F_2^c \qquad \textit{Eq. 2.35}$$

Where F_2^c is the mean crushing force of one SE described in [25].

The equation for the approximate instantaneous crushing force of one SB with the small angle approximation can be given by Eq. 2.36:

$$F^b(\alpha) = F_2^b \left[0.576 + \frac{1}{2\alpha}\right] \qquad \textit{Eq. 2.36}$$

2.4.4 Tools for hastening concept design phase in practice

As mentioned before, the concept design phase of a car body structure is characterised by frequent changes in its design. Thus, various concept designs need to be analysed quickly and without excessive efforts. Various computer aided tools are developed and are available in the market for fast construction, modification and analysis of the designs concerning the crashworthiness of vehicle structures. This section gives a brief overview of such tools available in the market. First two tools presented in Sections 2.4.4.1 and 2.4.4.2 below, Fast Concept Modelling and SFE Concept, are used for fast and parametric CAD and CAE modelling of vehicles. Whereas, Secollapse / Vcrush and Visual Crash Studio (VCS) presented in Sections 2.4.4.3 and 2.4.4.4 are based on the analytical methods summarised in Section 2.4.2.2 and 2.4.3.2 and are used for performing preliminary crash analysis of car body structures.

2.4.4.1 Fast Concept Modelling (FCM)

Fast concept modelling (FCM) [39], [40] is offered by Contact Software GmbH, Bremen (headquarters), Germany. It is a CAD-driven tool which couples the CAD and CAE fields for the purpose of creating parametric models in the automotive design process. It is developed as a construction tool integrated into the CATIA V5 environment. It allows for parametric 3D modelling of automotive structures and thereby makes it possible to rapidly modify the constructed structures. Using FCM, the properties necessary for FE analysis can also be assigned to the structures in the CAD environment. FCM, thereby, allows for a rapid transfer of data between CAD and CAE fields compared to a fully manual operation. Owing to such modelling strategy, the concept design process can be accelerated [40].

2.4.4.2 SFE Concept

Computational tool SFE Concept [41] is offered by SFE GmbH, Berlin (headquarters), Germany. In contrast to FCM, this tool follows a CAE-driven approach. It offers fast and efficient means to create and modify parametric FE models. The FE models are simulated and optimised in an automatic feedback loop with external FE solver and optimiser. The optimised results can be directly integrated into the initial FE model by instantly updating the FE mesh. Using this approach, frequent and time-consuming data transfers between CAD and CAE models can be avoided, thereby quickening the concept design process [41].

2.4.4.3 Secollapse / Vcrush

Using the semi-empirical approach for the analytical analysis of box columns loaded in axial and combined axial and bending loads presented in [29], [42], [43], Mahmood and Paluszny developed the computer programs VCRUSH, a system code, and SECOLLAPSE, a component code, for analysing complex vehicle structures [21], [44], [45]. In these computer programs, a single thin walled component of a vehicle structure is considered as a tapered beam element with defined end cross-sections. The cross-section is then divided into sub-elements as plates or shells. For a given load, the stress levels and deformation state in each sub-element are calculated and reviewed using the semi-empirical equations. With each increment in the load the changed stress levels and thereby the deformation phase, either elastic, local buckling or post buckling, are updated for each sub-element. Thus, the full loading and collapse characteristics of beam elements are evaluated iteratively. Mahmood and Paluszny presented these programs as a design aid for engineers for analysing vehicle structures composed of open or closed thin-walled sections of arbitrary shapes, predominantly for the concept design phase. To the best of the author's knowledge, these tools are not in use today.

2.4.4.4 Visual Crash Studio (VCS)

Abramowicz developed a computer program Visual Crash Studio (VCS) [46], which is offered by Impact Design, Europe, Michalowice (headquarters), Poland, founded by Abramowicz. VCS finds application in pre-design and early design stages of a vehicle structure. The program is conceptualised for analysing the crashworthiness of complex structural components and cross sections based on the concept of the macro elements, i.e. superfolding and superbeam elements, presented in [25], [26]. The program discretises given structural components into a finite number of macro elements, which have prescribed knowledge of

deformation behaviour under loads. This knowledge is based on the analytical basics presented in [25], [26]. Thereby, assembling the behaviour of all the macro elements, behaviour of the full structural component is simulated by the program. VCS uses the basic theory of structural mechanics supported by experimental observations to assemble the performance of individual macro elements and to predict the performance of the structural component [47]. Due to the limitations imposed by analytical formulation of the macro elements, the types of structures that can be modelled by this method are limited to thin walled structures.

In addition to calculating the deformation behaviour of structural components, VCS also suggests geometrical corrections in the complex cross-sectional shapes of the components, so that the components would deform in a desired mode, for example, folding mode under axial load. The program also applies the theory of macro elements for analysing structural components of complex shapes, for example, for analysing the response of a longitudinal front rail under frontal impact loads [47], [48].

2.4.5 Limitations of available tools

The tools listed above are evaluated on the basis of steps of car body design that can be carried out using these tools. Table 2.3 presents this evaluation. The steps that can be executed using each tool are marked by "√".

Table 2.3: Evaluation of available tools

Design steps	**FCM**	**SFE Concept**	**Secollapse / Vcrush**	**VCS**
Precise definition of performance targets				
Initial layout of car body structure				
CAD construction	√			
Creation of analysis model	√	√	√	√
Analytical or FE analysis		√	√	√
Optimisation of geometry		√		√
Adaption of optimised geometry in CAD	√	√		

Amongst the above mentioned computational tools available to the car body design engineers and analysts, two limitations can be clearly seen. First, there is no tool or guideline available for defining the crash performance targets for the car body and its components at the beginning of the design. Without specific targets, it is often difficult for the design engineer to start *planning* the design. Second, there are no guidelines available for *guessing* the initial cross-sectional geometry and materials for the car body components, which are required to be given as input for all the available tools listed above. Both these functions are generally carried out using the experience of the engineer and previous data available with the vehicle manufacturer. As a result, often the components are overdesigned in the concept design phase, which in turn results in a heavy car body structure. This may also lead to lack of required crashworthiness. The optimisation of this designed structure requires extra efforts and time.

Therefore, deduction of appropriate performance targets and choosing appropriate component geometry and materials in the concept design phase becomes highly beneficial, as it can help in reducing further optimisation cycles. Consequently, the design process of the car body can be accelerated. For the small series manufacturers, who have limited resources and time for vehicle development, accelerating the design process is of utmost importance. This work focuses on overcoming these shortcomings of the design process.

As in the self-supporting car body structures complex component geometries and cross sections are involved, it is difficult to guess an appropriate initial cross-sectional shape. Due to multiple number of functions assigned to the components in these structures according to the integral construction concept, deducing and assigning appropriate performance targets to these components is also tedious. However, for simpler structures involved in the profile based car body structures with regular cross-sections, guidelines can be developed for defining performance targets and designing the initial geometry of the components.

2.5 Task formulation

As discussed in the previous Section 2.4.5, design of a crashworthy and lightweight car body structure in limited amount of time and at a low cost, is very advantageous, but at the same time, is also a huge challenge for the small series manufacturers. By generating an optimum concept design of the car body structure in a short duration, this challenge can be successfully met. Deciding the crash performance targets for the car body structure and its components initially, and then choosing the appropriate geometry and material for the components will be highly beneficial in generating an optimum concept design. Guidelines for

defining the performance targets and for choosing suitable component geometry can be generated by performing FE simulations on a defined set of structures of practical importance. With an intelligent synthesis of the data obtained, a performance oriented design approach can be developed for the car body structure considering its crash performance.

This work aims at developing a performance oriented design approach for generating a crashworthy profile-based car body structure with regular cross sections. Using FE simulation techniques, this work targets at developing guidelines for defining the crash performance targets for a profile based structure with regular cross sections. Taking advantage of the simplicity of the profile based structures, this work also aims at developing simplified methods for designing the cross-sectional dimensions and materials of these structures to satisfy the pre-defined performance targets.

3 The Multi Objective Knowledge-based Approach

The *Multi Objective Knowledge-based (MOK)* approach proposes a methodical technique for creating an optimum concept design of a new target car body structure constructed using the profile based construction concept. The knowledge-base integrated in this approach helps to generate a performance oriented concept design of the body structure, considering its crashworthiness. This knowledge-base is developed from the basic understanding of the vehicle crashworthiness and information extracted from numerous FE simulations performed on car body structures and profile structures with regular cross-sectional shapes. The MOK approach provides guidance to the design engineer through the entire car body development process, by supplying important design information in the concept design phase. The knowledge-base integrated in the MOK approach optimises the design process in terms of efforts, time as well as costs.

The MOK approach is based on the VDI guideline 2221 [49] describing a "Systematic approach to the development and design of technical systems and products". This VDI guideline describes a systematic design process and various steps to be followed, in order to design a product. The MOK approach divides the entire car body design process into seven steps to create an optimum concept design of the target car body. In each step, certain features of the target body structure are configured. The steps in the MOK approach and their association with the VDI guideline 2221 is explained briefly in Section 3.1. Section 3.2 concisely describes the three fields of knowledge-base integrated in the MOK approach. Developing an optimum concept design by deducing crash performance targets and choosing appropriate component geometry is realised through the structural knowledge-base. Section 3.3 briefly explains the focus of the structural knowledge-base.

3.1 The steps of the MOK approach

Figure 3.1 and Figure 3.2 respectively illustrate the design process according to the VDI guideline 2221 and the seven steps conceptualised in the MOK approach. This section explains these steps in the MOK approach and their respective tasks, and presents their similarities with the steps described in the VDI guideline 2221 [2], [49]. As will be discussed in the following paragraphs, although a one to one correspondence cannot be established between the steps of the MOK approach and the VDI guideline 2221, the MOK approach follows a similar process

of thinking, sequencing and formatting of the design steps.

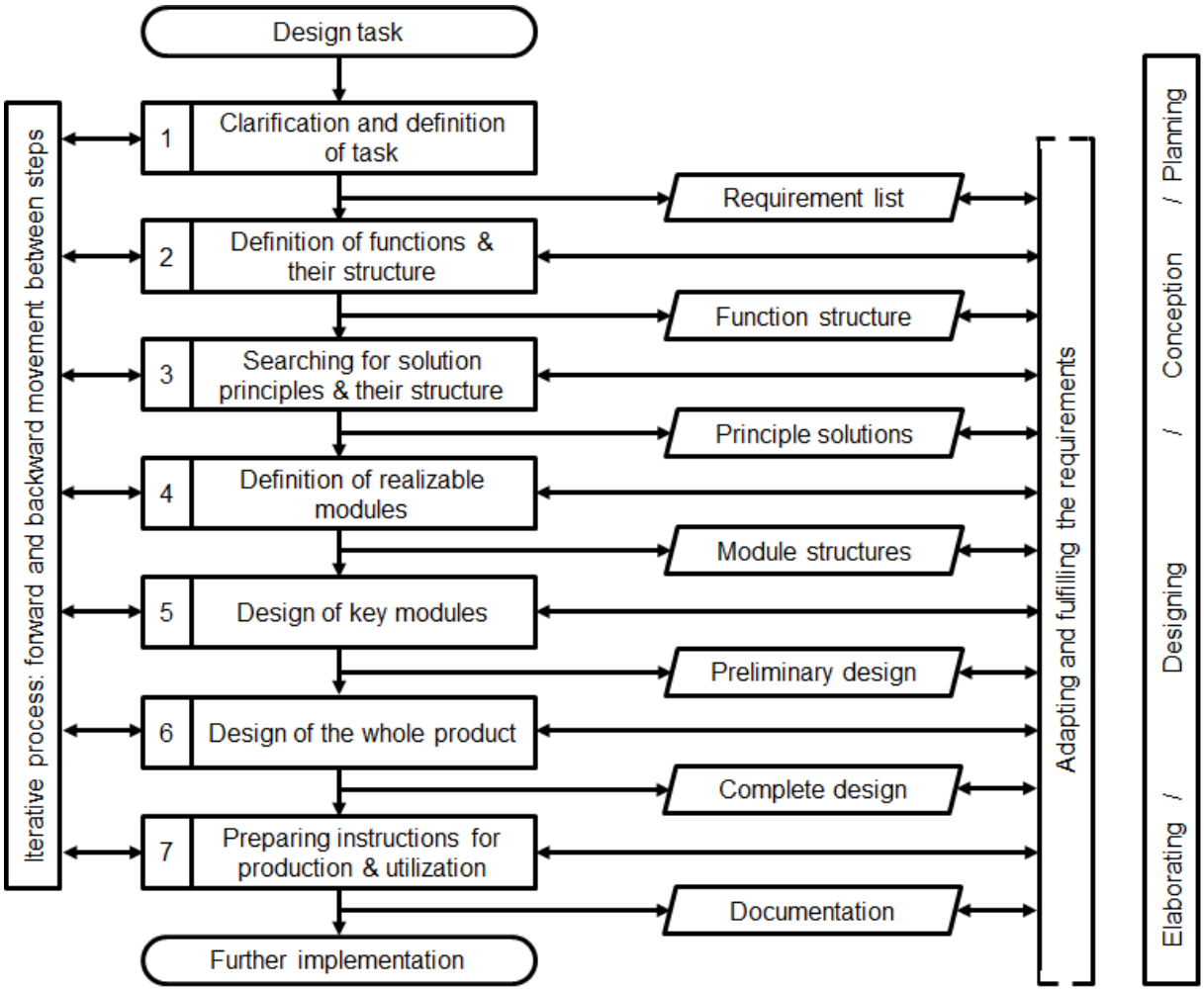

Figure 3.1: Design process according to VDI-guideline 2221 [2], [49]

In the view of the MOK approach, a crashworthy car body structure is considered as a machine which converts the kinetic energy before impact into deformation energy after impact. This is achieved by controlled deformation of the car body structure in definite zones. Thereby, the body structure fulfils the function of protecting the occupants in the event of an impact.

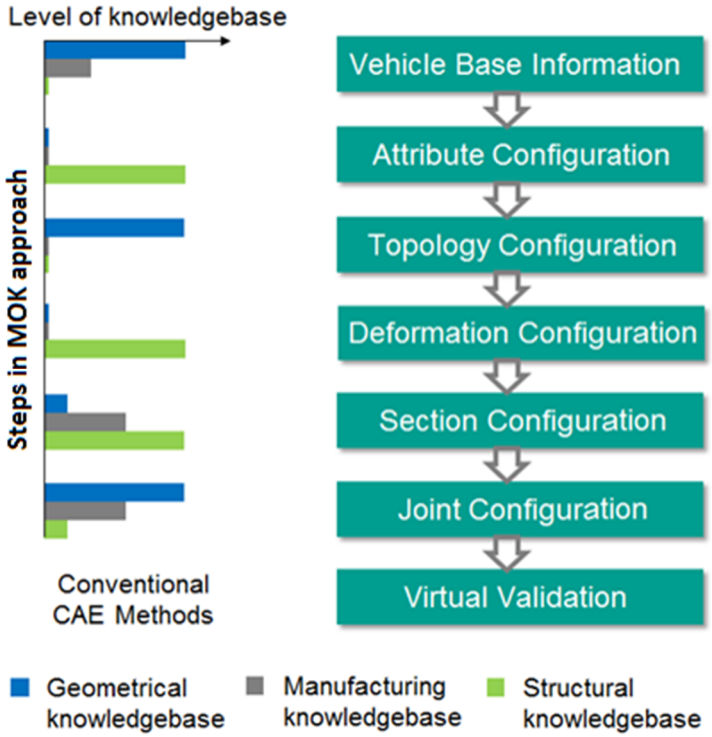

Figure 3.2: Steps in the MOK approach

In order to design a car body structure, it is first important to know the requirements and constraints that should be considered while designing. Therefore, similar to the first step of the VDI guideline 2221, “creating a requirements list”, the aim of the first two steps in the MOK approach is to list down design requirements for the target car body structure. In *Vehicle Base Information*, constraints, such as target mass, maximum allowable payload, dimensions of the target vehicle, package layout and exterior design are listed down, as illustrated in Figure 3.3. These constraints are defined by the manufacturer to suit the business model of the target vehicle.

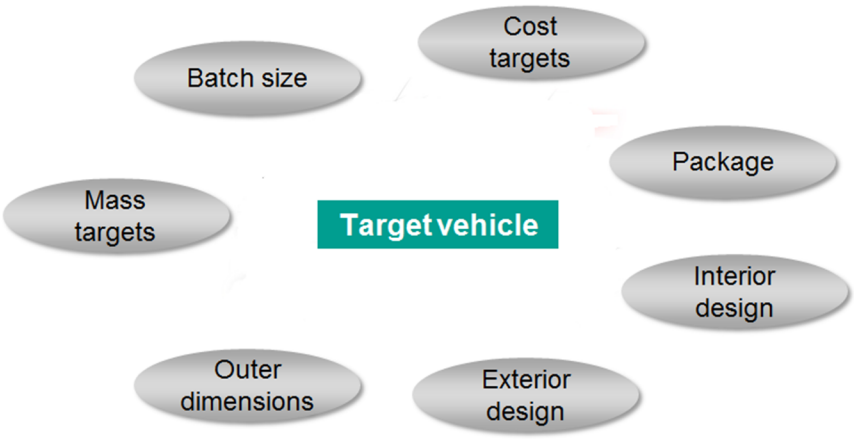

Figure 3.3: Vehicle Base Information

The second step in MOK, the *Attribute Configuration*, summarises the requirements related to the crash performance of the target car body those need to be considered during the design. These requirements are mainly defined in the form of:

- Crash scenarios to be considered during the design.
- Concrete structural performance targets to be achieved by the target car body in each of these crash scenarios.

At the start of the design, it is generally not possible to define the performance targets concretely, due to the lack of information about the geometry. The structural knowledge-base developed in this work gathers information about typical trends of the behaviour of the car body in various crash scenarios, and thereby provides a basis for definition of such performance targets in the concept design stage.

The next step in the VDI guideline 2221 is "creating a function structure", where the main function of the target product is defined and broken down into smaller sub-functions. In case of designing a crashworthy car body, creating a function structure can be viewed as dividing the global performance targets of the whole body structure into performance targets for different areas of the car body. This task is also carried out, to a certain extent, in the attribute configuration.

The third and fourth steps in the MOK approach can be compared to the third step of the VDI-guideline 2221, "creating a principle solution", i.e. developing the basic design concept. The main tasks carried out in creating a principle solution are, creating a qualitative design and choosing suitable physical effects, which would carry out the sub-functions defined in the function structure, in order to realise the main function. On similar lines, the third and fourth steps in the MOK approach create a principle solution for the target car body structure. The *Topology Configuration* develops the basic qualitative design concept of the new target car body. In this step, a wireframe topology of the target car body is created, as depicted in Figure 3.4. While creating this wireframe, the requirements, such as the overall dimensions, package components etc., listed in the vehicle base information, are taken into account.

The next step in the MOK approach, the *Deformation Configuration*, develops the physical effects for realising the performance targets set in the attribute configuration. It sets the deformation targets for individual car body components so that the overall target behaviour of the car body in a crash scenario could be achieved.

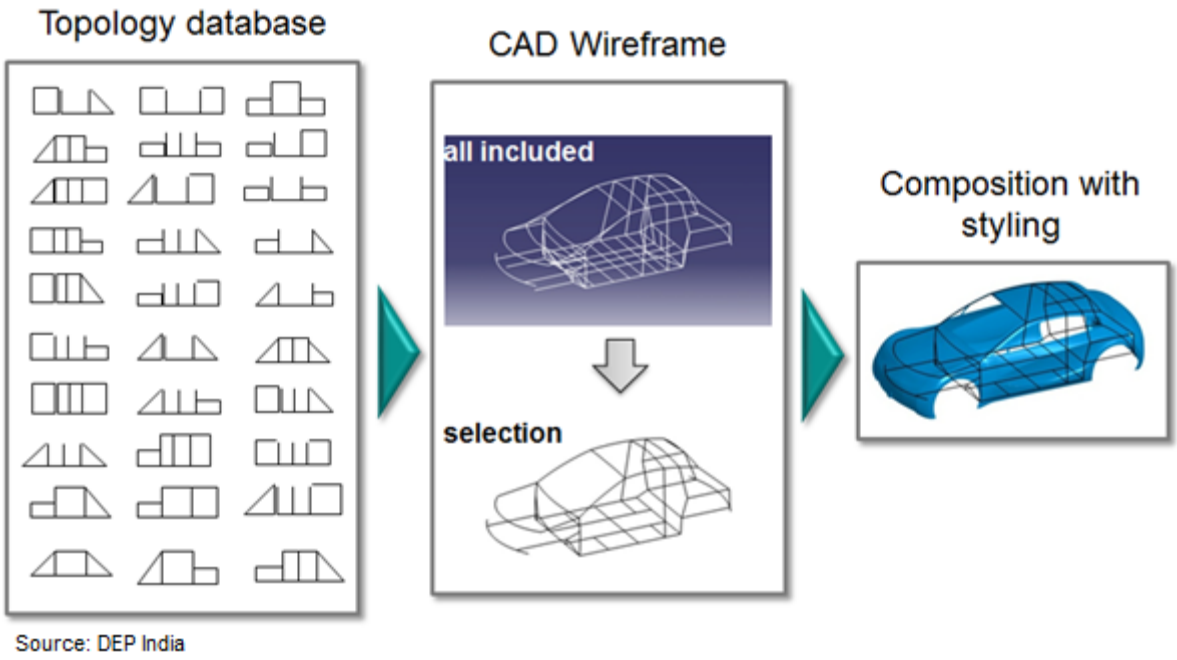

Figure 3.4: Topology Configuration [22]

Similar to the next two steps in the VDI guideline 2221, “module structures and preliminary design”, for constructing the geometry of the product, the subsequent steps conceptualised in the MOK approach also aim at designing and constructing the geometry of the target car body. The *Section Configuration* designs the sections and materials of the profile structures of the new car body, whereas the *Joint Configuration* constructs the joints connecting the profile structures. The last step in the MOK approach, *Virtual Validation*, validates the constructed structure using conventional CAE techniques. The next steps in the VDI guideline, “complete design and documentation” are included in the detailed design phase and therefore are not considered in the MOK approach.

3.2 Fields of knowledge-base in the MOK approach

The MOK approach proposes integration of knowledge-base into three fields in the car body design: geometrical, manufacturing and structural design. The basic concept of each of the knowledge-base fields is illustrated in Figure 3.5.

The task of the *geometrical knowledge-base* is to apply parametric CAD construction techniques for construction of the target profile based car body structure. The construction is initiated by defining the topology of the target car body. The profile structures and joints of the body structures are then constructed parametrically, as the design progresses.

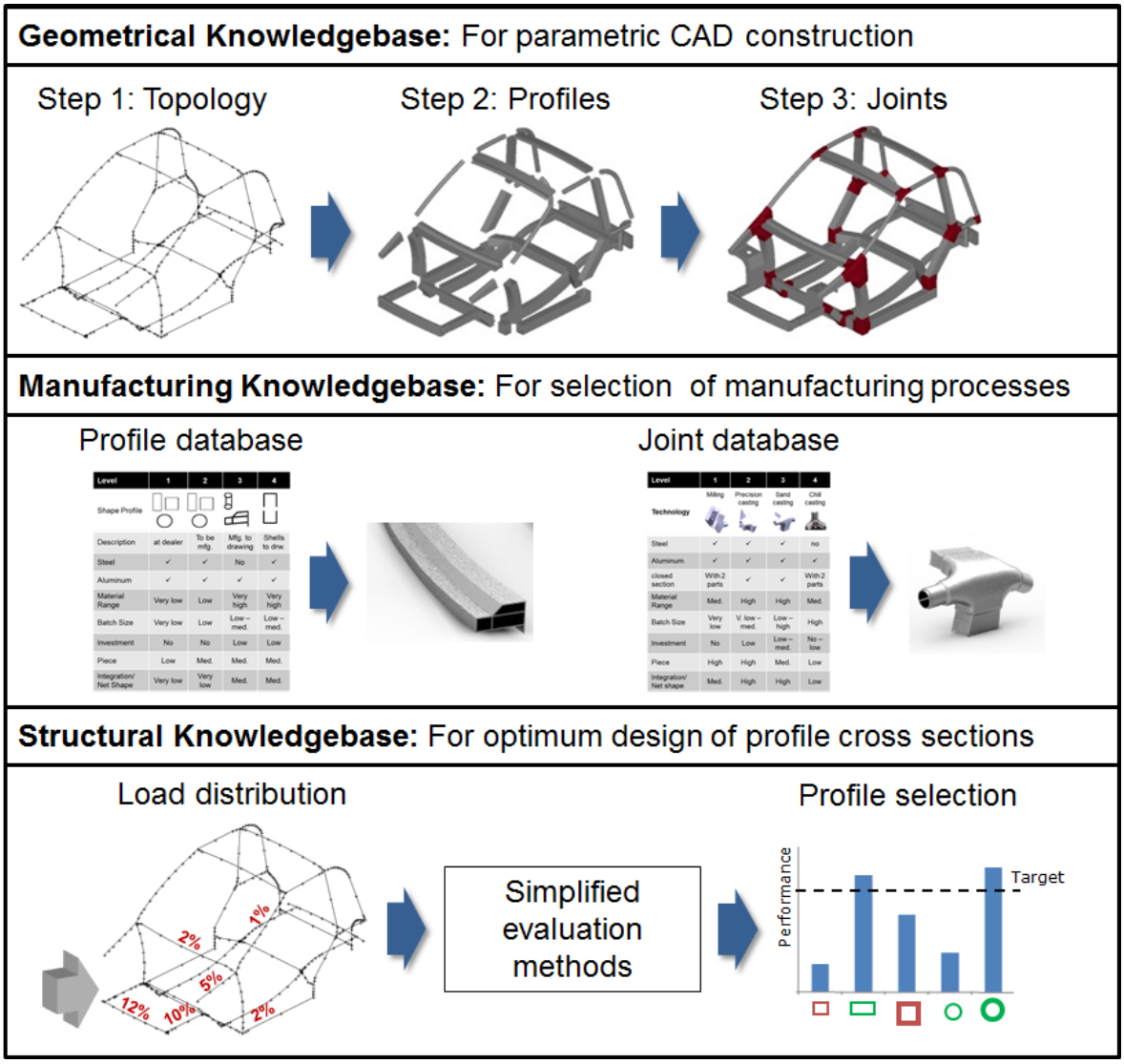

Figure 3.5: Fields of knowledge-base in the MOK approach [11]

The *manufacturing knowledge-base* is essentially conceptualised for assisting in the selection of appropriate manufacturing processes for the car body components. These processes are selected based on the vehicle batch size and the materials of the components, keeping the overall targets for the initial investments and production costs in mind. The manufacturing concepts for the FlexBody profile structure and joints presented in Section 2.2.2, Table 2.1 and Table 2.2, demonstrate an example of integration of manufacturing knowledge-base in the FlexBody concept.

The *structural knowledge-base* targets at developing and validating simplified and time efficient methods. These methods can be used in the concept design phase for predicting the performance of the car body components, and synthesising their performance to predict the behaviour of the full car body in impact scenarios.

3.3 Focus of structural knowledge-base

This work focuses on the development of the structural knowledge-base. The aim of structural knowledge-base is to facilitate performance oriented design of a crashworthy profile based car body structure with regular cross-sections in its concept design stage. Crashworthy design of a car body is realised by designing its components to absorb sufficient amount of energy in an event of impact, so that the integrity of the passenger compartment is maintained. The structural knowledge-base aims at pre-defining the targets for the structural performance of these car body components during a crash scenario, and choosing appropriate cross-sectional geometry and materials for these components, matching the targets. In this work, information extracted from FE simulations of full vehicles and profiles with regular cross sections is extensively used for developing this knowledge-base. Due to the performance oriented design concept employed here, the optimisation time required during the detailed design phase can be considerably reduced. The development of structural knowledge-base in the MOK approach is divided into three steps namely; attribute configuration, deformation configuration and section configuration. As specified in Section 3.1, definite functions are allotted to each of the configurations.

- In the attribute configuration, the main performance targets of the target car body structure, such as global energy absorption and deformation targets for different crash scenarios, are defined. A benchmark developed using FE simulations is used as a guideline for defining these targets.
- The performance targets for individual components of the car body structure are defined in the deformation configuration. These include, definition of the desired deformation mode, deformation sequence and energy to be absorbed. The global performance targets defined in the attribute configuration and the wireframe model created in the topology configuration are taken as basis for the deformation configuration.
- In the section configuration, simplified methods are developed for the basic deformation modes relevant for the profile structures with regular cross sections, in order to predict their behaviour under crash loads. Knowing their behaviour and performance under basic loads, geometry and material, suitable for the pre-defined performance targets, can be chosen for the target car body components.

This work demonstrates the development of the structural knowledge-base using available CAE techniques and its application for design of a crashworthy profile based car body structure with regular cross sections. Generating a full-fledged database, ready for commercial use is not the aim of this work, and is left for further development.

4 Development of Structural Knowledge-base

This chapter describes the various tasks conducted in the course of this work for developing the structural knowledge-base. The description is divided into three sections corresponding to the three configurations of the MOK approach, relevant for developing the structural knowledge-base. Each section describes the objectives of each configuration and presents the tasks carried out in each configuration to develop the structural knowledge-base.

4.1 Attribute configuration

4.1.1 Objectives

Two important tasks in the concept design phase of a car body structure are, the clear definition of the design tasks and the definition of the concrete performance targets for the body structure. The attribute configuration carries out following steps for developing the knowledge-base for the profile based structures for realising the above tasks.

- All load cases which should be considered during the concept design of the target vehicle are listed in a so-called *safety model*. As the scope of this work is limited to the design of a car body considering crash loads, only these scenarios are considered during the development of the knowledge-base.
- A vehicle is exposed to different types of loads in different crash scenarios and thereby, also behaves differently in each case. The desired behaviour or the target performance of the vehicle to be designed (or the target vehicle) is defined as concretely as possible for the considered crash scenarios, using guidelines obtained from a numerical benchmark developed in the course of this work.

The concept and the process of creating a safety model for the target vehicle is described in Section 4.1.2. The process of applying the knowledge obtained from the numerical benchmark database as a guideline for defining the global performance targets for the target vehicle, is explained in Section 4.1.3

4.1.2 Safety model for a target vehicle

A safety model lists and gives a detailed description of all the crash scenarios that should be considered during the design of a crashworthy target vehicle. A large number of crash regulations are available, which can be considered for the design and assessment of

crashworthiness of a vehicle. These regulations are set by different agencies, both governmental and non-governmental, all over the world. In Europe, mainly following regulations are considered important: ECE [50], FMVSS [51] and EuroNCAP [52]. It is the task of the vehicle program management to decide which regulations should be considered while designing a particular vehicle in a particular design phase. This decision depends on number of factors such as:

- Phase of the design (concept phase or detailed design phase)
- Class and type of the target vehicle
- Target market segment and vehicle batch size
- Intended usage of the vehicle
- Legal safety requirements
- Internal (Manufacturer's) safety policies
- Capacity and competence available
- Time and finances available

Figure 4.1 gives an overview of the legal regulations in Europe and the USA generally considered during design of a vehicle.

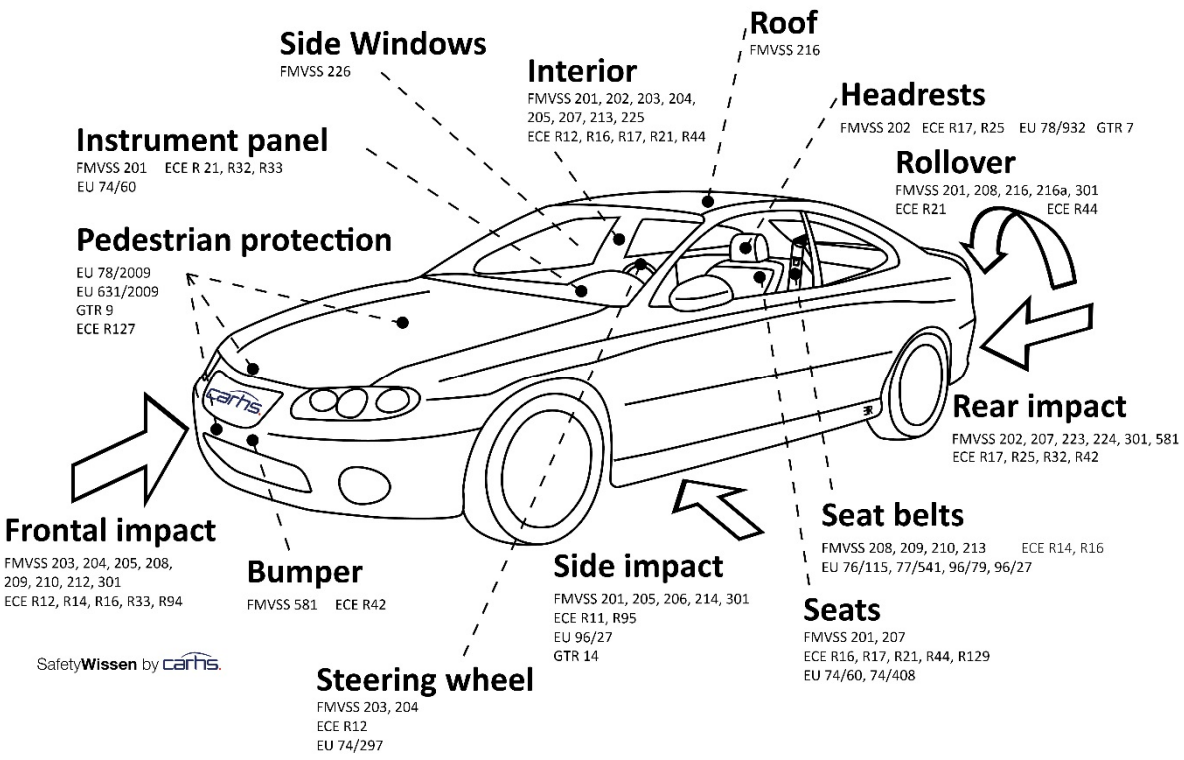

Figure 4.1: Regulations in Europe and USA [53]

4.1.2.1 Selecting appropriate crash scenarios for safety model

The market segment aimed for by the vehicle under consideration and its planned batch size per year are decisive factors for choosing the crash scenarios for validation of the vehicle. The European Union directive 2007/46/EC [54] about "establishing a framework for the approval of motor vehicles and their trailers, and of systems, components and separate technical units intended for such vehicles" provides guidelines for type-approval of vehicles, including small series, considering their safety requirements. According to this directive, a vehicle batch size is called small series, if a maximum of 1000 vehicles are produced per year. For small series vehicles the legal requirements are less in number as well as in terms of strictness. For the small series scenarios no destructive tests apart from ECE-R12 [55] (behaviour of steering system during front crash) were mandatory until the end of year 2012 [54]. New amendments to the European Union directive 2007/46/EC require certain small series vehicles to be tested for frontal crash according to ECE-R94, side crash according to ECE-R95 and pedestrian protection according to EC 78/2009, in addition to ECE-R12 [56]. The safety model for the target vehicle should include all regulations that are made mandatory considering the planned vehicle batch size. Additionally, future modifications in the laws should also be considered while developing the safety model, whenever applicable.

For small series vehicles certain tests are made mandatory by law for individual subsystems [54]. These tests are not very useful for the concept design of a car body structure and therefore can be ignored while creating the safety model. Certain other regulations, such as ECE-R26 [50] (protruding outer edges), are relevant while planning the layout (exterior, topology etc.) of the target vehicle and do not directly affect the crashworthiness of the vehicle. Such regulations should not be included in the safety model.

Apart from the vehicle batch size, the type of vehicle also plays an important role in defining the homologation for the target vehicle. For example, different considerations should be made while designing an electric vehicle as compared to those made for the design of a conventional vehicle. There are certain directives, such as ECE-R100 [50] and FMVSS 305 [57], specifically directed towards the design of electric vehicles. Such regulations should be included in the safety model for the target vehicle.

The intended usage of the target vehicle, additionally, should also be considered while developing the safety model. For example, vehicles used for car-sharing purpose as a mode of public transport will have different safety requirements as compared to small series vehicles used as sports cars. Although there are no special regulations set for car-sharing vehicles, it is

advisable to design the vehicle for the crash scenarios described for the mass production vehicles.

The crash regulations defined in other countries such as FMVSS-directives developed by the National Highway Traffic Safety Administration (NHTSA) in the USA [51] include some crash scenarios which are not included in ECE regulations. FMVSS 208 [58], a high speed frontal crash with rigid wall, is one such example. Such regulations should be given appropriate consideration while setting up the safety model for the target vehicle.

4.1.2.2 Concept of level system

As explained in Section 4.1.2.1, depending on various commercial and economic factors the crash scenarios to be considered while designing a target vehicle are strategically selected. Some of these scenarios, which are of key importance for the initial design, can be considered during the concept design phase. As the design progresses additional crash scenarios may also be considered. For example, the regulations ECE-R94 and EuroNCAP regulation for frontal crash with offset deformable barrier are almost similar. The only difference between these regulations is the higher vehicle speed used while testing according to the EuroNCAP regulation. Thus, for the concept design phase of a small series vehicle, only ECE-R94 regulation can be considered. When the vehicle development advances to the detailed design phase, the EuroNCAP regulation can be considered, if essential and if possible.

In order to facilitate the classification of the chosen crash scenarios for the target vehicle depending on the design phase and resources available, a level system is conceptualised in the MOK approach. All the regulations relevant for the target vehicle are assigned one of the three levels: 0, 1 or 2. Here:

- 0: Mandatory crash scenarios (legally required)
- 1: Recommended scenarios
- 2: Reference or best-in-class scenarios

Depending on the facts specified earlier, such as design phase, costs, vehicle class etc., a suitable level is chosen and is considered while designing the crashworthy target car body. For example, when a design engineer chooses a safety level 0 for the target vehicle, all the crash tests that are made compulsory for that particular vehicle class will be considered while designing its car body. On the other hand, if level 2 is chosen, all crash scenarios with level 0, 1 and 2 will be considered during the design. All the crash scenarios listed under the chosen level constitute the safety model for the target vehicle for that particular design phase.

This initial task in the attribute configuration, choosing a safety level, should be carried out carefully as it affects many parameters related to the design. Some of the important parameters affected are listed below.

- Complexity of design
- Risk involved during impacts
- Costs of design
- Designing time
- Weight of the car body structure

With increasing safety level from 0 to 2, the complexity of design, cost of design, time required for design and weight of the car body structure increase, while the level of risk involved during impacts decreases.

4.1.3 Development of benchmark database

4.1.3.1 Purpose of benchmark

A crashworthy vehicle undergoes a controlled amount of deformation and absorbs impact energy during an event of crash. The vehicle behaves differently in different crash scenarios. The difference lies in the manner of deformation, the amount of energy absorbed, the car body components undergoing deformation and the motion of the vehicle after the impact. There are no guidelines available for determining the targets for the global performance for a new vehicle, such as energy to be absorbed, in the event of a crash at the start of design. These targets are generally defined using previous experience by the design engineer. For the small series manufacturers, who generally lack such resources, it is difficult to define these performance targets and set the initial inputs, important for the design.

In this work a benchmark is developed by conducting numerical crash simulations of benchmark vehicles. The results of these simulations are used for acquiring the basic knowledge about the behaviour of a car body structure in different impact scenarios. Thereby, the knowledge obtained is used for demonstrating the process of defining the global performance targets for the target profile based car body structure. This numerical benchmark provides basic information about:

- Typical behaviour of a vehicle in different crash scenarios
- Typical deformation behaviour of car body components
- Distribution of deformation energy in different subsystems of the vehicle

4.1.3.2 Benchmark vehicles

The National Crash Analysis Center (NCAC) at The George Washington University's Virginia Campus, USA provides an archive of validated finite element models of full vehicles [59]. At NCAC, these models are validated for certain selected crash scenarios by using the results of actual tests. These FE models are developed in LS-Dyna nonlinear FE program, and are made freely available.

In order to develop the benchmark for this work, two vehicles, namely the Chrysler Neon (1996) of the Chrysler Corporation, and the Ford Taurus (2001) of the Ford Motor Company, USA, are taken from the NCAC website. The Chrysler Neon is a compact passenger vehicle, whereas the Ford Taurus is a mid-sized passenger vehicle. Although old and constructed using the self-supporting body structure, these benchmark vehicle models provide the basic idea about the performance of vehicles in different crash scenarios. In this work, these models are solely used for demonstrating the process of deducting the global performance targets for the target vehicle. While applying this approach for vehicle design commercially, a benchmark with more recent vehicle models, especially those constructed as profile based structures, should be developed.

In the following text, the vehicle models Chrysler Neon and Ford Taurus are respectively termed as benchmark vehicle 1 and 2 (BV1 and BV2). These FE models are simulated using the LS-Dyna code, from LSTC, for different crash scenarios. The vehicles are analysed for the following scenarios:

- Frontal crash with rigid wall at 0° (FMVSS 208)
- Frontal crash with rigid wall at 30° (FMVSS 208)
- Frontal crash with offset deformable barrier (ECE-R94)
- Frontal crash with rigid pole
- Side crash with rigid pole (EuroNCAP)
- Side crash with moving deformable barrier (ECE-R95)
- Rear crash with moving rigid impactor (ECE-R34)

Table 4.1 gives an overview of the test conditions prescribed in the crash regulations for the respective scenarios listed above.

Table 4.1: Description of crash scenarios analysed for benchmark database

Crash test	Regulation	Barrier			Velocity of travel [km/h]	Angle of travel w.r.t. position of barrier
		Type	Overlap [%]	Dimensions [mm]		
Frontal crash	FMVSS 208	Rigid	100	-	32 – 56	0°
	FMVSS 208	Rigid	100	-	32 – 56	30°
	ECE-R94	Deformable	40	1000 x 450 x 650	56	0°
	Pole-front	Rigid	-	φ 250	30	0°
Pole crash	EuroNCAP	Rigid	-	φ 250	29	90°
Side crash	ECE-R95	Deformable	-	1500 x 500	50	90°
Rear crash	ECE-R34	Rigid	100	2500 x 800	35 – 38	0°

Mostly, the passenger vehicles have a weight in the range of 700 – 2100 kg [59], [60]. As this work takes a small passenger vehicle as a basis for validating the MOK approach, the two passenger vehicles, mentioned above, are chosen for setting the benchmark. Table 4.2 outlines the essential information about the FE models of these benchmark vehicles.

Table 4.2: Description of FE models of benchmark vehicles

Description	**BMV 1**	**BMV 2**
Interior Components	No	Yes
Number of Parts	336	778
Weight [kg]	1317	1665
Total Number of Elements	270768	1057113
Number of Nodes	283859	936258
Number of Shells	267786	805505
Number of Solids	2852	99486
Number of Beams	122	4

4.1.3.3 Results of numerical analysis of benchmark vehicles

The numerical analysis carried out on the two benchmark vehicles revealed some typical trends in the behaviour of vehicles in crash events. These trends can be followed while defining performance targets for the target vehicle. Typically, useful observations are made for the following:

- Energy of deformation during a crash event
- Energy absorbed by car body structure and other vehicle systems
- Trends in force displacement curves

Following paragraphs explain the observed trends and their use in defining the design targets.

Energy of deformation

During a crash event, a vehicle moving with high velocity is brought to rest in very short period of time. This sudden reduction in the velocity has an adverse effect on the passengers in the vehicle and can result in death of the passengers. As explained in Section 2.3.1, the car body structure plays an important role in keeping the passengers safe in the event of a crash. This is achieved by controlled deformation of the car body structure, and thereby absorbing much of the impact energy generated by sudden reduction in the velocity.

If it is assumed that the vehicle comes to a stand-still after impact, the total kinetic energy of the vehicle before impact should be completely absorbed by the body structure and other vehicle systems. However, in reality, often the vehicle has certain amount of velocity, generally a mixture of translational and rotational velocity, even after the impact. This motion after the impact can be attributed to the elasticity of the materials used for construction of the vehicle and the direction as well as type of the impact. Thereby, some part of the initial kinetic energy is absorbed by the vehicle as deformation energy and the remaining part is dissipated by the motion after impact. This energy dissipation can be represented by simple energy conservation equations for the crash scenarios. A general equation for the energy conservation in case of an impact between two vehicles, illustrated schematically in Figure 4.2, can be written as Eq. 4.1 [1].

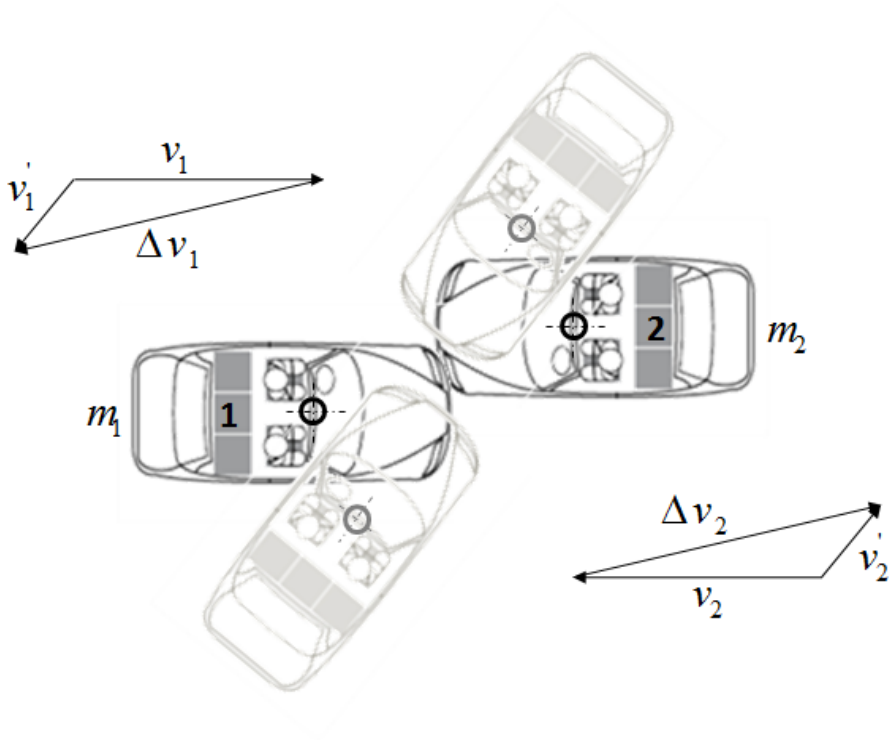

Figure 4.2: Kinematics of a crash impact between two vehicles [1]

$$\underbrace{\frac{1}{2}m_1v_1^2+\frac{1}{2}m_2v_2^2}_{\text{Initial Kinetic Energy (KE)}}=\underbrace{\frac{1}{2}m_1v'^2_1+\frac{1}{2}m_2v'^2_2}_{\text{Translational KE after Impact}}+\underbrace{\frac{1}{2}J_1\dot{\Psi}_1^2+\frac{1}{2}J_2\dot{\Psi}_2^2}_{\text{Rotational KE after Impact}}+\underbrace{E_{Def,1}+E_{Def,2}}_{\text{Energy of Deformation}} \quad \textit{Eq. 4.1 [1]}$$

Where,

m_1	:	Mass of vehicle 1
v_1	:	Velocity of vehicle 1 before impact
m_2	:	Mass of vehicle 2
v_2	:	Velocity of vehicle 2 before impact
v'_1	:	Velocity of vehicle 1 after impact
v'_2	:	Velocity of vehicle 2 after impact
Δv_1	:	Change in velocity of vehicle 1 ($v'_1 - v_1$) during impact

Δv_2 : Change in velocity of vehicle 2 ($v'_2 - v_2$) during impact

J_1 : Moment of inertia of vehicle 1

J_2 : Moment of inertia of vehicle 2

$\dot{\Psi}_1$: Angular velocity of vehicle 1 after impact

$\dot{\Psi}_2$: Angular velocity of vehicle 2 after impact

$E_{Def,1}$: Energy of deformation of vehicle 1 by plastic deformation during impact

$E_{Def,2}$: Energy of deformation of vehicle 2 by plastic deformation during impact

As seen from the above equation, the initial kinetic energy of both vehicles is converted into energy of deformation, energy of translational and rotational motion after the impact. Depending on the elements involved in the impact scenario, certain components of the above Eq. 4.1 may equal to zero. For example, Figure 4.3 and Eq. 4.2 represent the conservation of energy in case of a frontal crash with an offset deformable barrier (ECE-R 94).

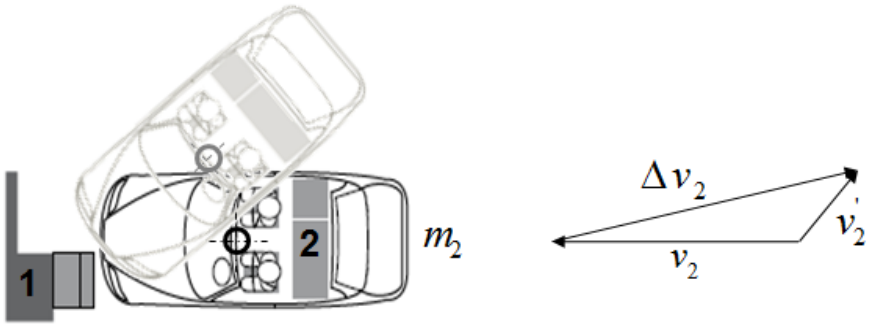

Figure 4.3: Kinematics of crash scenario according to ECE-R94

$$\frac{1}{2}m_2v_2^2 = \frac{1}{2}m_2v'^2_2 + \frac{1}{2}J_2\dot{\Psi}_2^2 + E_{Def,1} + E_{Def,2} \qquad \textit{Eq. 4.2}$$

Since the deformable barrier 1 in Figure 4.3 is stationary, it does not have any initial kinetic energy. Therefore, the first term on the left-hand side in Eq. 4.1 is zero. Similarly, after the impact, the barrier deforms but does not have any motion, thus both translational and rotational energies of the barrier after impact, the first and the third term on the right-hand side in Eq. 4.1, are also equal to zero.

The amount of impact energy absorbed by the vehicle varies depending on the crash scenario. It is observed from the FE simulations performed on the benchmark vehicles that the percentage of energy absorbed by the vehicles in a particular crash scenario by plastic

deformation remains approximately same. For example, the amount of energy absorbed by the benchmark vehicle 1 in case of the FMVSS 208 crash scenario is 88%, while that absorbed by the benchmark vehicle 2 is 86%. Figure 4.4 illustrates the division of initial kinetic energy into the energy of deformation and the energy of motion after impact for both the benchmark vehicles in various crash scenarios. In the bar diagrams presented in Figure 4.4, the y-axis shows the energy in percentage. Here, the total length of the bar, i.e. 100% of the energy, equals the initial kinetic energy. The different regions of the bars represent the division of this initial kinetic energy into the energy of deformation and the energy of motion after the impact, with their respective percentages. Different crash scenarios are presented on the x-axis. Legend for these crash scenarios is given in the Table 4.3.

Table 4.3: Legend for Figure 4.4, Figure 4.5, Figure 4.7, Figure 4.8 and Figure 4.9

Legend	Description
FCRW 0	**F**rontal **C**rash with **R**igid **W**all at **0**° (FMVSS208)
FCRW 30	**F**rontal **C**rash with **R**igid **W**all at **30**° (FMVSS208)
FCODB	**F**rontal **C**rash with **O**ffset **D**eformable **B**arrier (ECE-R94)
FCRP	**F**rontal **C**rash with **R**igid **P**ole
SCRP	**S**ide **C**rash with **R**igid **P**ole (EuroNCAP)
SCMDB	**S**ide **C**rash with **M**oving **D**eformable **B**arrier (ECE-R95)
RCMRI	**R**ear **C**rash with **M**oving **R**igid **I**mpactor (ECE-R34)

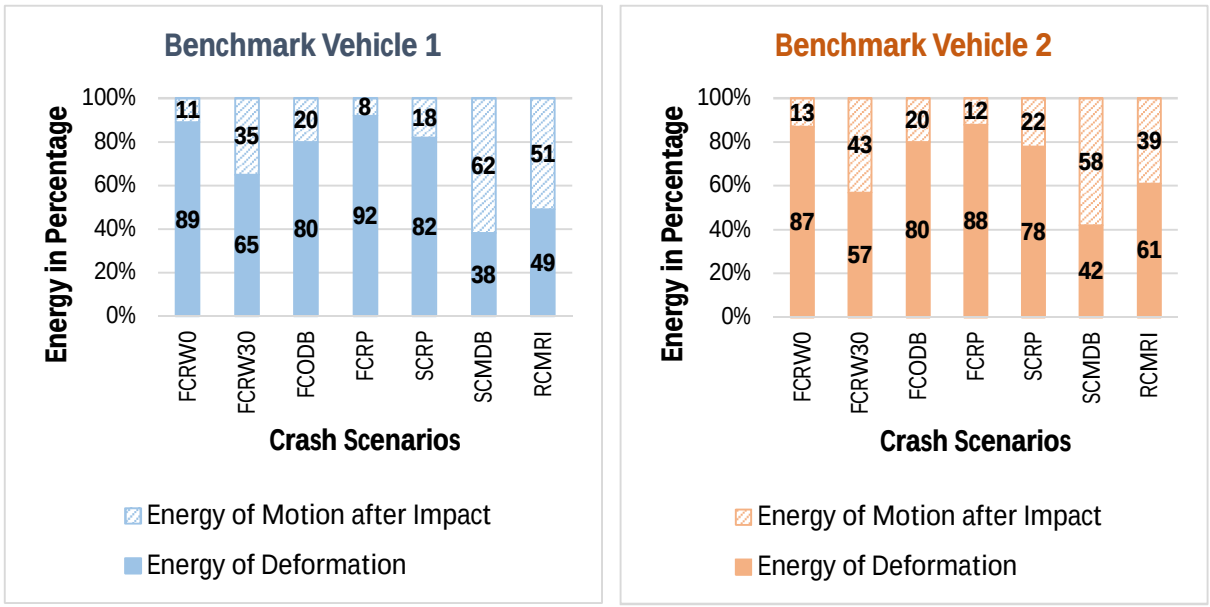

Figure 4.4: Percentage of deformation energy for benchmark vehicles in different crash scenarios

Using the above data, a general range of percentage of energy of deformation can be fixed for the target vehicle for each crash scenario. An example is shown in Figure 4.5 for a target vehicle constructed as a profile-based structure.

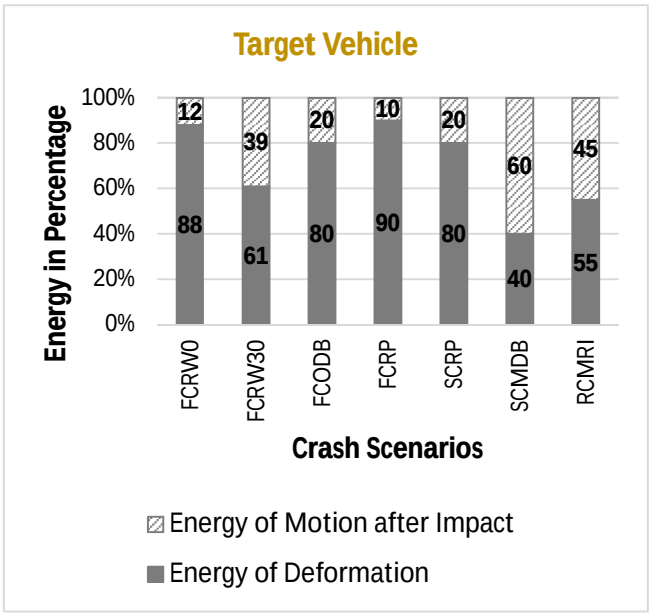

Figure 4.5: Percentage of deformation energy – example for a target vehicle comprising of a profile based body structure

These values of the percentage share of energy of deformation can be used as performance targets, according to which the profile based target car body structure is to be designed.

Energy absorbed by car body structure

Although, the energy dissipated in the vehicle during a crash scenario is mainly absorbed by the car body structure, various other vehicle systems, such as the outer skin, the chassis (suspensions, brakes, tires etc.), the inner body panels and the deformable barrier, if involved, also contribute in absorption of the energy. Figure 4.6 illustrates an example of the energy distribution during a frontal crash with offset deformable barrier (ECE-R94), observed from numerical simulations performed during this work for the benchmark vehicle 1. Since this benchmark vehicle is constructed as a self-supporting structure, the outer skin components and the inner body panels included in "other systems" in Figure 4.6, also have a considerable contribution in absorbing the energy. As mentioned before, the benchmark developed in this work, is used only for demonstrating and developing the basics of the MOK approach. Therefore, use of self-supporting structures as benchmark for the design of profile based structures focused in this work can be justified within the boundary of this work.

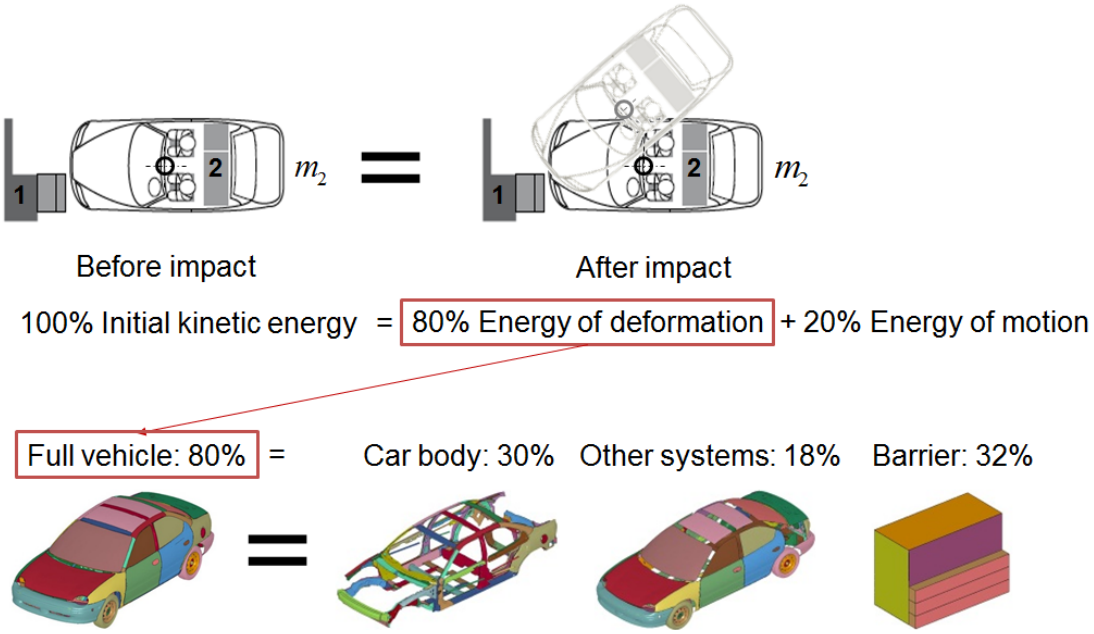

Figure 4.6: Distribution of energy of deformation in different systems of a benchmark vehicle (Example: ECE-R94)

For designing a car body structure, it is useful to know the typical trends of the distribution of the deformation energy in various vehicle systems. It is also helpful to know exactly how much energy should be absorbed by the body structure and how much should be absorbed by the rest of the systems. The benchmark vehicles simulated in the course of this work are analysed so as to find the energy absorbed by the car body, various vehicle systems and the deformable barrier, if involved, during different crash scenarios listed in Table 4.1. Figure 4.7 shows the energy

distribution in the benchmark vehicles. The energies of deformation, labelled as E_{Def} in Figure 4.7, and incurred by different systems involved in the impacts, are expressed as percentage of the total initial kinetic energy before the impact. The total length of the bars in Figure 4.7, equivalent to 100% energy, represents the total initial kinetic energy before the impact.

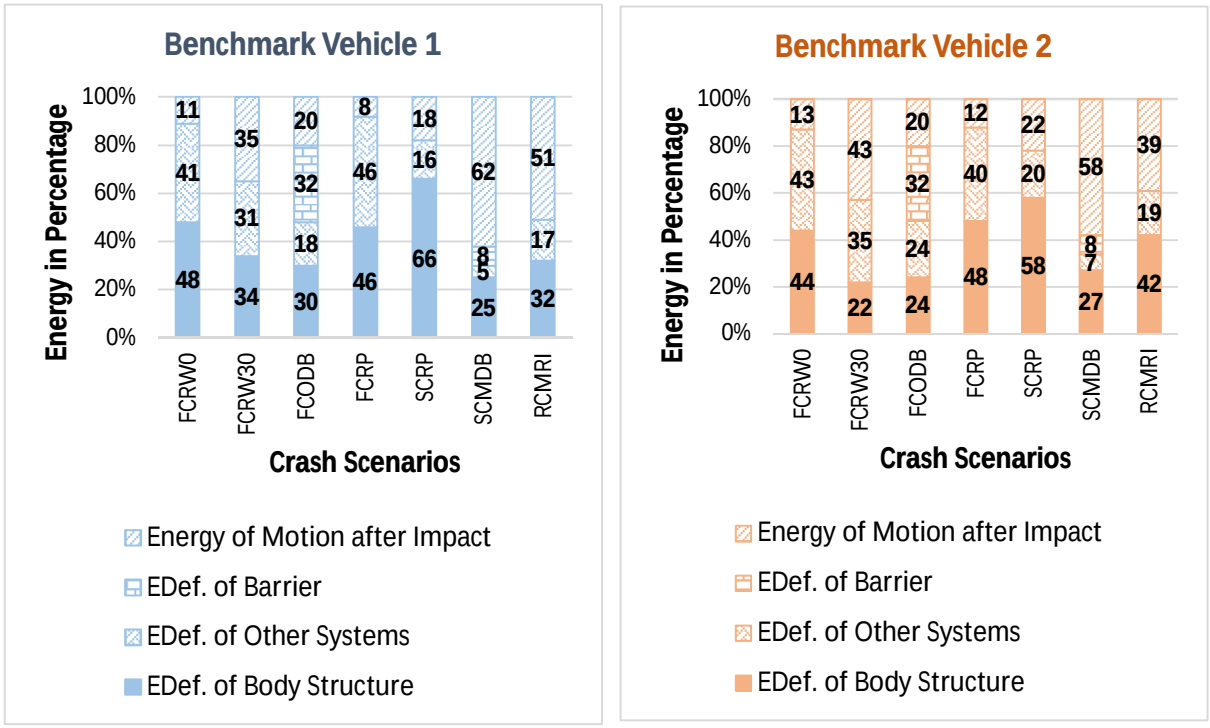

Figure 4.7: Percentage distribution of deformation energy in different systems of benchmark vehicles in various crash scenarios

Using the above data, a percentage distribution of deformation energy in different systems can be fixed for the target vehicle for each crash scenario. An example is shown in Figure 4.8 for a target passenger car.

On the basis of these benchmark data, energy absorption targets can be defined for the car body structure of the target vehicle and can be used as a basis for further design of the car body structure. Distribution of the energy in a vehicle differs with the type of the car body structure, for example, self-supporting structure or space frame structure. Therefore, while defining these targets, the type of the target car body should also be considered. Therefore, the energy absorption targets for the car body structure of the target vehicle are kept higher compared to those for other vehicle systems. Therefore, a percentage distribution of deformation energy in different systems can be fixed for the target vehicle for each crash scenario is modified as shown in Figure 4.9 for a target passenger car.

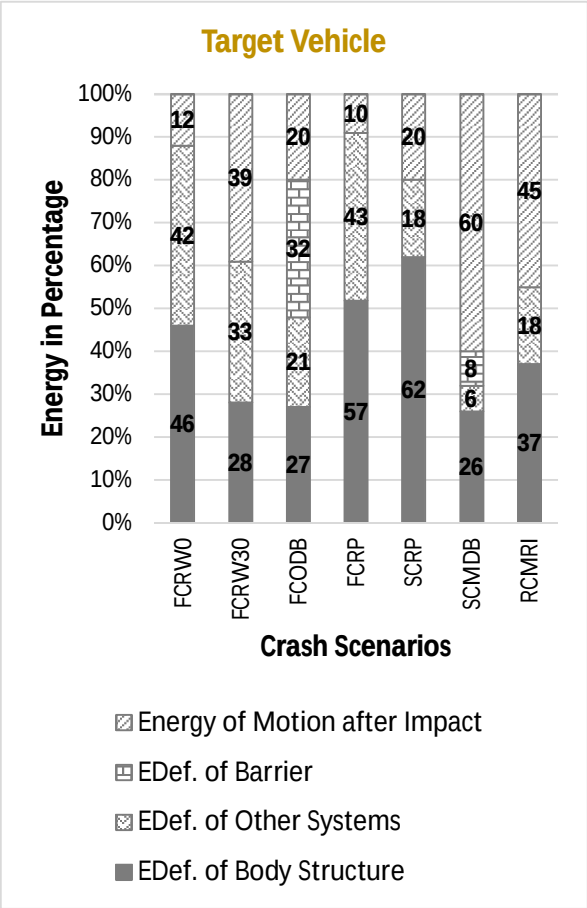

Figure 4.8: Percentage distribution of deformation energy in vehicle systems – example-1 for a target vehicle comprising of a profile based body structure

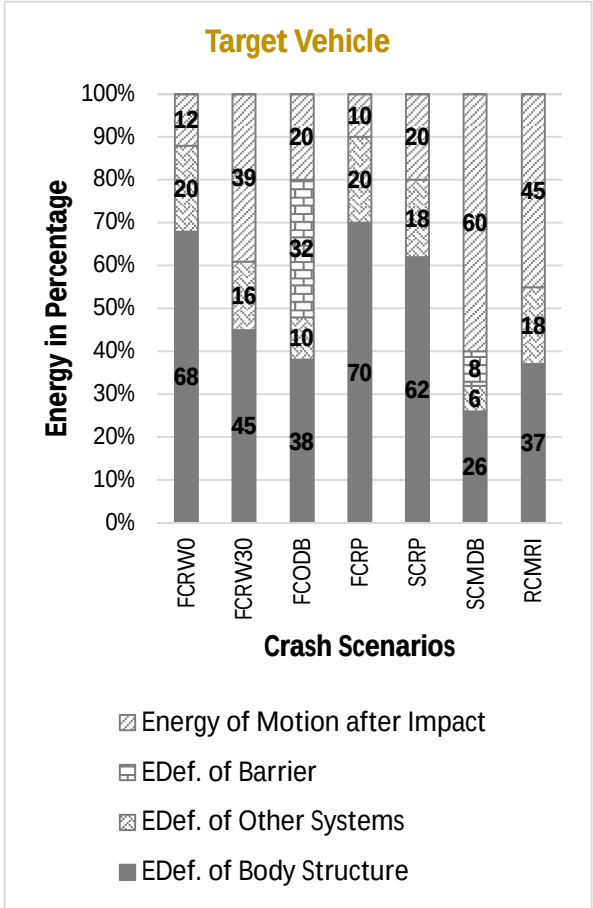

Figure 4.9: Percentage distribution of deformation energy in vehicle systems – example-2 for a target vehicle comprising of a profile based body structure

Trends of force displacement curves

Most of the vehicles behave in a similar manner regarding the force deformation behaviour in a particular crash scenario. Although, the actual values of force acting on the vehicle and the deformation incurred are different for different vehicles, typical trends can be found in their force deformation curves. Similar trends can be followed while setting the target force deformation curve for a target vehicle. Figure 4.10 illustrates force – time curves for the two benchmark vehicles in the event of a frontal crash with rigid wall (FMVSS 208). Deformation is a function of time, therefore a force – deformation curve will have a similar trend.

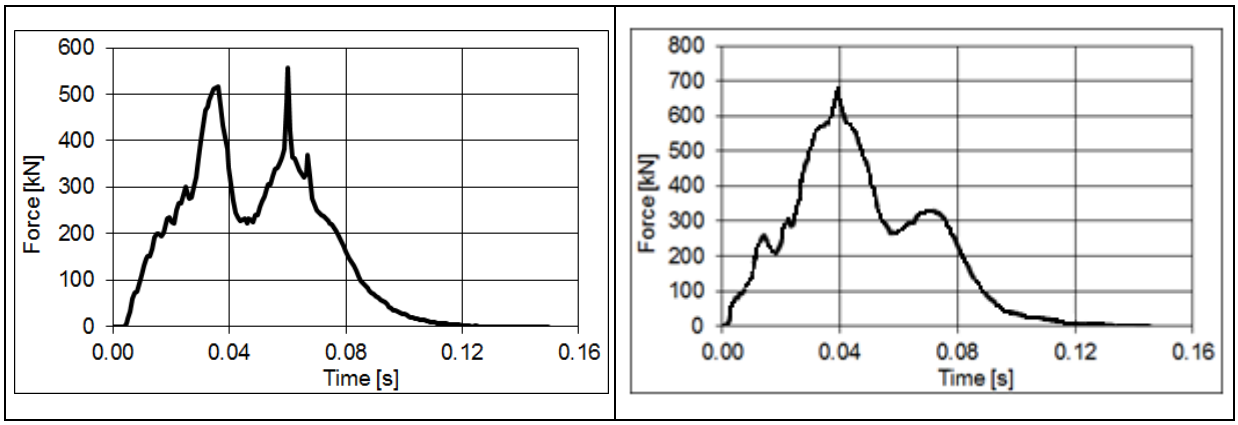

Figure 4.10: Trends of force – time curve for benchmark vehicles in FMVSS208 scenario

4.2 Deformation Configuration

4.2.1 Objectives

The deformation configuration is conceptualised to define the performance targets for the profile structures of the target profile based car body structure in a particular crash scenario. These targets are defined in accordance with the global targets determined for the target car body in the attribute configuration, as described in Section 4.1. The deformation configuration has following objectives:

- Identifying the car body profile structures active in a particular crash scenario.
- Defining the desired deformation modes for the active profile structures and defining their sequence of deformation. Additionally, the desired amount of deformation should also be predicted for each profile structure considering its deformation mode.
- Defining the targets of energy absorption for the profile structures.

The tasks carried out in the deformation configuration are partly based on the benchmark developed in the attribute configuration. However, the knowledge of crash kinematics and the understanding of behaviour of the car body components in different crash scenarios is required on the part of the design engineer for realising these tasks.

Different steps carried out in the deformation configuration are summarised in Section 4.2.2.

4.2.2 Steps in deformation configuration

4.2.2.1 Identification of active components

In real world, a car body structure can be subjected to a crash impact in different directions. These real-world impacts have been converted to definite crash tests by legislative bodies and

customer rating agencies. The safety model described in Section 4.1.2 and prepared in the attribute configurator lists the crash scenarios to be considered while designing the target car body structure.

In each of these crash scenarios only certain regions of the car body are supposed to deform and absorb energy, and thereby maintain the integrity of the passenger compartment and the rest of the car body structure. For example, in a frontal impact only the front structure of the car body should deform. The rear end of the car body structure can be practically assumed to be not loaded. Similarly, in the case of a side impact, only the side structure of the car body will absorb energy whereas the front and rear structures can be considered to be unloaded.

In the first step of the deformation configuration, the profile structures of the car body, which will be loaded, and therefore, those need to be designed as energy absorbing structures in a particular crash scenario, are identified. The profile structures that will be active in that particular crash scenario depend on the following factors:

- Direction of impact
- Overall dimensions of the car body
- Extents of deformation or crumple zones
- Positioning of the crash impactors with respect to the car body structure

Although, for different car body layouts, the active components in a crash scenario can vary, the basic knowledge about identifying these components can be obtained from the benchmark simulations carried out in the attribute configuration. This information can supplement the basic judgment of the design engineer. The energy absorbed by the car body components of the benchmark vehicles in an offset frontal impact with a deformable barrier (ECE-R94) is illustrated in Figure 4.11 and Figure 4.12, as an example. The bar diagrams give the percentage of energy absorbed by each component of the car body and the picture of the car body shows the distribution of plastic strain in the car body structure during the impact. The components that absorb a considerable amount of energy are considered as active for this particular crash scenario. These observations can be used as basis to identify the active profile structures for the target profile based car body.

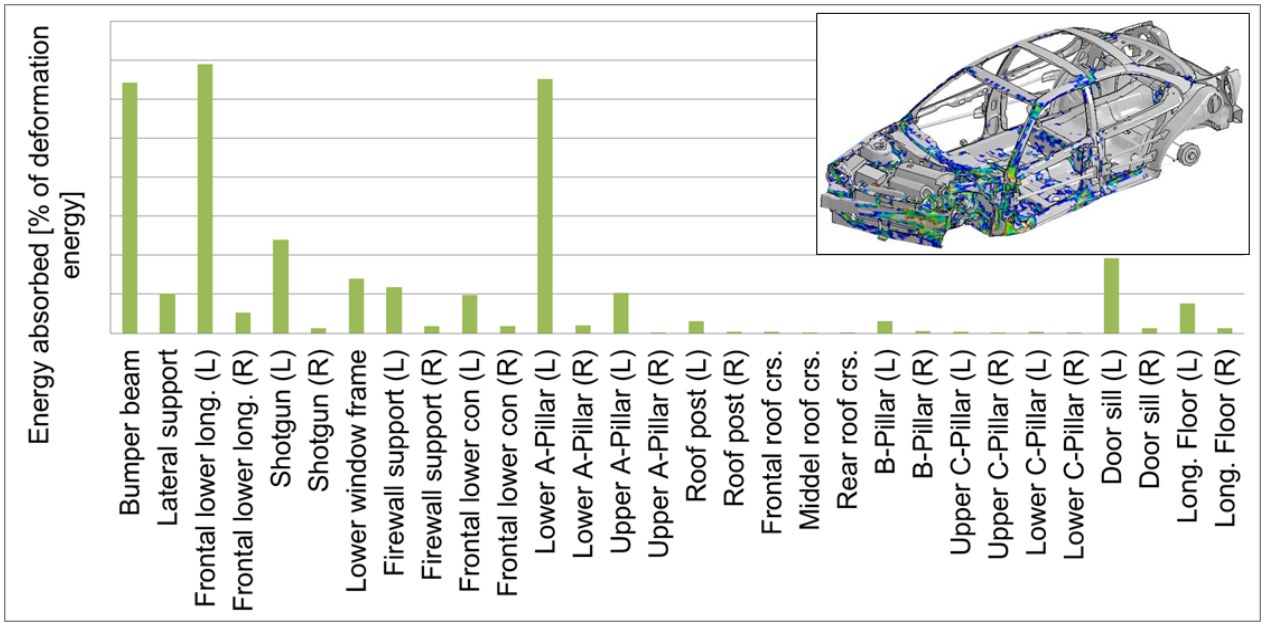

Figure 4.11: Active car body components of benchmark vehicle 1 in ECE-R94 scenario

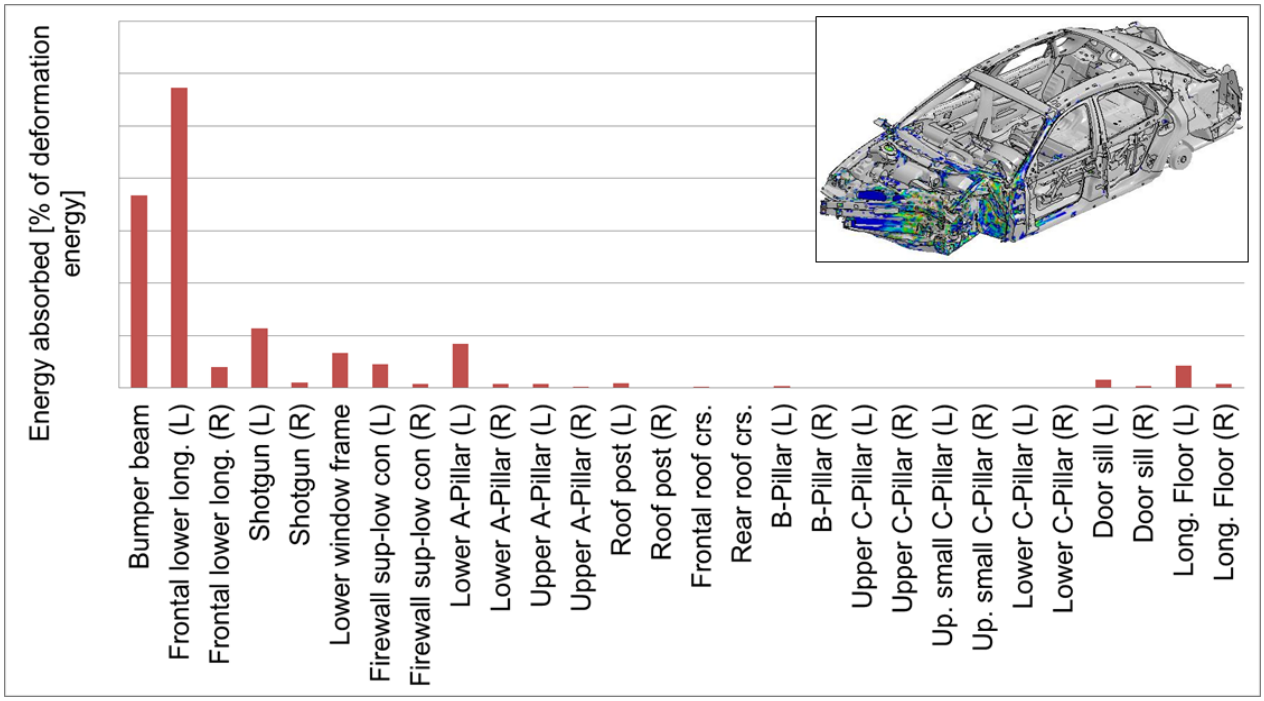

Figure 4.12: Active car body components of benchmark vehicle 2 in ECE-R94 scenario

The profile structures identified as active for a particular crash scenario are then divided into groups, representing an approximate deformation sequence of the car body in case of that particular crash scenario.

4.2.2.2 Basic modes of deformation of active components

As mentioned before, the profile based body structures consisting of regular or standard closed cross sections are focused in this work. The car body profiles that need to sustain more loads, which cannot be achieved by the standard cross sections, can later be optimised to integrate ribs. However, for the concept design phase all profiles can be assumed to possess standard closed cross sections.

As described in Section 2.4.2 and 2.4.3, two types of collapse modes are predominantly observed in the profile structures with regular cross sections: axial collapse and bending collapse. After identifying the active car body components in a particular crash scenario, next task in the deformation configurator is to assign a reasonable *preferred* deformation mode to each active profile structure or its part. Additionally, it is also advisable to define the type of deformation, in order to define whether the deformation would be elastic, elastic-plastic or plastic. Only those components that would be having a plastic deformation are required to be designed for the optimum cross section and material for that particular crash scenario. For other components, stronger cross sections and materials can be chosen, which will support the plastically deforming components. The basic deformation modes relevant for the profile structures with standard closed cross sections are:

- Regular axial folding
- Irregular axial folding
- Cantilever bending
- Three-point bending
- Crumpling due to bending

Depending on the direction of loading, the design engineer can assign one of the deformation modes listed above to each active profile structure or its part.

4.2.2.3 Defining deformations using spring model

The actual deformations of each of the active components can be determined on the basis of the total maximum possible deformation defined for the car body structure in the attribute configurator for a particular crash scenario. The initial definition of the target force – displacement curve and the deformations considered for this curve for individual groups of components can also be taken as basis. Additionally, the basic topology of the target car body, determined in the topology configurator according to the MOK approach, is required at this stage, which describes the lengths of the components and their positioning. Basic knowledge

of the package restrictions also helps in determining the deformation targets more concretely.

For determining the target deformations of the active components, a so-called *spring model* can be constructed. In this model all the active components undergoing deformation are represented by springs of definite lengths. These springs can be connected in series or parallel configuration representing the actual layout of the components. The areas of the components which would remain un-deformed due to overlaps between components or attachments to the components, can be represented by solid blocks. The lengths of the deformable and non-deformable areas can be deduced from the basic topology of the car body and the package layout.

Using the deformation sequence and the deformation modes defined earlier for each active component, the maximum possible deformations for each component can be defined. A check should be kept to guarantee that the deformations defined for the component groups in the attribute configurator are realised. According to the theory [31], [34], [61], [62], [63] a collapse efficiency of 70% – 75% can be assumed for the components deforming in the axial folding mode. The desired deformations in case of a bending collapse can generally be found from package restrictions and from the remaining length of deformation zones after determining the axial deformations.

4.2.2.4 Defining energy absorption targets

In a car body structure, the amount of energy absorbed by each of the active components differs largely depending on various factors, such as the design strategy followed, the mass of the vehicle and the construction concept used for the car body structure. Therefore, it is difficult to find a general trend in the energy absorbed by the active components. For the sake of this work, the energy absorption targets for individual components are decided depending on the global performance targets defined in the attribute configurator and the data obtained from the benchmark simulations. For each benchmark vehicle simulated, the percentage of the energy absorbed by the individual component with respect to the total energy of deformation of the vehicle is determined. An example is presented in Figure 4.11 and Figure 4.12. This percentage data can then be modified for the target car body depending on the global target set for the deformation energy in the attribute configurator. Additionally, the judgment of the design engineer regarding the energy to be absorbed by the active component plays an important role in this step. It is up to the design engineer to decide the relevance, sensibility and suitability of the guidelines provided by the benchmark data to the target car body.

4.3 Section Configuration

4.3.1 Objectives

The purpose of the section configuration is to assist in designing optimum cross sections of regular shapes for the active profile structures of the target car body, considering the performance targets defined for them in the deformation configuration. Moreover, aim of the section configuration is to develop simplified and time efficient analysis methods, which do not require any computer modelling of the profile structures. Using these methods, the behaviour of the active profile structures with regular cross sections, deforming in the basic deformation modes, can be predicted. Thereby suitable cross sections can be chosen for the profile structures matching the pre-defined performance targets. A car body thus constructed in the concept design stage will always possess a certain level of crash performance. In order to develop the simplified analysis methods for the profile structures, following tasks are carried out in the section configuration:

- Research various analytical and/or empirical methods available for calculating the crash performance of metal profile structures with standard thin walled sections collapsing in axial and bending deformation modes. The analytical methods considered in this work are summarised in Sections 2.4.2 and 2.4.3. The statistical method, regression analysis, described in appendix Section 9.1 is used as an experimental method in this work.
- Evaluate these methods using tests and FE simulations for a defined range of standard section components, relevant for the profile based car body construction concept.
- Find a suitable simplified method for predicting the crash performance of standard sections in axial and bending collapse modes.

4.3.2 Design of Experiments for profile structures

As mentioned before, in the course of this work, different analytical and empirical methods for predicting the crash behaviour of thin walled structures are assessed. In order to judge the suitability of these methods for analysing the behaviour of standard profile structures used in the profile based car body structures, under simple loading conditions, the technique of Design of Experiments (DoE) is used. Data obtained from a number of tests and numerical simulations performed in the course of this work are used as a basis for evaluating the simplified methods. Following sections describe the process followed during this assessment and discuss the results of the physical and numerical experiments.

4.3.2.1 Definition of design space and planning the DoE

As described in Section 2.1.2.4, the profile based car body structures employ profile structures as load carrying components of the car body. Regular profile cross sections are always preferred in this type of structures. However, depending on the strength requirements, compound sections, which combine different regular cross-sectional shapes, and irregular sections can also be found in profile based structures. Additionally, vehicle batch size and the initial investments required for the manufacturing tools, also influence the types of cross sections used in the profile based car body structures. Although, different cross-sectional shapes are used in these car body structures, the overall dimensions of these profile cross sections lie in a definite spectrum.

With the aim of identifying this spectrum, a benchmark is created by measuring cross sectional dimensions of the car body components used in different profile based car body structures and self-supporting body structures [64], [65]. In order to obtain a complete overview of the car body component sections normally used in the passenger vehicles, the dimensions of the self-supporting car body components are also included in this benchmark. The dimensional spectrum or the design space, thus identified, is used for conducting the DoE for the standard profile structures.

Figure 4.13 a) and b) respectively illustrate examples of compound and irregular cross sections found in the car body structures included in this benchmark. The profile based car body structures considered here are often observed to use compound sections consisting of two or more box sections. The dimensions noted in the benchmark represent the dimensions of the individual box sections and not the total dimensions of the compound sections. In case of the irregular cross sections, the extreme dimensions of the cross sections are indicated in the benchmark.

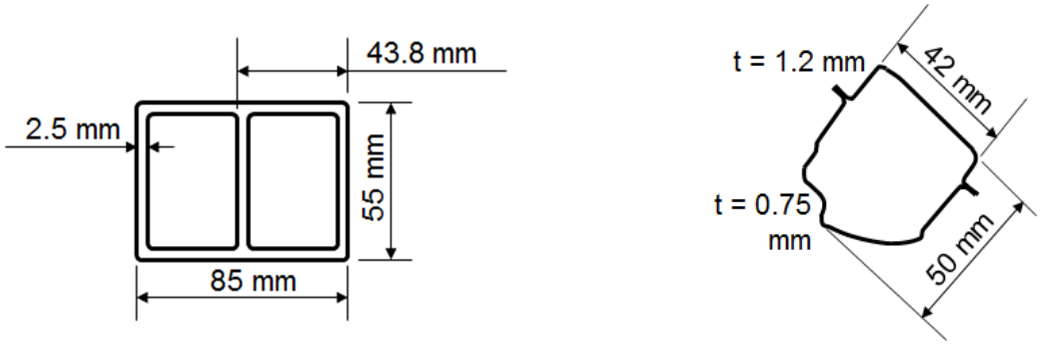

a) Compound sections b) Irregular sections

Figure 4.13: Examples of compound and irregular cross sections found in car body structures

Figure 4.14 and Figure 4.15 summarise the dimensions of the cross sections included in the benchmark. These figures also illustrate the chosen dimensional spectrum or the design space, enclosed in the dotted lines, for the DoE conducted in this work.

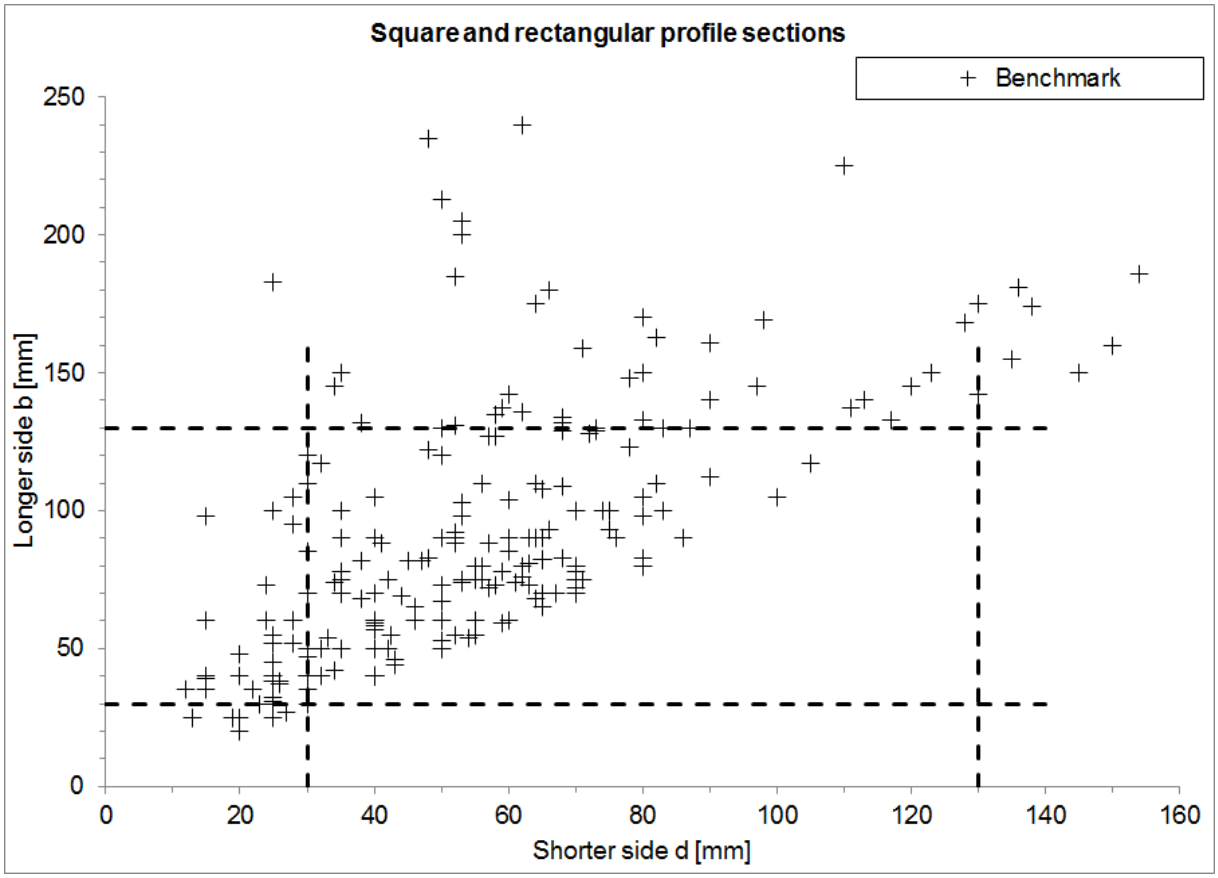

Figure 4.14: Benchmark of cross sectional dimensions and chosen design space – longer side vs. shorter side of cross-section

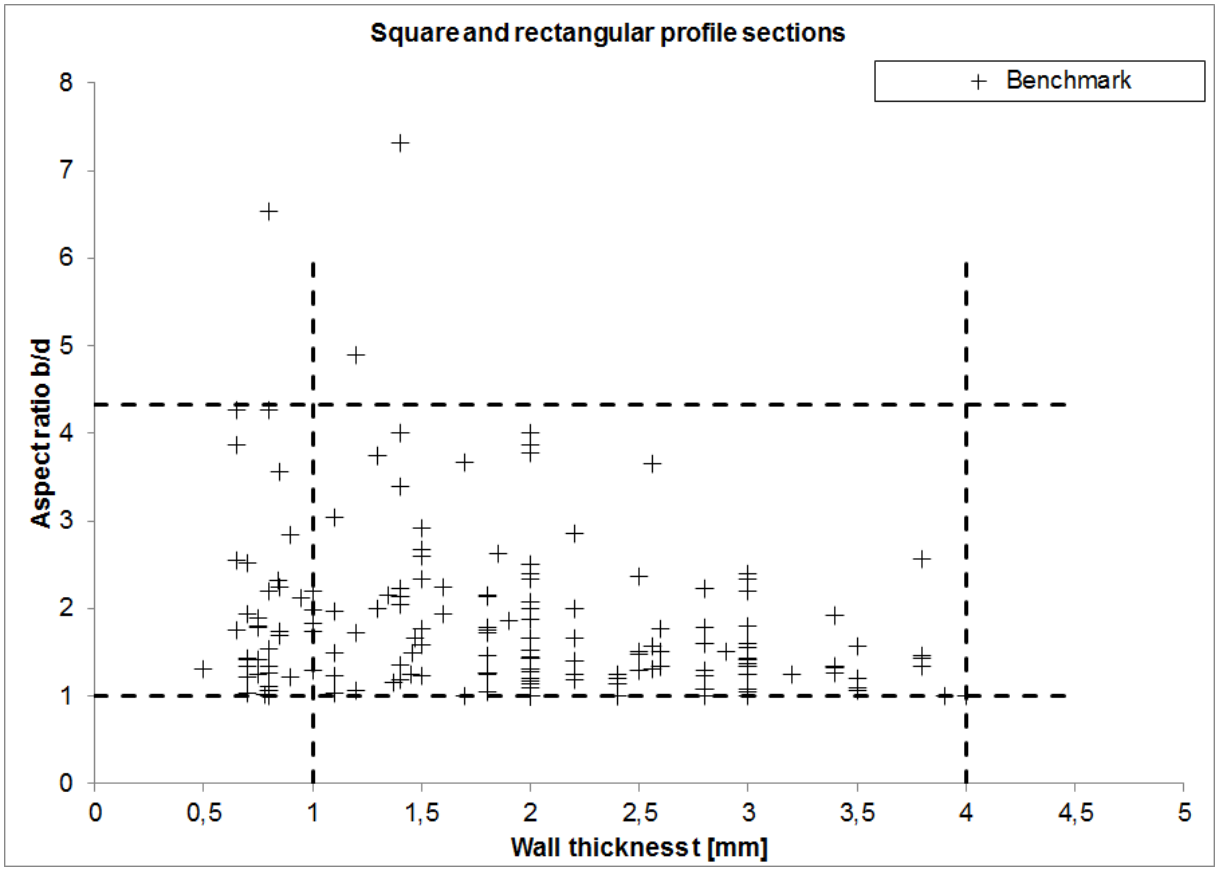

Figure 4.15: Benchmark of cross sectional dimensions and chosen design space – aspect ratio vs. wall thickness of cross-section

The theories summarised in Sections 2.4.2 and 2.4.3 give basic knowledge of the parameters that affect the behaviour of thin walled structures under axial and bending loads. Using this knowledge, following parameters are chosen as variables of DoE in this work for assessing the analytical and experimental methods:

- Cross sectional shape: square, rectangular
- Cross sectional dimensions: longer and shorter side
- Wall thickness
- Length of the profile structure
- Materials

The spectrum for cross-sectional dimensions and wall thickness of the profile structures is decided using the benchmark data illustrated in Figure 4.14 and Figure 4.15. The lengths of the structures normally used in a car body depend on the overall dimensions of the vehicle and the topology of the car body. Considering these parameters of the target ec2go FlexBody structure used for validating the structural knowledgebase developed in this work and summarised in Chapter 5 later, the spectrum for the length of the profiles is decided for this

DoE. Additionally, the profile lengths generally tested in the literature, such as [28], [31], [37], [66] etc., are also considered while defining the profile length spectrum.

The profile based car body structures generally use different construction materials, including different grades of steels and aluminium alloys. In order to assess the suitability of the simplified methods considered in this work for different materials, profile structures made of four material grades are included in the DoE design space. These include a low grade and a high grade variety each of steel and aluminium alloys. These varieties are chosen considering their application in automotive structures, their material properties and the availability of thin walled profiles made of these materials in the market in stock.

After deciding the geometrical and material spectrum for the profile structures as summarised in Table 4.4 [65], [67], individual experimental points are chosen for each parameter such that the whole spectrum is evenly covered. Market availability of the structures chosen for the tests is also considered while choosing these experimental points. Using these chosen values for the parameters and the techniques of DoE, an experimental plan is created to include various combinations of the parameter values. D-optimal plan is used in this work for creating this experimental plan. Statistical software "Visual-XSel" from the company CRGRAPH, Munich, Germany [68] is used for this purpose.

Table 4.4: Spectrum of DoE variables for physical testing and numerical simulations

Parameter	**Range**
Longer and shorter side: b and d	30 – 130 mm
Wall thickness: t	1 – 4 mm
Profile length: l	100 – 950 mm
Material	2 Steels grades (S 235, S 355) 2 Aluminium grades (AW 6060, AW 6082)

The D-optimal experimental plan created different combinations of values in the spectrum defined in Table 4.4 and created a list of around 450 experimental runs. Considering the efforts and costs required for the physical testing of all these experimental runs, method of numerical simulation is chosen for this work for executing the experiments. In order to guarantee realistic numerical results, tests are performed for some chosen experimental runs

and the numerical models are validated on their basis. The validation of the numerical models is explained in detail in Section 4.3.2.2.

Following figures, Figure 4.16 to Figure 4.19, depict the experimental points chosen for conducting the numerical simulations and the tests, overlaid on the benchmark of profile structure dimensions explained earlier in this section.

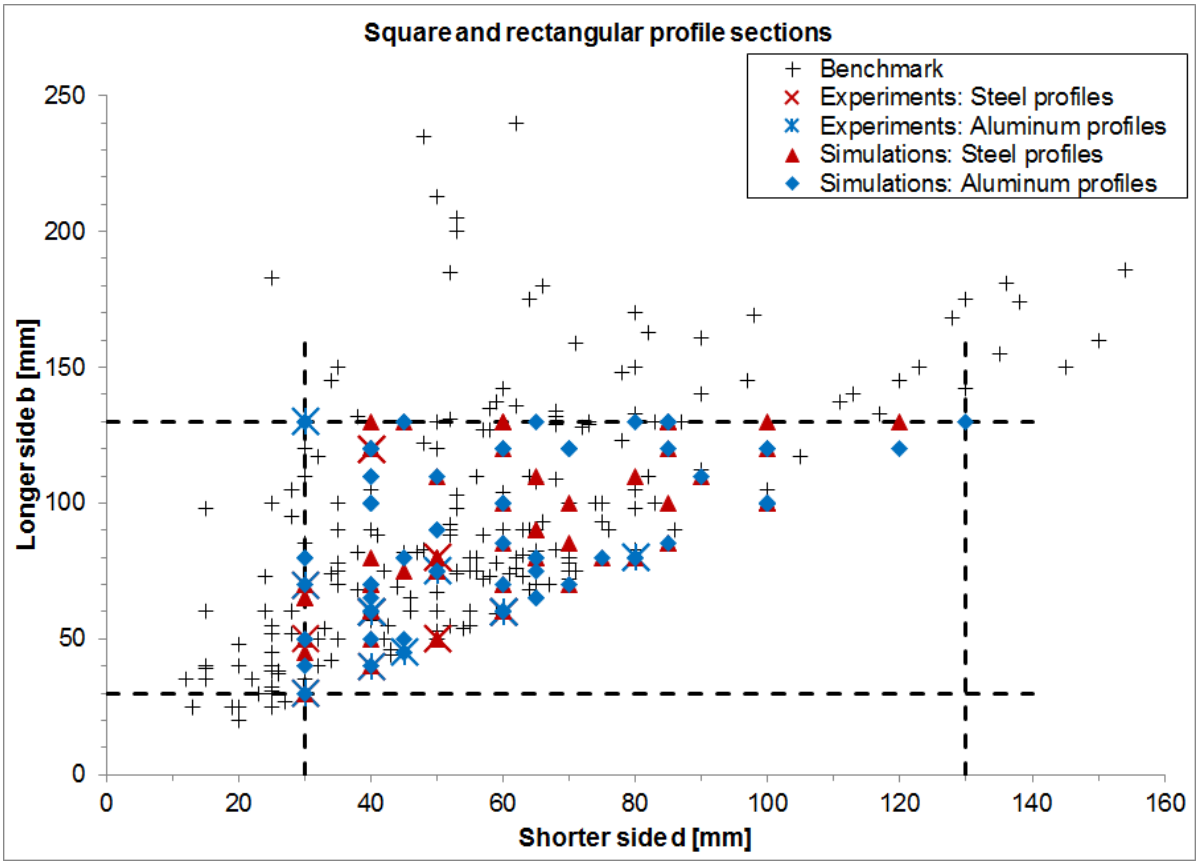

Figure 4.16: Experimental points chosen for analysis – longer side vs. shorter side of cross section

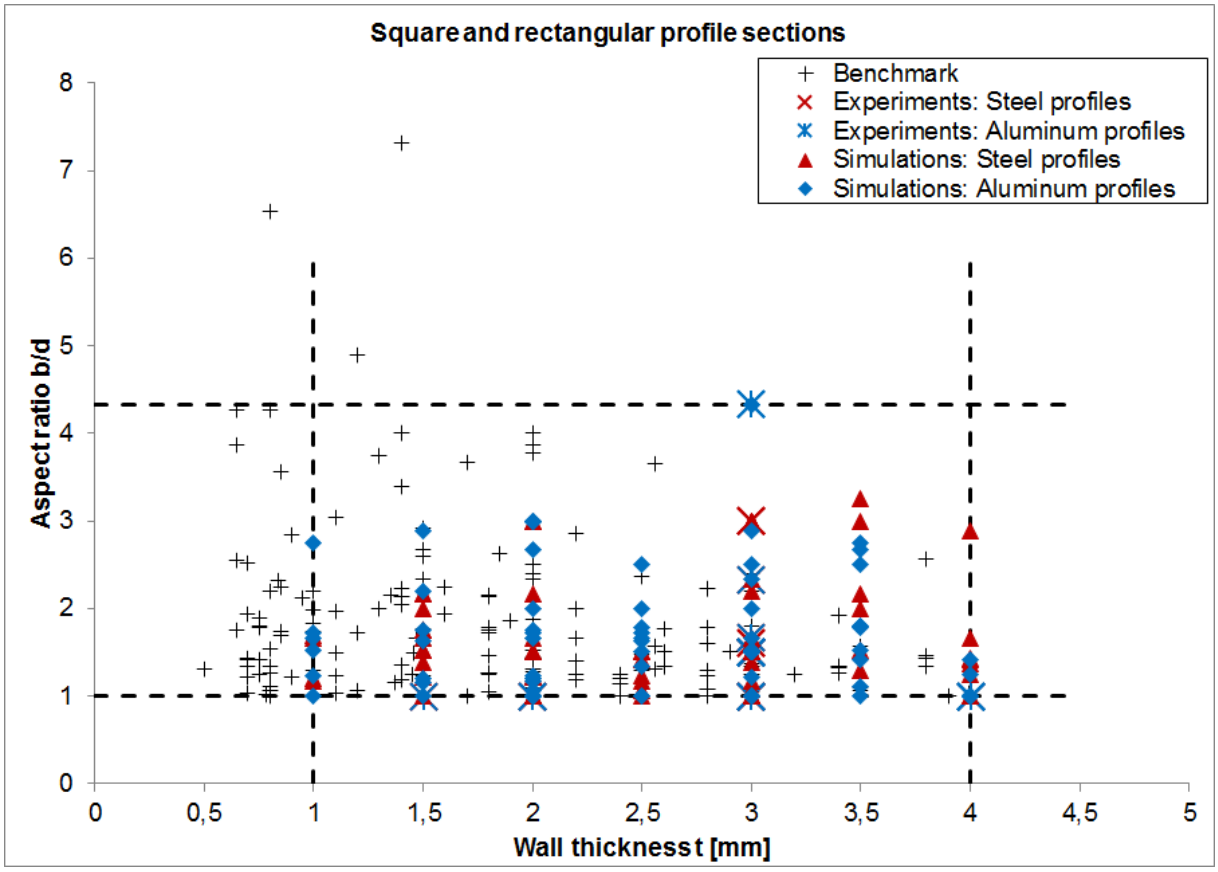

Figure 4.17: Experimental points chosen for analysis – aspect ratio vs. wall thickness of cross section

In the automotive structures, the axial folding mode is generally observed for profile structures with smaller length. Thus, for the axial loading scenario, a larger number of profile structures with shorter lengths are analysed. For bending loads, it is difficult to accommodate very short length structures in the experimental setup. Additionally, for these structures it is also difficult to get a distinct plastic hinge in the bending scenario. Therefore, a larger number of profile structures with longer lengths are analysed for the bending scenario. This difference in the chosen experimental points can be observed from Figure 4.18 and Figure 4.19.

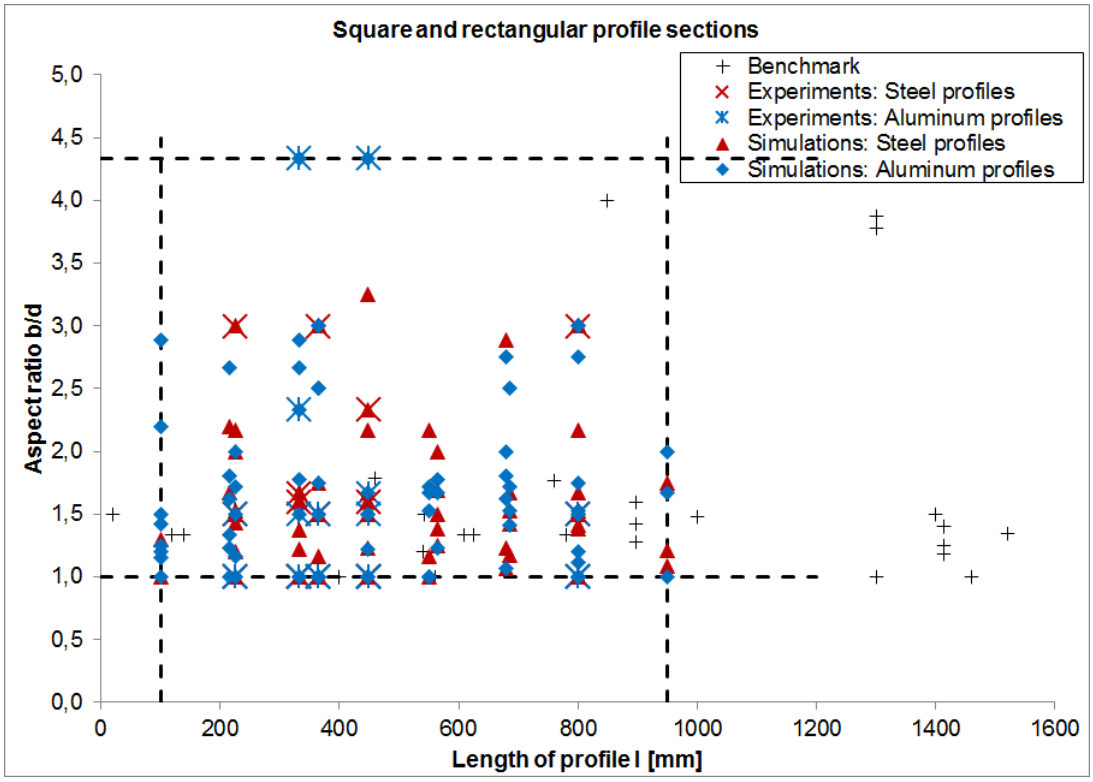

Figure 4.18: Experimental points chosen for analysis with axial load – aspect ratio vs. profile length

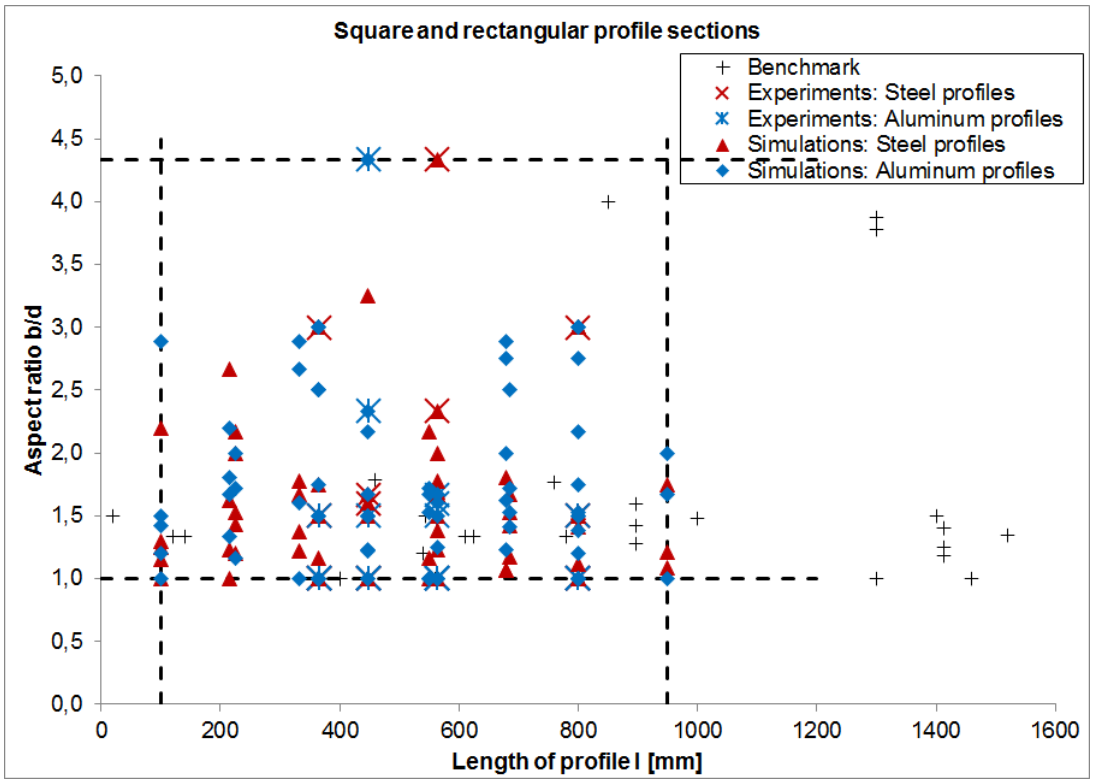

Figure 4.19: Experimental points chosen for analysis with bending load – aspect ratio vs. profile length

4.3.2.2 Validation of the numerical models using physical tests

The D-optimal plan created around 450 experimental runs by combining different values of the DoE variables listed in Table 4.4. Performing physical tests for all these experimental runs was not feasible due to the following reasons:

- All the profile cross-sections and material combinations generated in the DoE are not readily available in the market.
- In order to maintain the repeatability and account for any unseen errors during the tests, it is advisable to repeat each single test. Therefore, the number of tests to be carried out is further increased.
- Performing all the experimental runs physically would increase the material costs as well as human efforts.

Thus, the experimental runs generated through DoE are carried out using numerical simulation techniques. The numerical models are validated using the tests carried out at selected experimental points, illustrated in Figure 4.16 to Figure 4.19. These points for performing the tests are selected considering following factors:

- Profile sections readily available in the market
- Covering the chosen spectrum as evenly as possible
- Capacity of the testing facilities available
- Cost of materials and experiments

One important input required for generating realistic numerical models is the stress-strain curve of the material of the profile section. These material properties may vary from profile to profile depending on the origin of the material, the manufacturer, the manufacturing process and to some extent the geometry of the profile. Therefore, it is advisable to generate material curves from the specimen cut from the profiles that are to be tested.

For the present DoE, the material stress-strain curves are generated by performing tension tests on such specimens cut from the profile sections tested. The tension test specimen are cut in accordance with the DIN 50125 [65] guideline. The tests are carried out on the tension-compression testing machine at the Ritza Technologies client location. Figure 4.20 shows the test setup of the tension tests and an example of an aluminium specimen after the test [65].

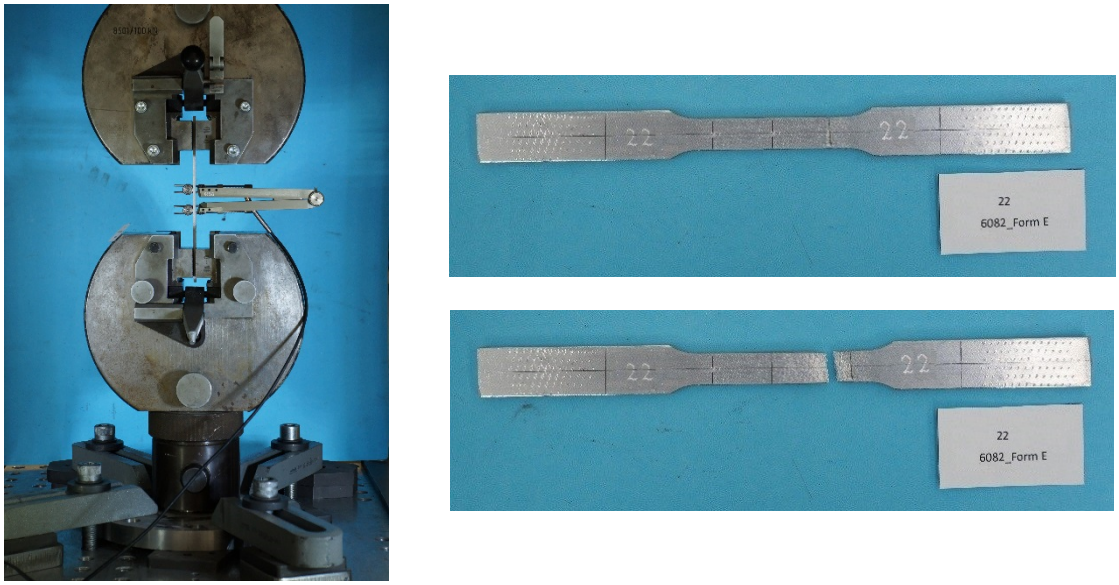

a) Test setup for tension test b) An aluminium specimen (AW 6082)

Figure 4.20: Test setup for tension test and example of a tested specimen

Figure 4.21 shows an example of the material stress-strain curves generated from the tension tests performed on a specimen cut from a square and a rectangular profile made of aluminium alloy AW 6082.

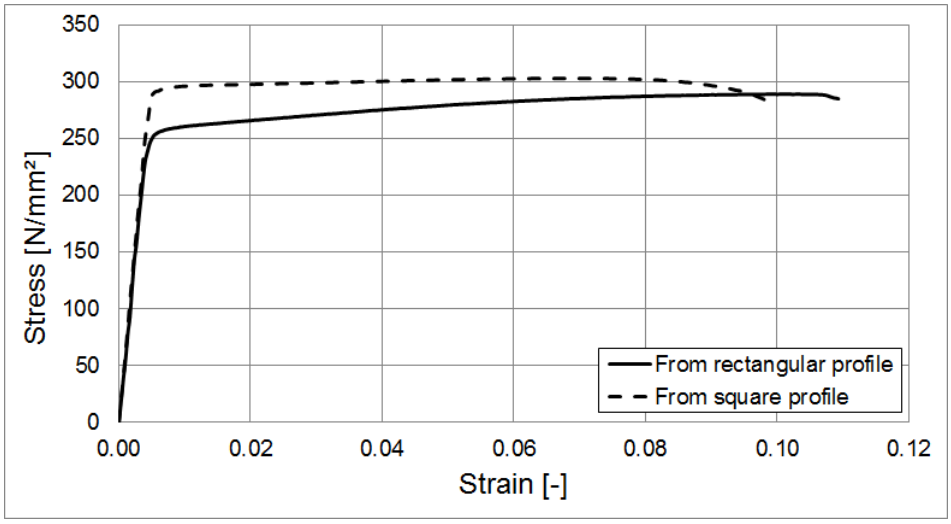

Figure 4.21: Material stress-strain curves of AW 6082 obtained from specimen cut from square and rectangular profiles

The material stress-strain curves obtained from the tension test specimen taken from square and rectangular profile sections made of same material were often observed to differ from each other. This fact can be attributed to the variation in the residual stresses in the square and rectangular profiles originating from difference in their cross-sectional geometry and manufacturing. It was observed from the comparison of test and simulation results that the

material models obtained from square profiles matched with all the experiments performed with deviations in acceptable range. Therefore, in order to maintain consistency in all the simulations, these material models are used for further numerical analysis of all profile structures.

Description of numerical model

The numerical simulations are carried out using the explicit nonlinear FE code LS-Dyna developed by LSTC. All the models are built using 2D shell elements with a size of 5 mm. This element size gave a satisfactory compromise between the accuracy of the FE results and the simulation time. The cross section of each profile is built as an ideal mid-surface. The geometrical imperfections that may exist in the actual profile sections are not considered while generating the FE models in this work. This was decided in order to avoid a more time-consuming modelling process. Also, as not all the profiles simulated are tested physically, there is no reference available for generating imperfections for these profiles. Some of the profile sections tested had rounded corners whereas some profiles had no radius at the corners. This difference was unavoidable, as the profiles were procured from different suppliers and manufactured using different manufacturing processes. In order to maintain consistency in all the numerical models, the models are built without any radius at the corners. An automatic single surface contact is defined between all the parts in the FE model.

The material data generated from the tension tests is used for the simulations. The material is described using MAT_024 [66], an elasto-plastic material. Material failure is not modelled in the material model, as these numerical results match better with the results of the physical tests. Figure 4.22 shows the force – displacement curves of an axially folding aluminium profile as an example of the comparison between the test results and the numerical results with and without considering the material failure.

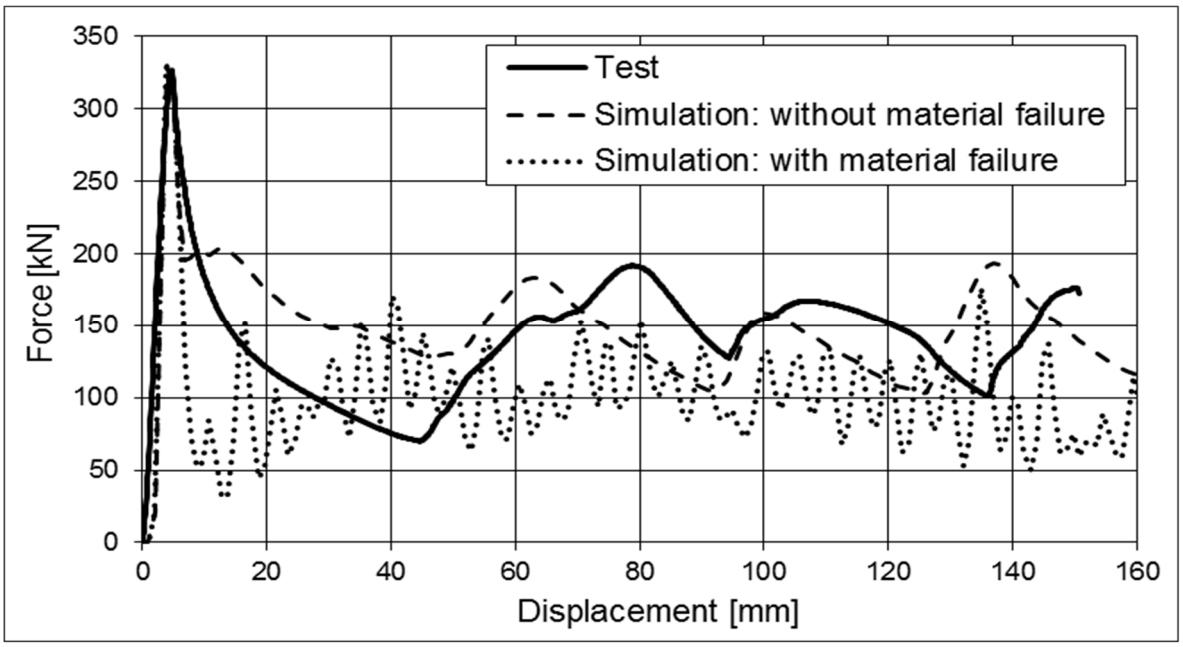

Figure 4.22: Comparison of results of physical test and simulation with and without considering material failure

Load scenarios

The tests are carried out for two load scenarios, namely axial compression and three-point bending. The numerical models are validated by comparing the results of the simulations with the tests. The comparison is made on the basis of the force – displacement curves and the deformation behaviour of the profile under consideration. The loading scenario, cantilever bending, is analysed using only numerical simulations as it requires a more complex experimental setup as compared to other scenarios.

- Axial compression:

In this load case the profile structure is compressed between two rigid plates, called as impactor and the support. The geometries of the impactor and the support are built such that the profile ends are inserted in the plates, in order to avoid the profiles from snapping out of place during the tests. All degrees of freedom (DOF) of the support are fixed, whereas one translational DOF of the impactor parallel to the longitudinal axis of the profile structure is kept free. The impactor is given a pre-defined constant velocity v_0 of 2 mm/s during the tests and 1000 mm/s in the simulations over a definite time interval, so that the profile is compressed quasi statically by 40 to 50% of its length. Figure 4.23 illustrates the experimental and numerical setup for the axial compression loading.

a) Experimental setup b) Numerical model setup

Figure 4.23: Experimental and numerical setup for axial compression

- Three-point bending (3PB):

In this load case, the profile structure is loaded in bending, perpendicular to its longitudinal axis, using a cylindrical impactor and two fixed cylindrical supports. All DOFs of the supports are fixed. The impactor has one free translational DOF in the direction perpendicular to the longitudinal axis of the profile. Impactor is given a pre-defined velocity of 2 mm/s during the tests and 1000 mm/s in the simulations over a definite time interval in order to realise quasi-static loading. The profiles are loaded until they incur a plastic hinge with a hinge angle between 40 to 50 degrees. Figure 4.24 illustrates the numerical and experimental setup for three-point bending loading scenario.

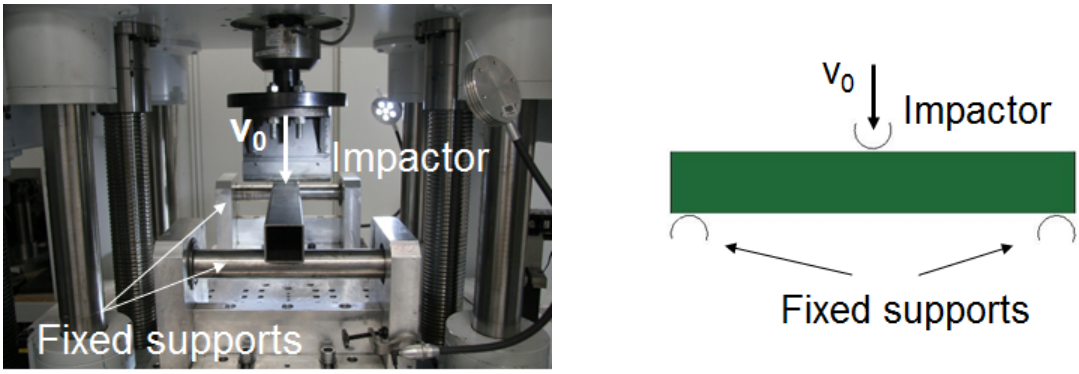

a) Experimental setup b) Numerical model setup

Figure 4.24: Experimental and numerical setup for three-point bending

Figure 4.25 and Figure 4.26 illustrate some examples of the comparison between the physical tests and the numerical simulations for profile structures made of each of the four materials. The examples are presented for axial compression and three-point bending loading.

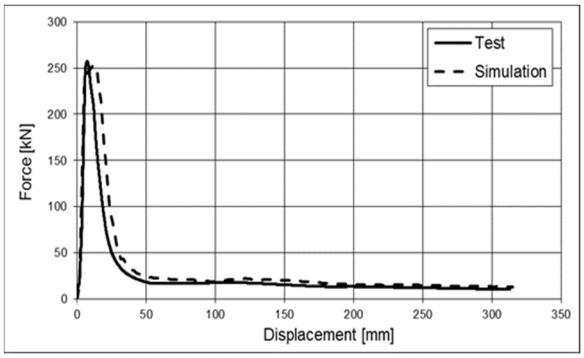

a) Square profile 60x60x3mm, 800mm long, made of S 235

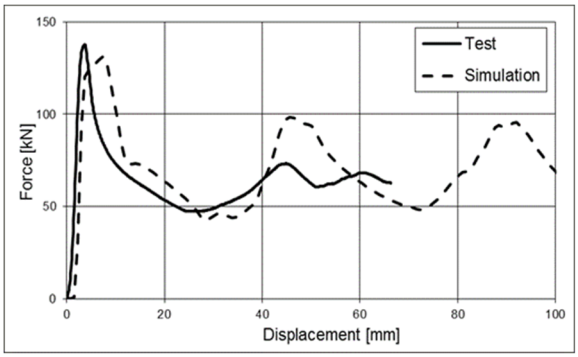

b) Square profile 60x60x3mm, 225mm long, made of AW 6060

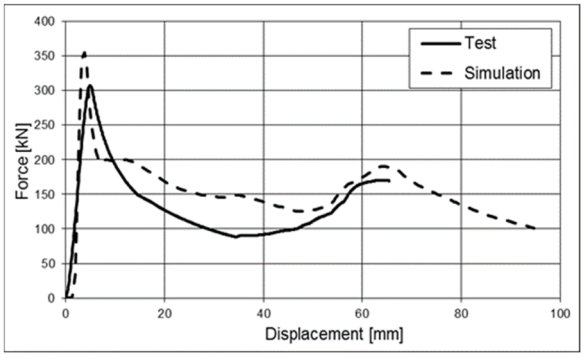

c) Rectangular profile 120x40x3mm, 225mm long, made of S 355

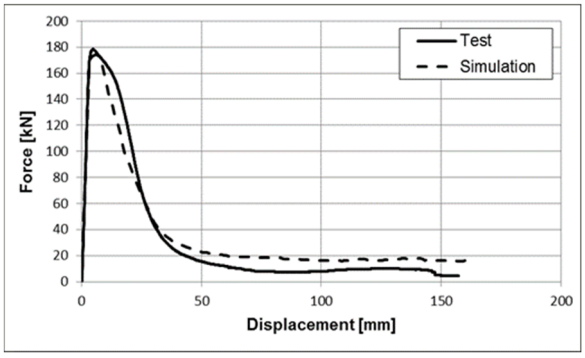

d) Square profile 40x40x4mm, 332mm long, made of AW 6082

Figure 4.25: Comparison between tests and numerical simulations for axial compression

The differences observed in the tests and the numerical simulations can be attributed to some unavoidable errors incurred in the tests as well as to the following assumptions made while generating the numerical models:

- The wall thickness of the profile structures is even at each point of the structure.
- The walls of the profile structures are free of any geometrical imperfections.
- The corner radii present in some profiles are neglected in the numerical models.
- The loading conditions imposed on the profile structures are assumed to act ideally. For example, in an axial loading scenario, the ends of the profile structure are assumed to be exactly parallel to the support and the impactor.
- The welded connections present in some profiles, mainly in steel profiles, are neglected.
- Material properties are constant in the whole profile including the corners and the welded connections.

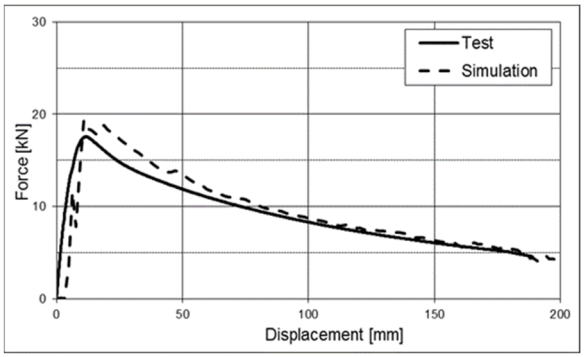

a) Rectangular profile 60x40x3mm, 800mm long, made of S 235, loaded on longer side

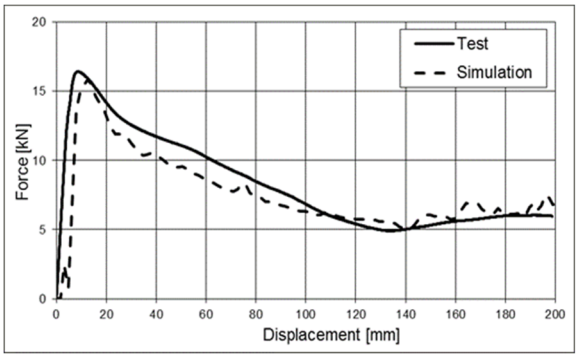

b) Square profile 60x60x3mm, 800mm long, made of AW 6060

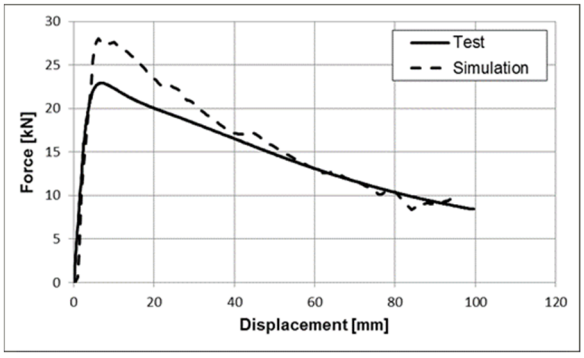

c) Rectangular profile 50x30x3mm, 448mm long, made of S 355, loaded on longer side

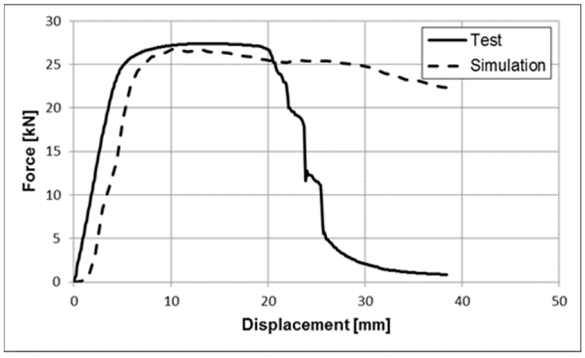

d) Square profile 40x40x4mm, 564mm long, made of AW 6082

Figure 4.26: Comparison between tests and numerical simulations for three-point bending

Building an exact model is a considerably tedious and time-consuming task. Considering the high number of experimental runs to be performed and the foreseen application of the generated data in the concept design phase, these assumptions are considered acceptable for this work. Thereby, the nominal differences observed in the simulation and test results are also considered tolerable for the current application.

4.3.2.3 Setup of the numerical models

As per the number of experimental runs involved in the DoE performed in this work, using the geometrical dimensions each structure was constructed in CREO 2.0, and the CAD models created for each experimental run were exported as '.prt' files.

The CAD models saved as '.prt' files are then meshed to create FE models using the HyperWorks 13.0 software. After meshing the FE models were exported in the '.k' file format. The final numerical model for each experimental run is prepared manually by importing the impactor and supports, and assigning the material properties and thickness to the appropriate

meshed geometrical model for each experimental run. Each of the runs is then simulated using LS-Dyna.

4.3.3 Regression analysis of numerical results

The results obtained from FE analysis of the experimental runs are used for performing regression analysis. This analysis investigates influence of the DoE variables presented in Table 4.4 on the behaviour of box profiles deforming in axial folding and cantilever bending modes. Results of this regression analysis can be used to predict the performance of box profiles loaded axially and in cantilever bending in the defined design space.

The variables of DoE, presented in Table 4.4, are chosen as independent variables for this regression analysis. The load levels F_{max} and F_2 in axial collapse and M_{max} and M_m in the cantilever bending collapse are chosen as dependent or response variables. As these load levels are the main criteria that can be used to calculate energy absorbed by the profile structures of a car body in the respective deformation modes and in deciding the sequence of deformation, they are chosen as response variables. Table 4.5 summarises the independent and response variable chosen for the regression analysis performed in this work.

Table 4.5: Independent and response variables of regression analysis

Independent variables	Response variables
Longer side of cross section b	Maximum crush load F_{max} (axial collapse)
Shorter side of cross section d	Mean crush load F_2 (axial collapse)
Wall thickness t	Maximum moment M_{max} (bending collapse)
Profile length l	Mean moment M_m (bending collapse)
Yield stress of material σ_y	
Ultimate stress of material σ_{ult}	

The regression analysis is carried out using Visual-Xsel software. Depending on the chosen design model and the transformation of the response variable, Visual-XSel fits a mathematical model, called the regression model, to the numerical results obtained for the experimental runs. The values of the quality parameters R^2, R^2_{adj}, Q^2 and p-value are also given

as output for the regression model. Design model represents the type of relationship between the independent and response variables and can be selected from one of the following models:

- Linear model
- Linear model with interactions
- Quadratic model with or without interactions
- Cubic model with or without interactions
- Fourth order model

The response variables can also be transformed. Following options are available in Visual-XSel for the transformation of the response variable Y:

- No transformation
- Y^2
- Root Y
- Ln Y
- 1/Y
- 1/Root Y
- $1/Y^2$

The quality parameters, summarised in Appendix 8.1.2, are used for choosing suitable design model and transformation of the response variables, and thereby the best fitting regression models are chosen for the response variables. Additionally, the difference between the numerical results and the values of the response variables calculated for each experimental run using the regression models is also used as a criterion for selecting the suitable regression model.

Regression models chosen for axial folding and cantilever bending modes of regular profile sections in the defined design space are presented below.

For axial folding mode:

- Maximum crush load F_{max}

$$F_{\max}=[473.514+14.679\left(\frac{b-80}{50}\right)+85.774\left(\frac{d-80}{50}\right)-7.494\left(\frac{l-525}{425}\right)+199.202\left(\frac{t-2.5}{1.5}\right)$$
$$+78.203\left(\frac{\sigma_y-291.125}{170.613}\right)+45.351\left(\frac{\sigma_{ult}-368.376}{168.534}\right)-38.522\left(\frac{b-80}{50}\right)\left(\frac{d-80}{50}\right)$$
$$+43.025\left(\frac{b-80}{50}\right)\left(\frac{t-2.5}{1.5}\right)+18.607\left(\frac{b-80}{50}\right)\left(\frac{\sigma_y-291.125}{170.613}\right)+37.647\left(\frac{d-80}{50}\right)\left(\frac{t-2.5}{1.5}\right) \quad \textit{Eq. 4.3}$$
$$+54.388\left(\frac{d-80}{50}\right)\left(\frac{\sigma_y-291.125}{170.613}\right)-41.159\left(\frac{d-80}{50}\right)\left(\frac{\sigma_{ult}-368.376}{168.534}\right)$$
$$+60.57\left(\frac{t-2.5}{1.5}\right)\left(\frac{\sigma_y-291.125}{170.613}\right)-40.753\left(\frac{t-2.5}{1.5}\right)^2-17.311\left(\frac{\sigma_y-291.125}{170.613}\right)^2]^2$$

The values of the quality parameters obtained for this regression model are presented in Table 4.6.

Table 4.6: Quality of regression model in Eq. 4.3

Parameter	Value	Quality
R^2	0.983	Good
R^2_{adj}	0.981	Good
Q^2	0.978	Good

- Mean crush load F_2

$$F_2 = \exp\ [10.987+0.108\left(\frac{d-80}{50}\right)-0.084\left(\frac{l-525}{425}\right)+1.161\left(\frac{t-2.5}{1.5}\right)+1.122\left(\frac{\sigma_y-291.125}{170.613}\right)$$

$$+0.141\left(\frac{d-80}{50}\right)\left(\frac{l-525}{425}\right)-0.118\left(\frac{d-80}{50}\right)\left(\frac{\sigma_y-291.125}{170.613}\right)+0.941\left(\frac{\sigma_y-291.125}{170.613}\right)^2 \qquad \textit{Eq. 4.4}$$

$$-0.712\left(\frac{\sigma_y-291.125}{170.613}\right)^3-0.198\left(\frac{d-80}{50}\right)^4-0.308\left(\frac{t-2.5}{1.5}\right)^4-0.879\left(\frac{\sigma_y-291.125}{170.613}\right)^4\ ]$$

The values of the quality parameters obtained for this regression model are summarised in Table 4.7.

Table 4.7: Quality of regression model in Eq. 4.4

Parameter	**Value**	**Quality**
R^2	0.961	Good
R^2_{adj}	0.957	Good
Q^2	0.937	Good

For bending collapse mode:

- Maximum moment M_{max}

$$M_{max} = \exp[\,15.779 + 0.852\left(\frac{b-80}{50}\right) + 0.218\left(\frac{d-80}{50}\right) + 0.007\left(\frac{l-525}{425}\right) + 0.706\left(\frac{t-2.5}{1.5}\right)$$

$$+ 0.204\left(\frac{\sigma_y - 291.125}{170.613}\right) + 0.42\left(\frac{\sigma_{ult} - 368.376}{168.534}\right) - 0.121\left(\frac{b-80}{50}\right)\left(\frac{d-80}{50}\right)$$

$$- 0.051\left(\frac{b-80}{50}\right)\left(\frac{l-525}{425}\right) + 0.071\left(\frac{b-80}{50}\right)\left(\frac{t-2.5}{1.5}\right) + 0.051\left(\frac{d-80}{50}\right)\left(\frac{l-525}{425}\right)$$

$$+ 0.109\left(\frac{d-80}{50}\right)\left(\frac{t-2.5}{1.5}\right) + 0.25\left(\frac{d-80}{50}\right)\left(\frac{\sigma_y - 291.125}{170.613}\right) - 0.175\left(\frac{d-80}{50}\right)\left(\frac{\sigma_{ult} - 368.376}{168.534}\right) \qquad \textit{Eq. 4.5}$$

$$- 0.085\left(\frac{t-2.5}{1.5}\right)\left(\frac{\sigma_y - 291.125}{170.613}\right) - 0.339\left(\frac{b-80}{50}\right)^2 + 0.028\left(\frac{l-525}{425}\right)^2 - 0.443\left(\frac{t-2.5}{1.5}\right)^2$$

$$- 0.072\left(\frac{\sigma_y - 291.125}{170.613}\right)^2 - 0.127\left(\frac{\sigma_{ult} - 368.376}{168.534}\right)^2 + 0.139\left(\frac{b-80}{50}\right)^3 + 0.127\left(\frac{d-80}{50}\right)^3$$

$$+ 0.279\left(\frac{t-2.5}{1.5}\right)^3 + 0.192\left(\frac{\sigma_y - 291.125}{170.613}\right)^3 - 0.153\left(\frac{\sigma_{ult} - 368.376}{168.534}\right)^3\,]$$

The values of the quality parameters obtained for this regression model are summarised in Table 4.8.

Table 4.8: Quality of regression model in Eq. 4.5

Parameter	Value	Quality
R^2	0.997	Good
R^2_{adj}	0.996	Good
Q^2	0.995	Good

- Mean moment M_m

$$M_m = \exp\left[15.12 + 0.902\left(\frac{b-80}{50}\right) - 0.155\left(\frac{d-80}{50}\right) + 0.077\left(\frac{l-525}{425}\right) + 1.047\left(\frac{t-2.5}{1.5}\right)\right.$$
$$- 0.683\left(\frac{\sigma_y - 291.125}{170.613}\right) + 0.973\left(\frac{\sigma_{ult} - 368.376}{168.534}\right) + 0.109\left(\frac{b-80}{50}\right)\left(\frac{d-80}{50}\right)$$
$$- 0.131\left(\frac{b-80}{50}\right)\left(\frac{l-525}{425}\right) + 0.068\left(\frac{b-80}{50}\right)\left(\frac{t-2.5}{1.5}\right) + 0.075\left(\frac{b-80}{50}\right)\left(\frac{\sigma_y - 291.125}{170.613}\right)$$
$$- 0.067\left(\frac{d-80}{50}\right)\left(\frac{\sigma_y - 291.125}{170.613}\right) + 0.085\left(\frac{l-525}{425}\right)\left(\frac{t-2.5}{1.5}\right) - 0.049\left(\frac{t-2.5}{1.5}\right)\left(\frac{\sigma_y - 291.125}{170.613}\right)$$
$$- 0.288\left(\frac{b-80}{50}\right)^2 + 0.096\left(\frac{l-525}{425}\right)^2 - 0.409\left(\frac{t-2.5}{1.5}\right)^2 - 0.35\left(\frac{\sigma_{ult} - 368.376}{168.534}\right)^2$$
$$\left. + 0.133\left(\frac{t-2.5}{1.5}\right)^3 + 0.572\left(\frac{\sigma_y - 291.125}{170.613}\right)^3 - 0.307\left(\frac{\sigma_{ult} - 368.376}{168.534}\right)^3\right] \quad \textit{Eq. 4.6}$$

The values of the quality parameters obtained for this regression model are summarised in Table 4.9.

Table 4.9: Quality of regression model in Eq. 4.6

Parameter	Value	Quality
R^2	0.991	Good
R^2_{adj}	0.989	Good
Q^2	0.986	Good

The regression models presented above for response variables describe the relationship between independent and response variables in the best possible way for the numerical results obtained in the course of this work. These models can be used for predicting the performance of the box profiles having dimensions and materials in the selected design space in axial folding and cantilever bending collapse modes.

4.3.4 Comparison of numerical results with analytical and experimental methods

This section presents the comparison of the results obtained through different analysis methods, namely numerical, analytical and experimental, for the regular profile sections for the modes of axial folding and cantilever bending. It is assumed that the numerical results obtained through the DoE represent the reality, and are, therefore, taken as the basis for the comparison.

The results compared include:

- For axial collapse: F_{max} and F_2
- For bending collapse: M_{max} and M_m

4.3.4.1 Axial collapse

The equations summarised in Section 2.4.2.2 are applied directly, without any computer programming, for calculating F_{max} and F_2 for all the experimental runs analysed in the DoE. As inputs, the cross-sectional dimensions, profile lengths and the material properties are provided corresponding to different experimental runs. The percentage differences between the numerical results and the analytical results are evaluated. All the results within the range of a ± 20% difference are considered to be acceptable for engineering applications in the concept design phase. The percentage differences are presented in Figure 4.27 - Figure 4.28 and Figure 4.30 - Figure 4.33. The figures depict the range of ± 20% and ± 10% differences using solid and dotted lines respectively. The greater the number of points lying in these ranges, more acceptable is the prediction made by the analytical or experimental methods for their application in the MOK approach. The comments following the figures also state the percentage of the experimental runs lying in the acceptable range of ± 20% when evaluated using the corresponding analytical or experimental method. The assumptions made while applying the theories are also listed below. The results calculated using regression equations are presented in Figure 4.29 and Figure 4.34 in a similar form.

Maximum crushing load F_{max}

Theory by Mahmood and Paluszny: Following assumption is made while applying this theory for calculating F_{max} and F_2.

- The values of empirical coefficients β, k_p and k_i are determined for steels as per [29]. Same values are used in the present work for analysing all the materials, since no separate values could be found for aluminium.

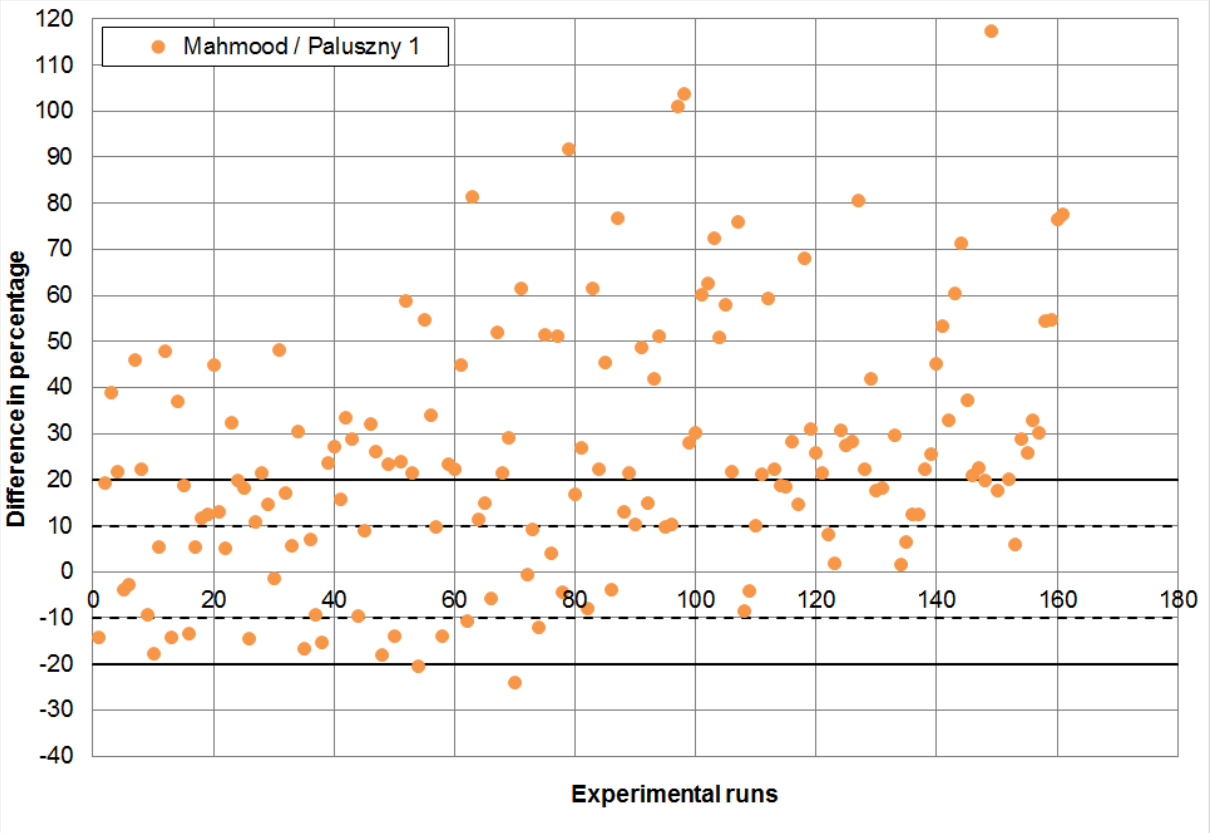

Figure 4.27: Comparison: F_{max} calculated using Mahmood's theory without considering length effect (Eq. 2.5)

Approximately 42% of the analytical results match with the numerical results in the range of ± 20% difference.

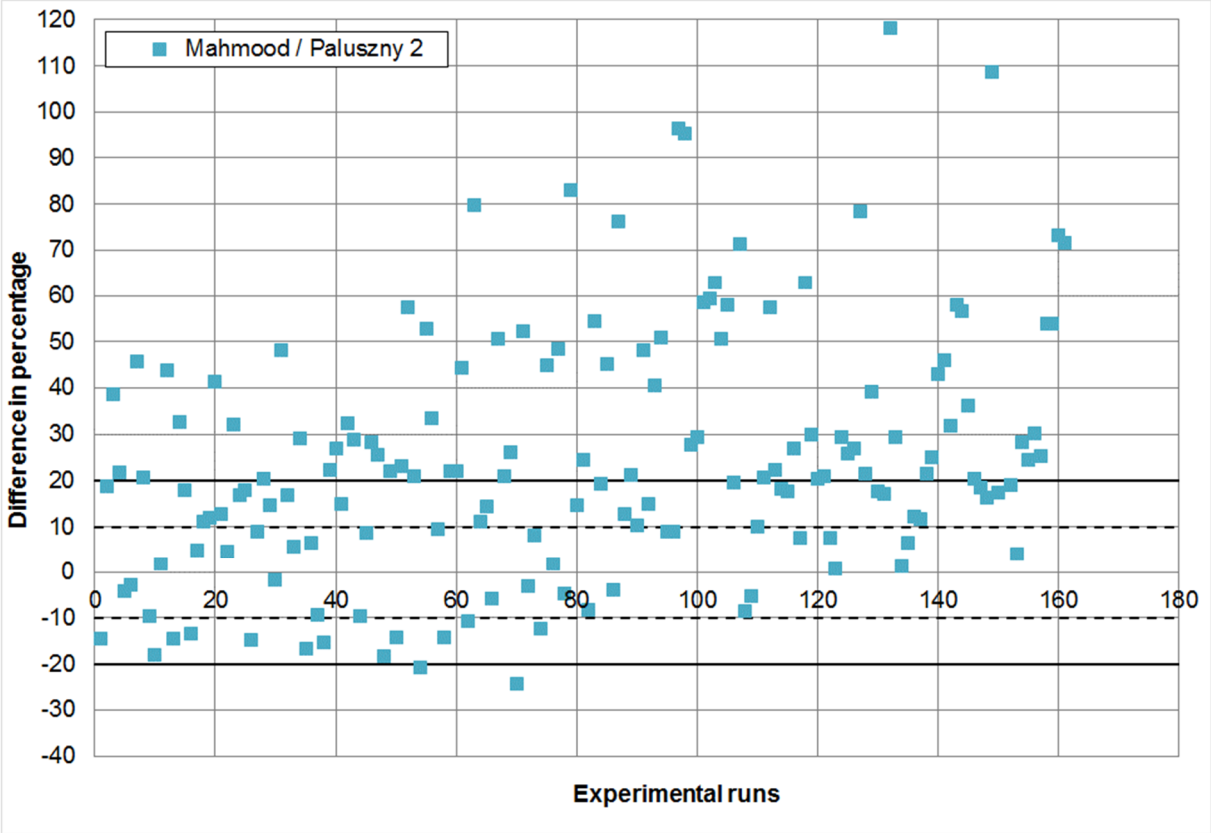

Figure 4.28: Comparison: F_{max} calculated using Mahmood's theory considering length effect (Eq. 2.6)

Approximately 45% of the analytical results match with the numerical results in the range of ± 20% difference.

Regression method:

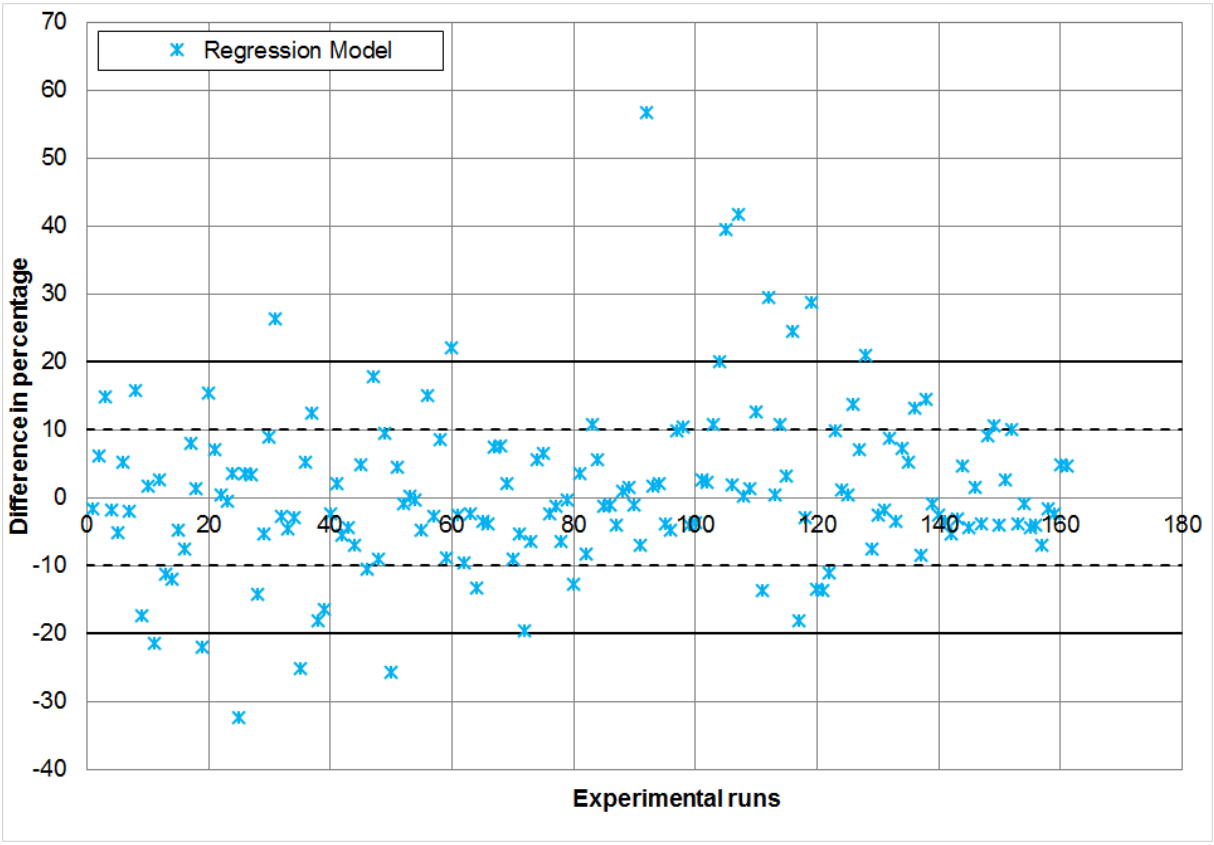

Figure 4.29: Comparison: F_{max} calculated using regression method (Eq. 4.3)

Approximately 91% of the regression results match with the numerical results in the range of ± 20% difference. Values of the quality parameters, summarised in Table 4.6, obtained for this regression equation represent an appropriately fitted model with a good prediction ability.

Mean crushing load F_2

Theory by Mahmood and Paluszny: The assumption made while applying this theory to calculate the value F_2 is mentioned previously.

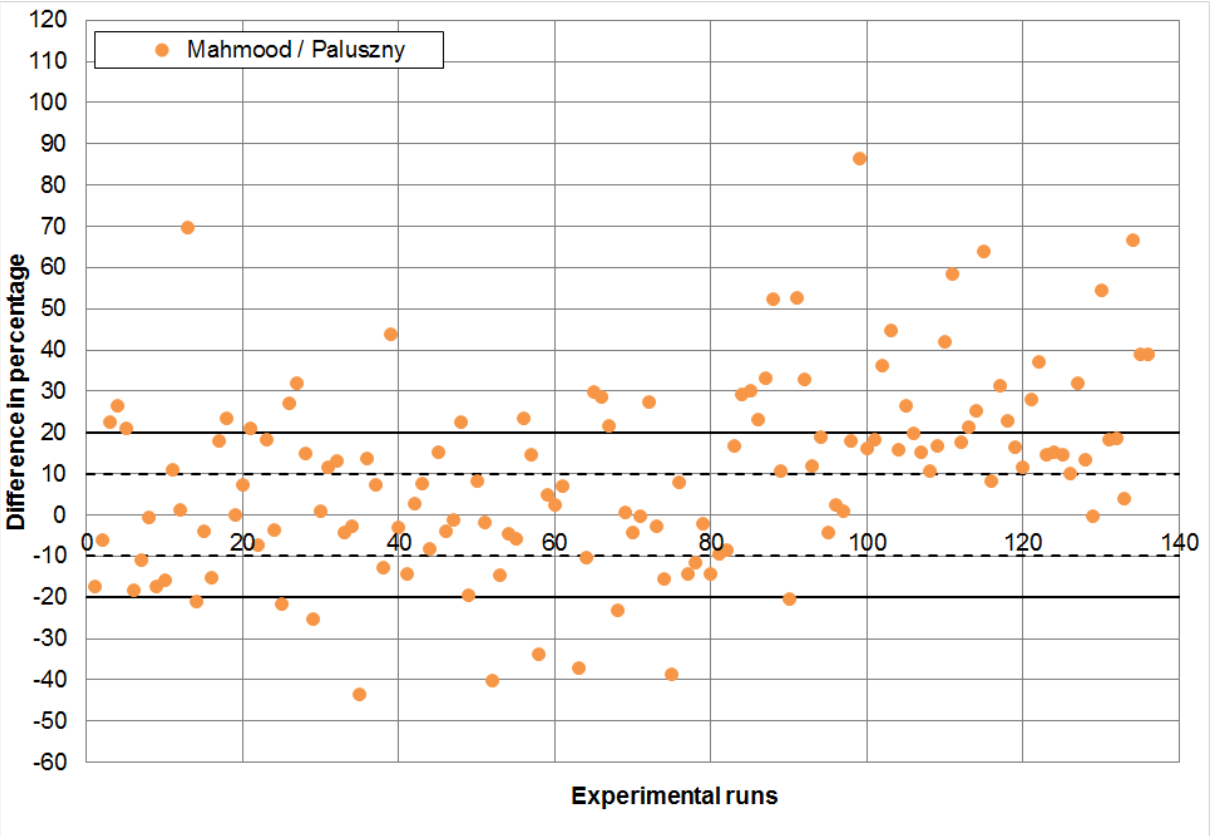

Figure 4.30: Comparison: F_2 calculated using Mahmood's theory (Eq. 2.7)

Approximately 62.5% of the analytical results match with the numerical results in the range of ± 20% difference.

Theory by Jones and Abramowicz: The assumptions made while applying this theory for the experimental runs are listed below.

- The values for Cowper-Symond's coefficients used are: D = 6844 s^{-1} and p= 3.91. These values are dependent on the material as per [35]. However, the values used in the present case are suggested in [31].
- Flow stress σ_0 is assumed to be equal to ultimate stress σ_{ult} of the material, as used in [31].

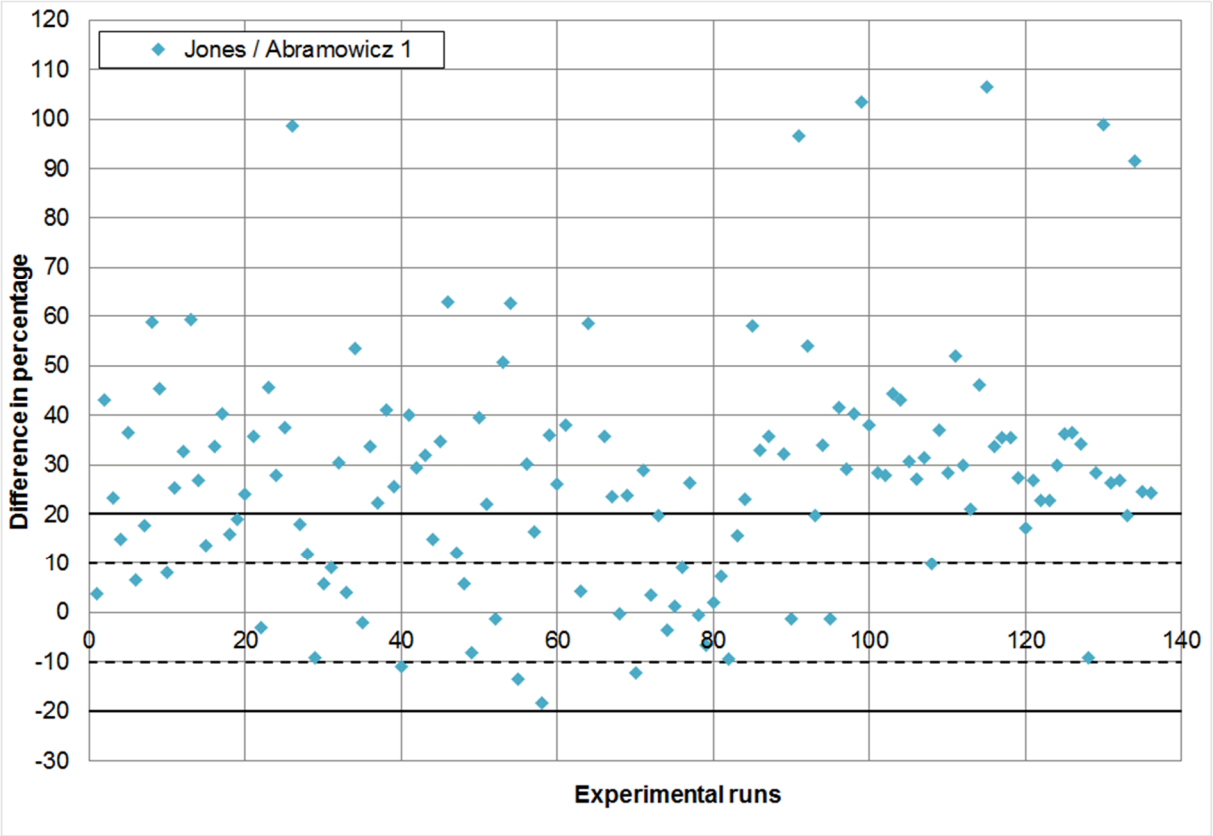

Figure 4.31: Comparison: F_2 calculated using Abramowicz's theory without considering dynamic effects (Eq. 2.9, Eq. 2.13, Eq. 2.15 or Eq. 2.17)

Approximately 34% of the analytical results match with the numerical results in the range of ± 20% difference.

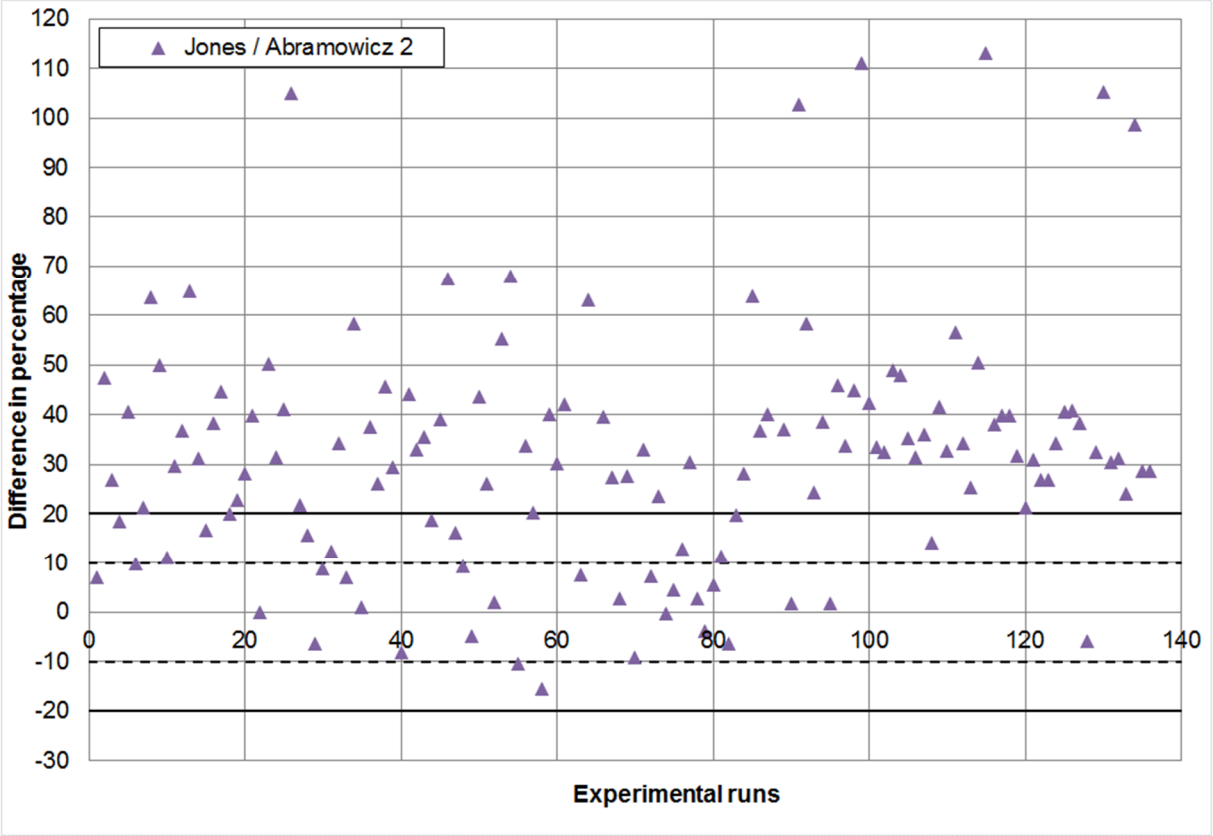

Figure 4.32: Comparison: F_2 calculated using Abramowicz's theory considering dynamic effects (Eq. 2.11, Eq. 2.14, Eq. 2.16 or Eq. 2.18)

Approximately 28% of the analytical results match with the numerical results in the range of ± 20% difference.

Theory of superfolding element by Wierzbicki and Abramowicz: The assumption made while applying this theory for the experimental runs is mentioned below.

- Flow stress is assumed to be $\sigma_0 = 0.92\sigma_{ult}$.

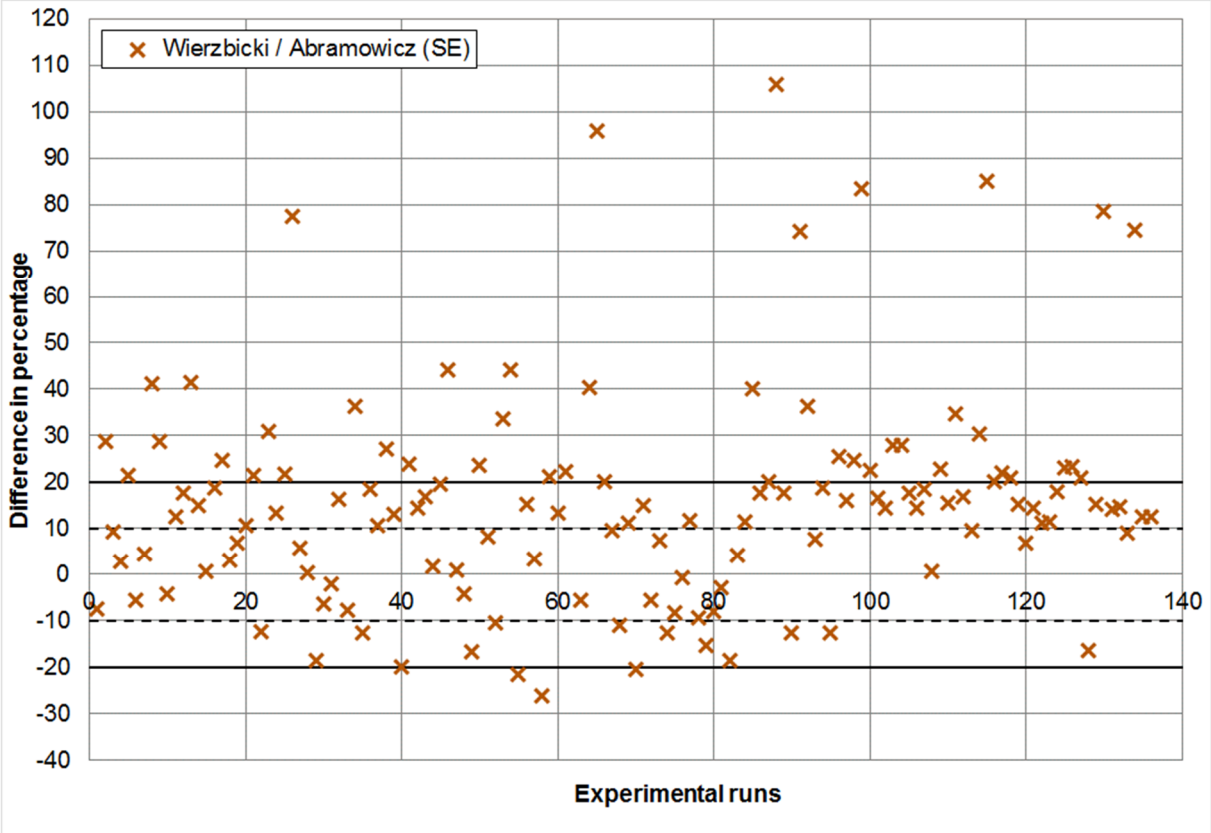

Figure 4.33: Comparison: F_2 calculated using theory of superfolding element by Wierzbicki and Abramowicz (Eq. 2.19)

Approximately 64% of the analytical results match with the numerical results in the range of ± 20% difference.

Regression method:

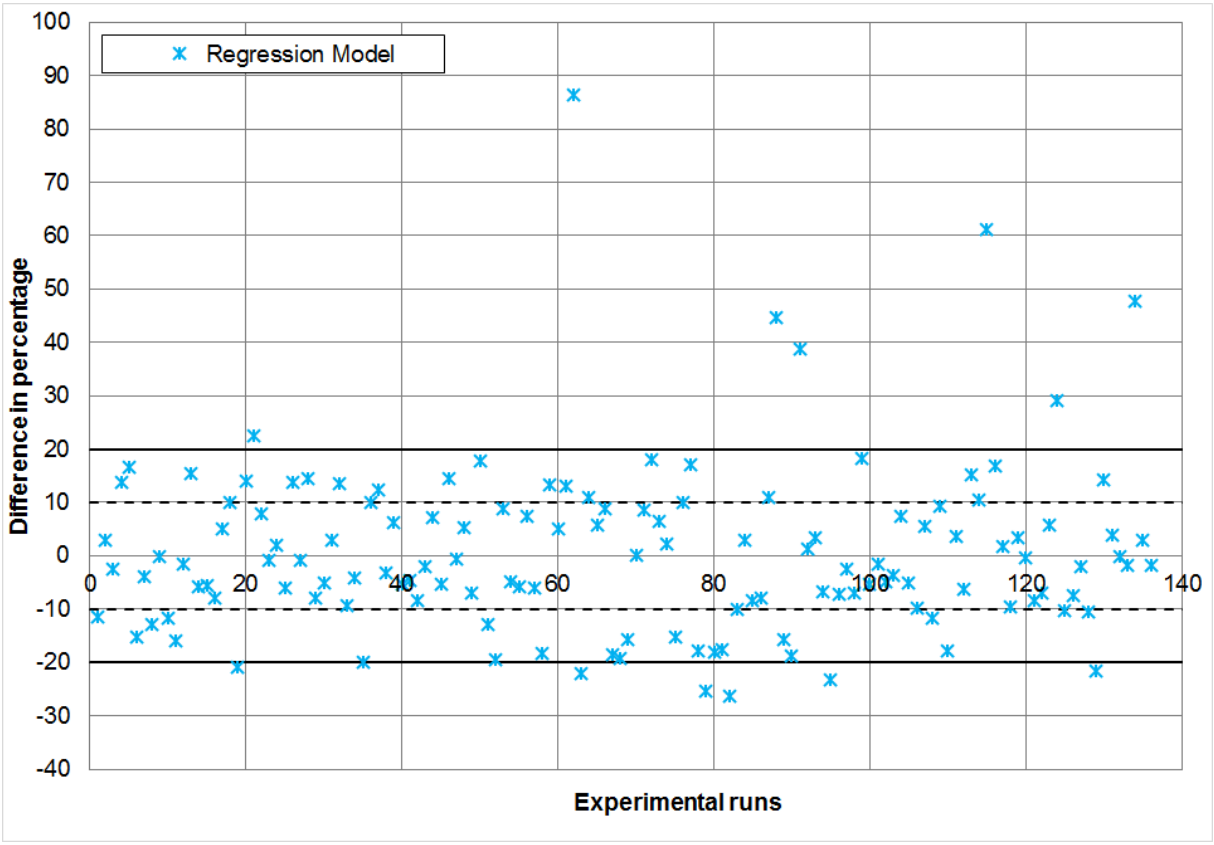

Figure 4.34: Comparison: F_2 calculated using regression method (Eq. 4.4)

Approximately 90% of the regression results match with the numerical results in the range of ± 20% difference. Values of the quality parameters, summarised in Table 4.7, for Eq. 4.4 represent an appropriately fitted model with a good prediction ability.

4.3.4.2 Bending collapse

The equations presented in Section 2.4.3.2 for bending collapse are applied directly, without any computer programming, for calculating M_{max} and M_m for all the experimental runs. The cross-sectional geometry, length of profiles and the material properties are given as inputs for these calculations. Similar to axial collapse, the percentage difference between the numerical and analytical results is evaluated for all the experimental runs. The results within the range of ± 20% difference are considered acceptable. The Figure 4.35 and Figure 4.37 - Figure 4.38 below illustrate the percentage differences, while the comments succeeding the figures state the percentage of experimental runs lying in the acceptable range. The figures are presented for cantilever bending with load applied only on the shorter side of the profile

structure, as similar results are obtained for bending load on the longer side. The assumptions made during the application of the theories are also listed for each individual theory. Finally, a similar comparison is shown in Figure 4.36 and Figure 4.39 for the results calculated using regression method applied to the numerical data.

Maximum bending moment M_{max}

Theory by Kecman: Following assumption is made while applying this theory for calculating M_{max} and M_m.

- The value of the maximum nominal flow stress σ_{pu} of the material in uniaxial tension is assumed to be equal to $0.9\sigma_{ult}$.

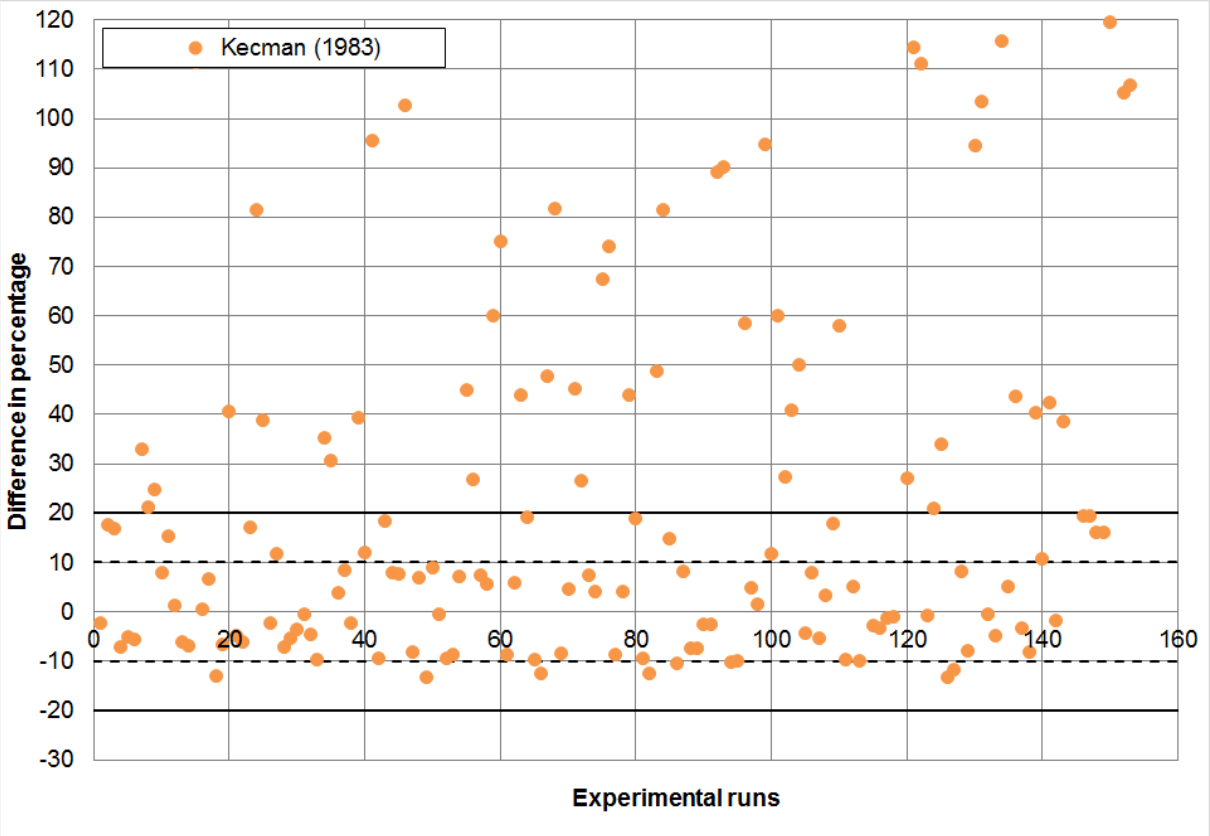

Figure 4.35: Comparison: M_{max} calculated using Kecman's method (Eq. 2.25, Eq. 2.26 or Eq. 2.27)

Approximately 64% of the analytical results match with the numerical results in the range of ± 20% difference.

Regression method:

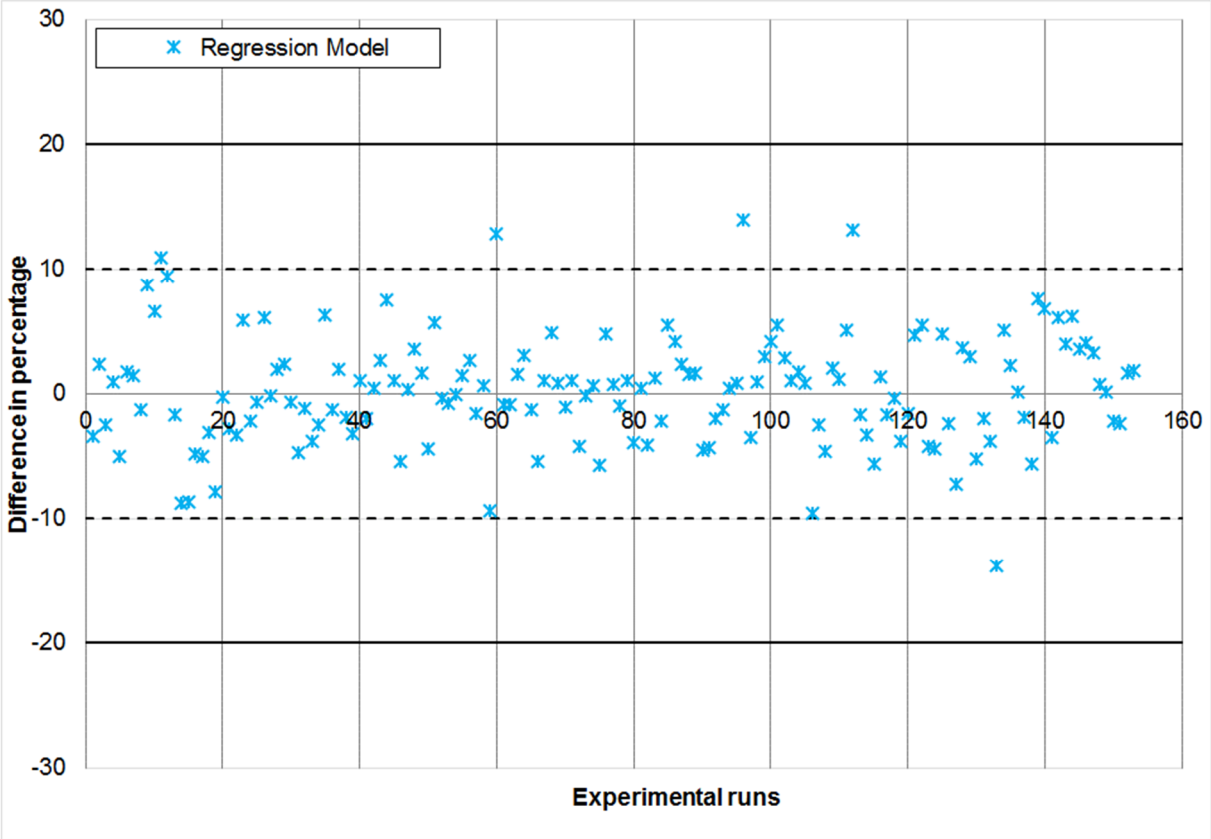

Figure 4.36: Comparison: M_{max} calculated using regression method (Eq. 4.5)

100% of the regression results match with the numerical results in the range of ± 20% difference. Values of the quality parameters, summarised in Table 4.8, for this regression equation represent an appropriately fitted model with a good prediction ability.

Mean bending moment M_m

Theory by Kecman: The assumption made during application of this theory is listed before.

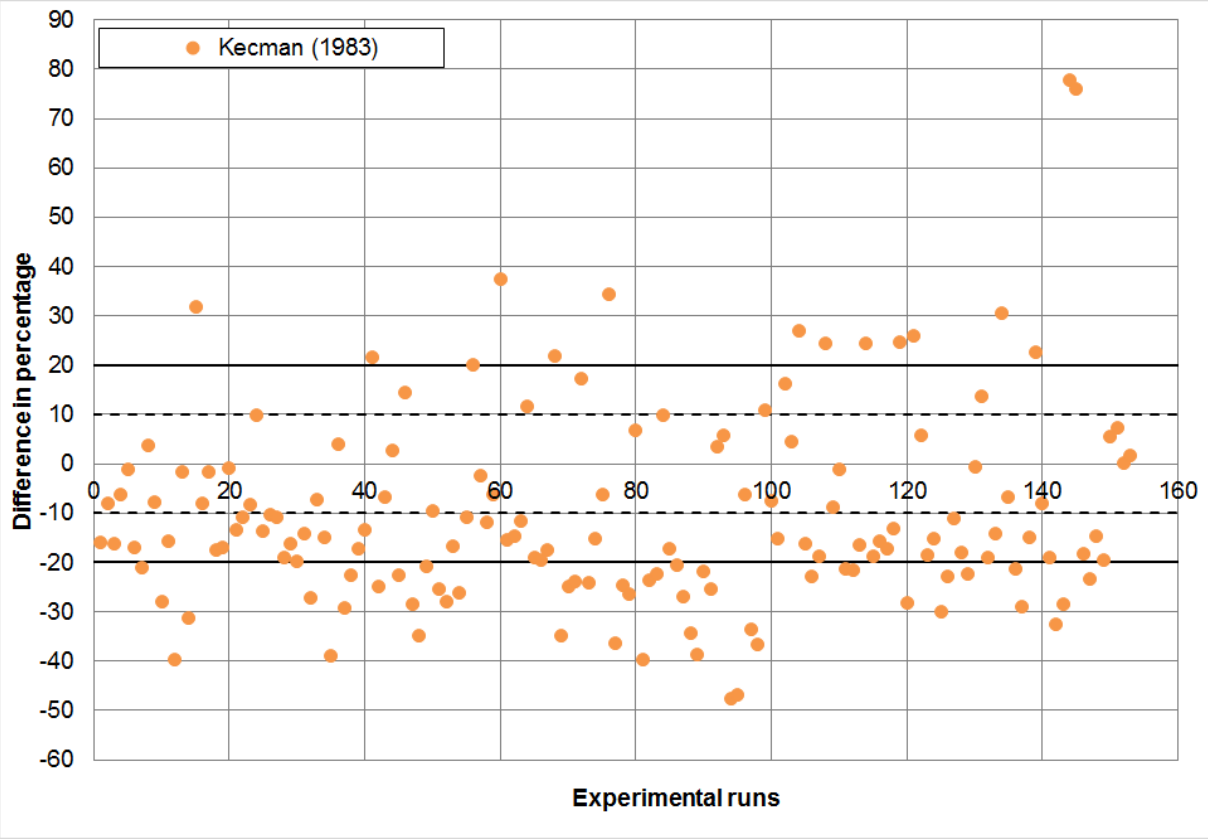

Figure 4.37: Comparison: M_m calculated using Kecman's method

Approximately 59% of the analytical results match with the numerical results in the range of ± 20% difference.

Theory of superbeam elements by Wierzbicki and Abramowicz: The following assumptions are made while applying this theory for calculating M_m.

- Flow stress is assumed to be $\sigma_0 = 0.92\sigma_{ult}$.
- In order to generate an approximate solution, the neutral axis is assumed to lie in the tensile flange.

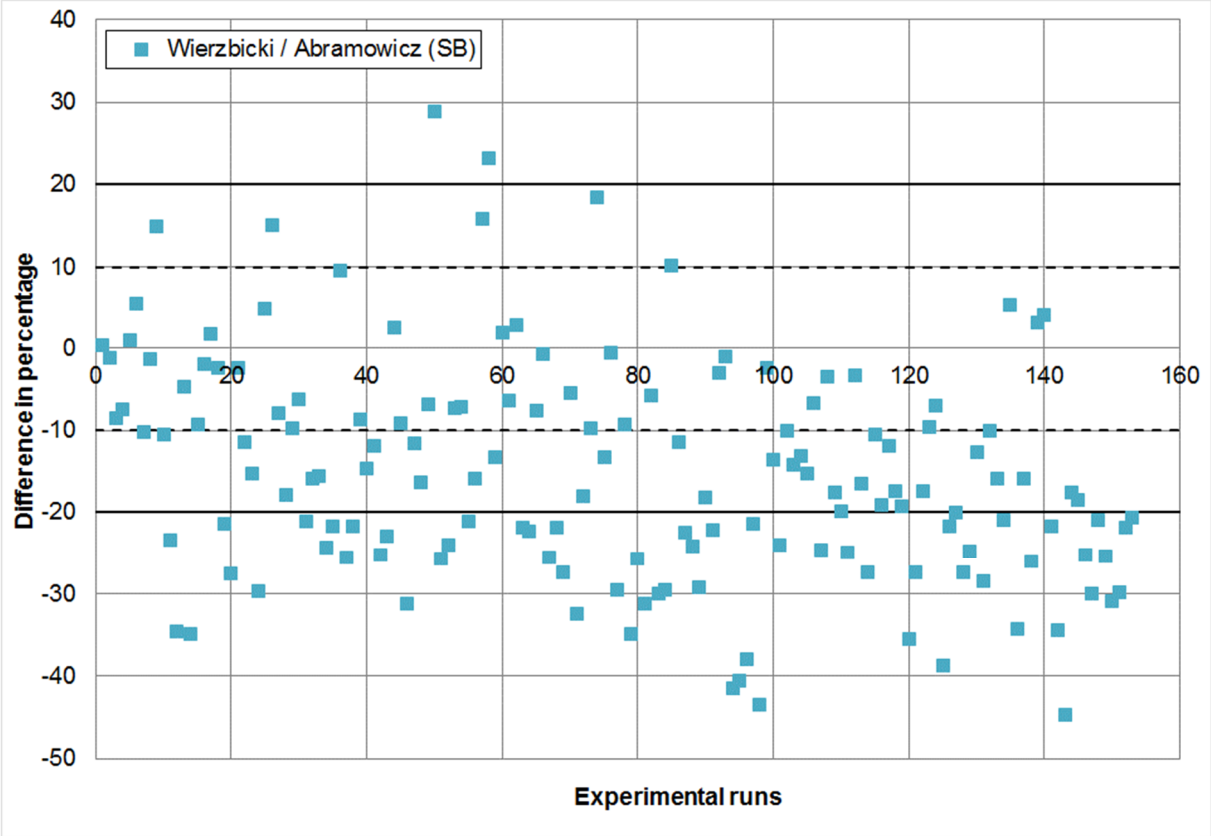

Figure 4.38: Comparison: M_m calculated using theory of superbeam element by Wierzbicki and Abramowicz (Eq. 2.35)

Approximately 57% of the analytical results match with the numerical results in the range of ± 20% difference.

Regression method:

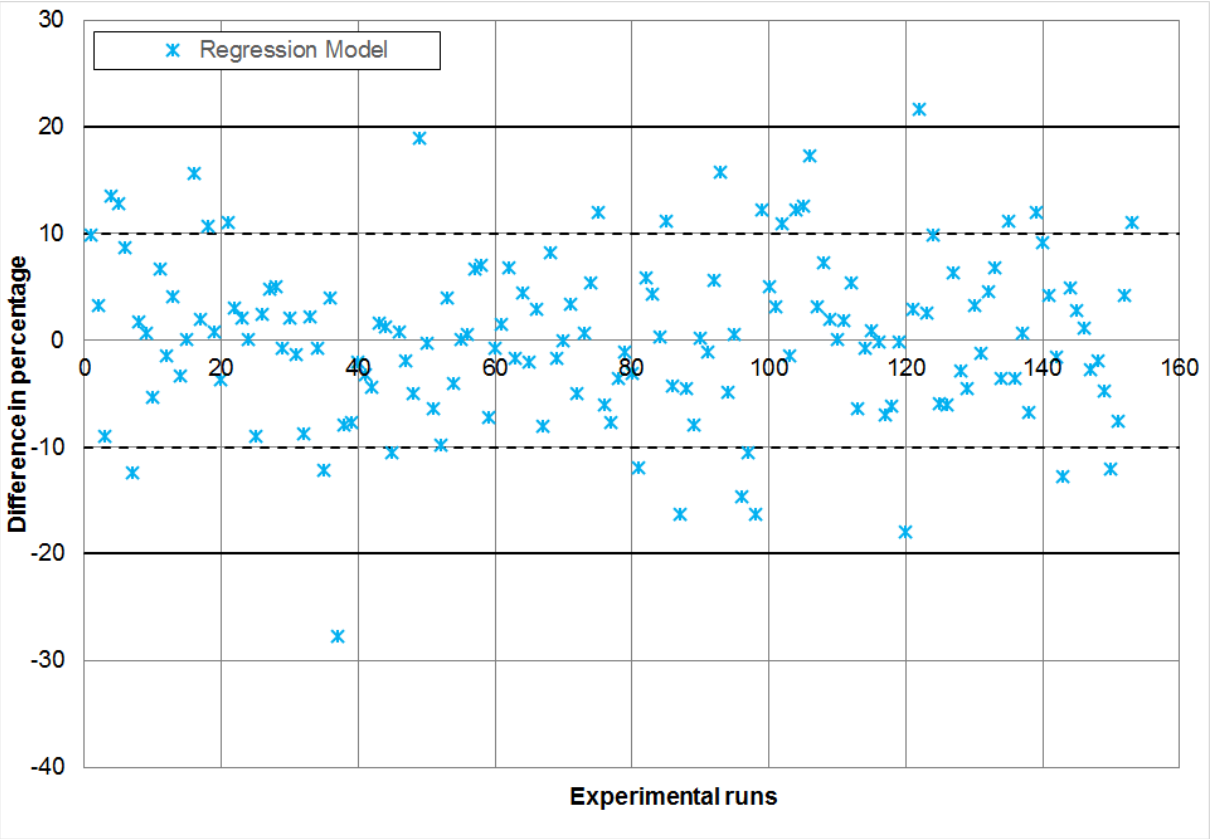

Figure 4.39: Comparison: M_m calculated using regression method (Eq. 4.6)

Approximately 99% of the regression results match with the numerical results in the range of ± 20% difference. Values of the quality parameters, summarised in Table 4.9, for this regression equation represent an appropriately fitted model with a good prediction ability.

4.3.4.3 Summary

The results of the comparison presented in previous Sections 4.3.4.1 and 4.3.4.2 are presented in the form of bar diagrams in Figure 4.40 and Figure 4.41. On the y-axis the percentage of analytical or regression results matching with the numerical results in the range of ± 20% difference is shown. On the x-axis the corresponding theory or regression model is presented.

As it can be observed from the Figure 4.40 and Figure 4.41, the classical theories when applied in their simplified form, without using any programming as used in VCS or Secollapse / Vcrush, for different box profile structures analysed in this work, give acceptable results for only a limited number of profile structures. When the profile structures are analysed using the

VCS software, the percentages of acceptable results increase approximately up to 80% in case of F_{max} in axial collapse and up to 90% in case of M_{max} in the bending collapse.

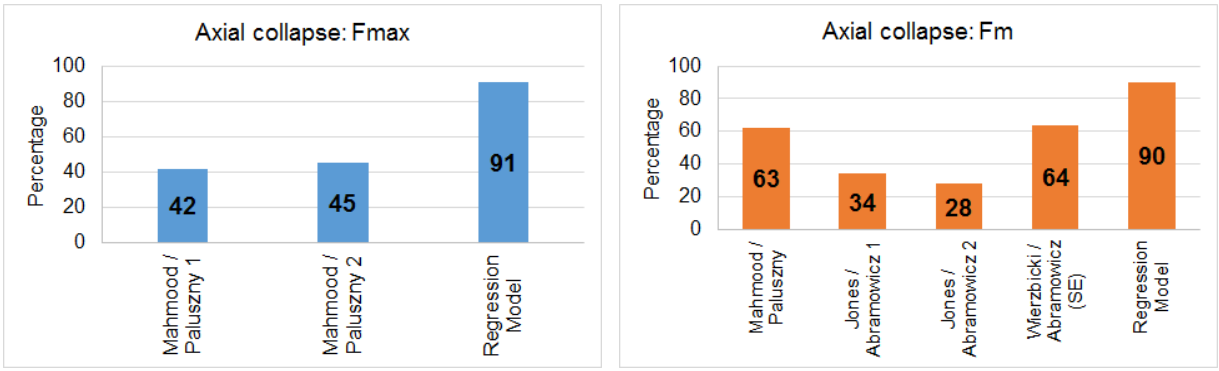

Figure 4.40: Overview of comparison of analytical and experimental methods with numerical method for axial collapse

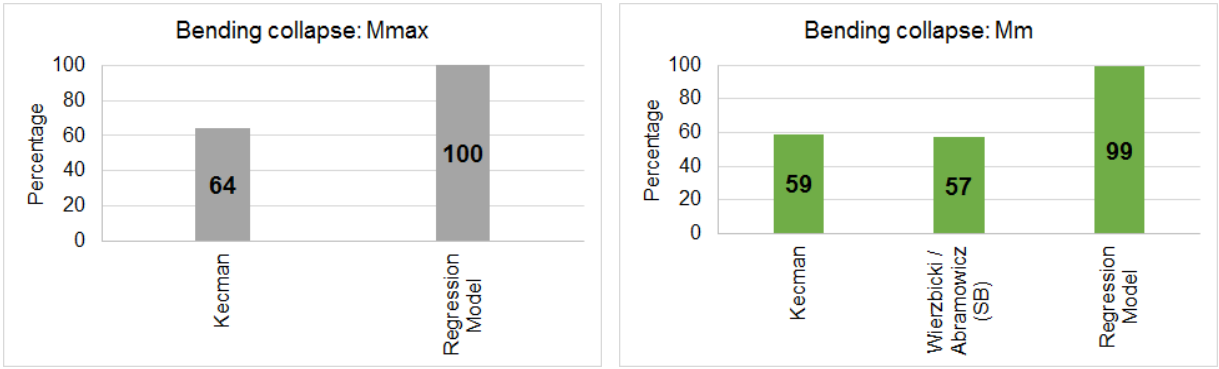

Figure 4.41: Overview of comparison of analytical and experimental methods with numerical method for bending collapse

The regression method, on the other hand, gives acceptable results for a much larger spectrum of the analysed structures. Additionally, the values reflecting the quality of the regression models suggest good prediction ability of the models. Therefore, for the purpose of the MOK approach developed for the profile based structures in this work, the regression method is found to be more appropriate.

The crumpling deformation due to bending load has a different geometry of deformation as compared to the cantilever bending mode. Therefore, the simplified methods analysed and developed in the section configurator cannot be applied for the crumpling bending mode. The methods developed in this work are applicable to regular and irregular axial folding and cantilever bending modes.

5 Application and Validation of Structural Knowledge-base

This work uses a micro-sized electric vehicle, Smart, “Electric Drive (ED)” [17] as basis for the application and validation of the structural knowledge-base. The micro-sized compact coupe passenger concept vehicle, named as **MiNIT** (**Mi**cro car by **NIT** Warangal) is developed using the MOK approach, in this work. The concept vehicle MiNIT is only 2.48 m in length and offers place for two people. The car body structure of MiNIT is a profile based structure, constructed using the FlexBody concept, using profile structures and joints.

Following sections demonstrate the application of the structural knowledgebase for designing the car body structure of the MiNIT considering scenario of frontal crash with a rigid wall. Sections 5.1, 5.2 and 5.3 demonstrate the application of the concepts of attribute configuration, deformation configuration and section configuration respectively, for generating a concept design of the front end of the MiNIT car body structure. The front end thus constructed is validated with the help of FE simulation techniques using LS-Dyna code. The results of the validation are presented in Section 5.4.

5.1 Application of attribute configuration

5.1.1 Safety model for MiNIT

In order to construct a safe vehicle, it is advisable to consider certain crash scenarios such as frontal crash, side crash, rear crash and roof crash during the design of MiNIT. Table 5.1 summarises different legal crash regulations and consumer protection regulations relevant for the MiNIT. A safety level is assigned to all the regulations according to the level system described in Section 4.1.2.2.

Table 5.1: Crash regulations relevant for micro-sized passenger vehicle, MiNIT

Crash test	Regulation			Level	Description
	Name	Country	Type		
Frontal crash	FMVSS 208	USA	Legal requirement	1	Vehicle travels against a stationary rigid wall at a speed of 56 km/h. The rigid wall should be at an angle of 0° to the direction of travel and should overlap the total width of the vehicle.
	FMVSS 208	USA	Legal requirement	2	Vehicle travels against a stationary rigid wall at a speed of 56 km/h. The rigid wall is obliquely placed at an angle of 30° to the direction of travel.
	ECE-R94	EU	Legal requirement	0	Vehicle travels against a deformable barrier at a speed of 56 km/h. The barrier overlaps 40% of the width of the vehicle on driver's side.
	EuroNCAP	EU	Consumer requirement	2	Vehicle travels against a deformable barrier at a speed of 64 km/h. The barrier overlaps 40% of the width of the vehicle on driver's side.
	ECE-R12	EU	Legal requirement	0	Vehicle travels against a stationary rigid wall at a speed of 53.1 km/h. The maximum allowable displacement of the steering column in horizontal and vertical direction is specified.
Side crash	ECE-R95	EU	Legal requirement	0	A moving deformable barrier is impacted on a stationary vehicle at a speed of 50 km/h. The direction of travel of the barrier is perpendicular to the longitudinal axis of the vehicle.
	EuroNCAP	EU	Consumer requirement	2	A moving deformable barrier is impacted on a stationary vehicle at a speed of 50 km/h. The direction of travel of the barrier is perpendicular to the longitudinal axis of the vehicle.

(Table 5.1 continued)

Crash test	Regulation			Level	Description
	Name	Country	Type		
Pole crash	EuroNCAP	EU	Consumer requirement	1	Vehicle travels against a stationary rigid pole sideways at a speed of 29 km/h. The direction of travel of the vehicle is perpendicular to the length of the vehicle.
	FMVSS 214	USA	Legal requirement	2	Vehicle travels against a stationary rigid pole sideways at a speed of 32 km/h and at an angle of 75°.
	Pole-front	-	-	1	Vehicle travels against a stationary rigid pole placed centrally in front at a speed of 30 km/h.
Roof crash	FMVSS 216	USA	Legal requirement	1	A rigid plate is pressed against the roof of a vehicle such that the force is brought on the A-pillar at a speed of 13mm/s
Rear crash	ECE-R34	EU	Legal requirement	1	A rigid plate with mass of 1100kg is impacted on a stationary vehicle at a speed of 38 km/h. The rigid plate should be impacted at an angle of 0° to the longitudinal axis of the vehicle and should overlap the total width of the vehicle.
	IIHS	USA	Consumer requirement	2	The driver's seat is tested against rear impact at a speed of 16 km/h.
	FMVSS 301	USA	Legal requirement	2	A moving deformable barrier is impacted on a stationary vehicle at a speed of 79.3 km/h. The direction of travel of the barrier is at 0° to the longitudinal axis of the vehicle.

Considering the design phase, namely the concept phase, and the cost and time constraints during the project MiNIT, the crash scenarios with levels 0 and 1 are chosen for the design of MiNIT. The modifications in the process of type approval of the small series vehicles that came into action recently [56] are also considered during the design of MiNIT. Figure 5.1 illustrates the safety model for the target micro-sized passenger vehicle.

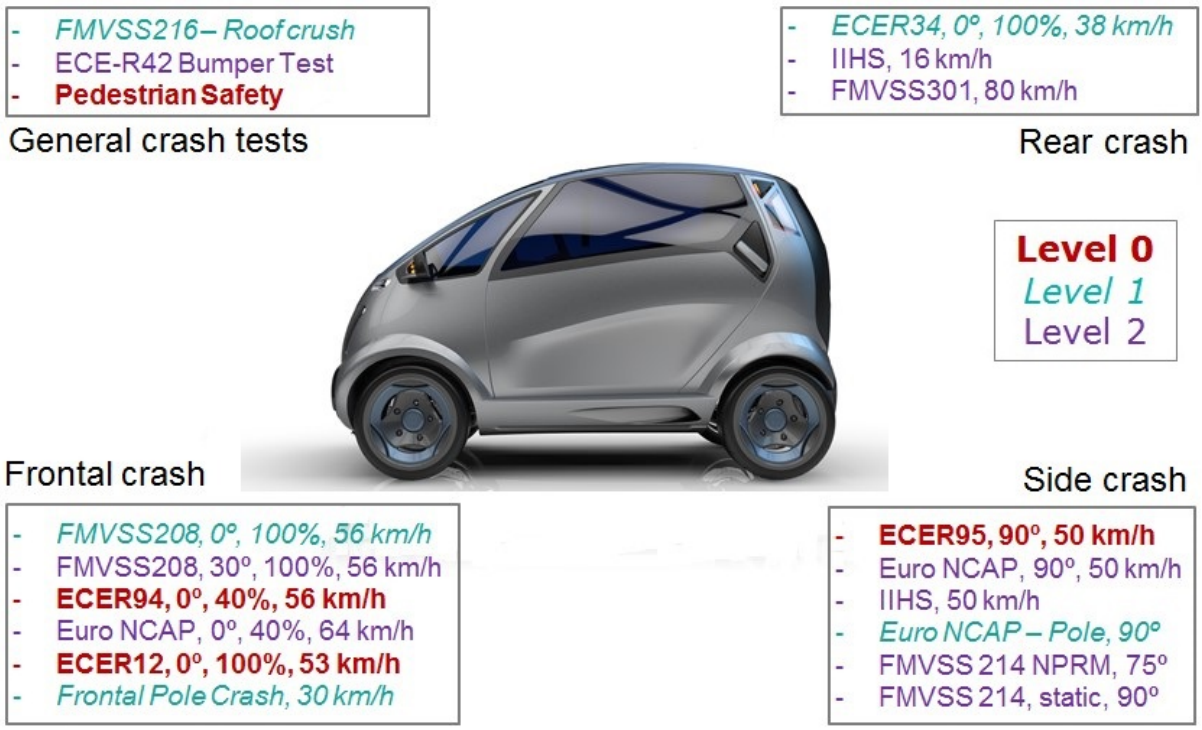

Figure 5.1: Safety model for the target micro-sized passenger vehicle, MiNIT

5.1.2 Definition of global performance targets

This section demonstrates the process of application of the benchmark developed, as described in Section 4.1.3, for the frontal impact scenario with a rigid wall at 0° (FMVSS 208), and thereby exemplifies the use of the attribute configurator in the MOK design process.

5.1.2.1 Basic information

Initially, the basic information about the target vehicle as well as the crash scenario, relevant for the crashworthy design of the MiNIT, is collected.

For the micro-sized passenger vehicle MiNIT the target curb weight is defined as 800 kg. The weight of fluids in the vehicle is approximated as 10 kg and the luggage capacity is assumed as 50 kg. As described in the FMVSS 208 directive, the test weight of the vehicle is calculated as [58]:

Test weight = Curb weight + weight of fluids + luggage capacity + 2 x 50th percentile male or 5th percentile female

For the MiNIT application, two 50th percentile male dummies, each weighing 77.7 kg [51], are considered. The total weight of the target vehicle to be tested for the frontal crash is, therefore, 1015.4 kg. Main features of the FMVSS 208 crash scenario are summarised in Table 5.2.

Table 5.2: Summary of FMVSS 208

Information about barrier	Rigid, immovable, overlapping 100% width of the vehicle, perpendicular to longitudinal axis of the vehicle
Velocity of impact	56 km/h (to the vehicle)
Picture	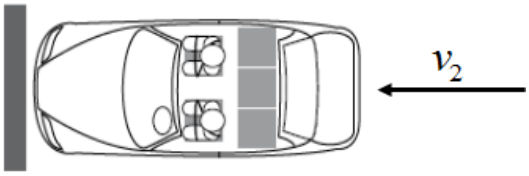

5.1.2.2 Energy of deformation

The conservation of energy in the case of FMVSS 208 impact scenario can be represented as in Figure 5.2 and written using Eq. 5.1. As the barrier is a rigid stationary wall, it has neither an initial nor a final velocity and it does not absorb any energy.

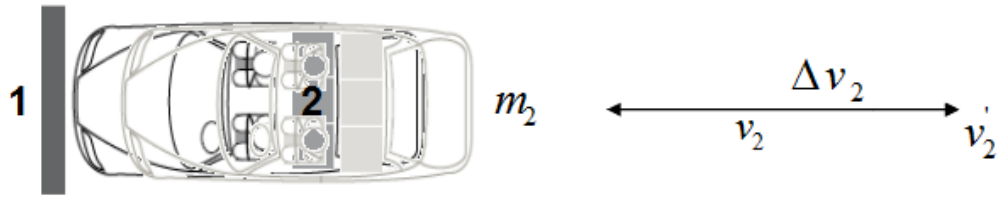

Figure 5.2: Crash scenario according to FMVSS 208

$$\frac{1}{2}m_2v_2^2 = \frac{1}{2}m_2v'^2_2 + E_{Def,2} \qquad \textit{Eq. 5.1}$$

As explained in the Section 4.1.3, the targets for the energy of deformation for the MiNIT vehicle can be defined using the benchmark data. Accordingly, for the FMVSS 208 crash scenario, the target vehicle should absorb approximately 88% of the initial kinetic energy while the remaining 12% of the energy will go in the translational motion after impact. Therefore, the vehicle should absorb a total of 108 kJ of energy by deforming in controlled manner, as given by Eq. 5.2.

$$E_{Def,2} = 0.88\left[\frac{1}{2}\times 1015.4kg\times\left(56km/h\right)^2\right] = 108.12kJ \qquad \textit{Eq. 5.2}$$

5.1.2.3 Allowable deformations of front end

In the next step, the extent of the deformations that the vehicle is allowed to undergo during the impact are set. For deciding these values, the overall dimensions of the vehicle, the topology of the target body structure and the information about package positioning in the vehicle are taken into consideration. In the view of these factors, the allowable deformations for the MiNIT in case of FMVSS 208 are set and illustrated in Figure 5.3. In order to give a better idea of the deformation zones, a schematic of the proposed topology of the MiNIT front structure is inserted in the background in Figure 5.3. The allowable deformation for the MiNIT during front impact are:

- Deformation of front end = maximum 300 mm
- Intrusion of firewall in the passenger compartment = maximum 50 mm

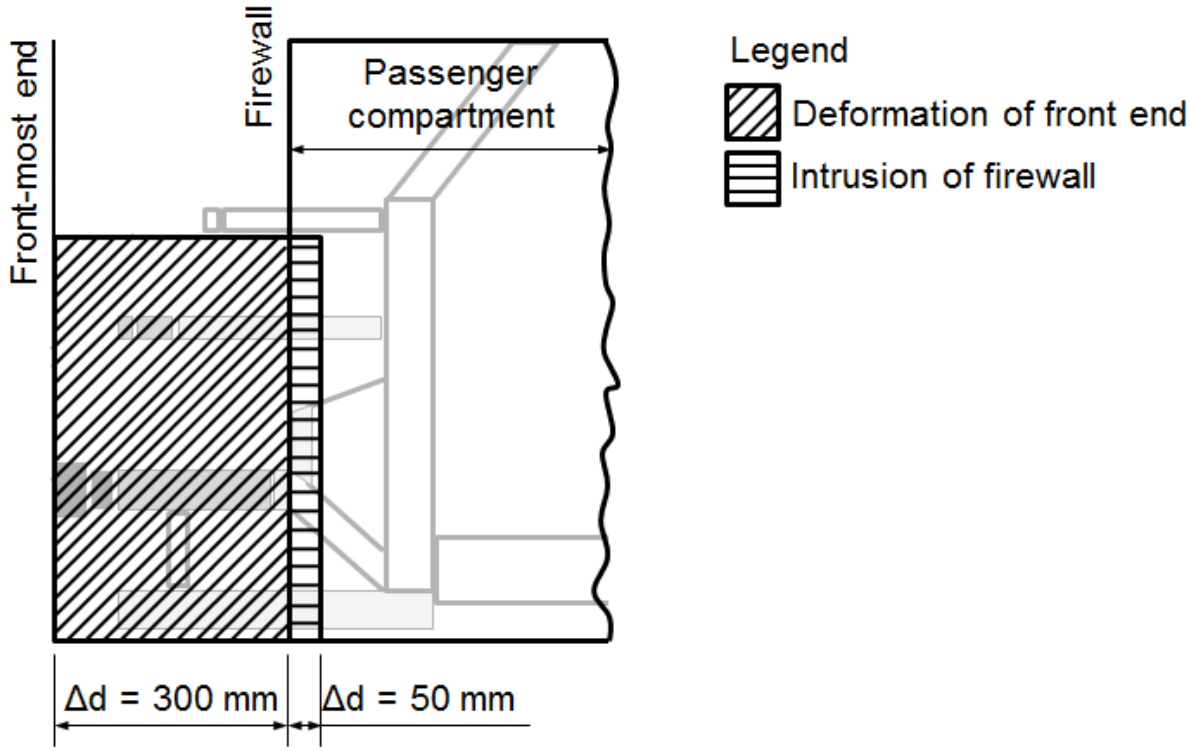

Figure 5.3: Deformation zones for frontal crash with rigid wall for MiNIT structure

5.1.2.4 Deceleration levels

As mentioned in Section 2.3.1, the allowable level of average vehicle deceleration in a particular crash scenario can be deduced from the limiting HIC value specified in the concerned crash regulation. For the FMVSS 208 crash scenario, the defined limit for the HIC value is 1000 within any time interval not more than 36 milliseconds [58]. The allowable value of the average deceleration the Smart ED vehicle can undergo corresponding to the defined limit for the HIC value can be calculated using a simplified calculation procedure [22], as described below.

For this simplified calculation, it is assumed that the vehicle and the occupant undergo a constant deceleration. Additionally, it is also assumed that the collision is perfectly plastic. Therefore, the vehicle does not possess any motion after the impact. Before the impact occurs, the vehicle and the occupant move with the same initial velocity v_0 of 56 km/h. During the frontal impact, the frontal vehicle structure deforms by the maximum allowable value of 350 mm, and thereby decelerates the vehicle with a deceleration of 346 m/s^2 (approximately 35g, g being the gravitational constant), and comes to a standstill.

The occupant is coupled to the vehicle via a seat belt. The seat belt system, however, does not act immediately as the impact takes place. Therefore, the occupant moves with the same initial velocity for some initial time until the seat belt tightens. This is called the *belt slack*. For the Smart ED vehicle, the displacement of the occupant's chest during belt slack is assumed to be 40 mm. Once the seat belt system tightens, the occupant's chest decelerates with a deceleration of 298 m/s^2 (approximately 30g), with a different deceleration value than that of the vehicle. The head of the occupant decelerates with a different deceleration value as compared to the rest of the occupant's body, the reason being the flexible connection between the head and the upper body realised through the neck. Thus, even after the occupant's body starts to decelerate the head moves freely through a certain amount of distance until the chin hits the chest. For the case of the Smart ED vehicle, this free flight of the occupant's head is assumed to be 140 mm. Thereafter the head moves with the same velocity as the chest and comes to rest at the same time as the chest. Thereby, the occupant's head experiences a higher amount of deceleration than the chest, and equals to 721 m/s^2 (approximately 73g). The velocity-time diagram and the decelerations experienced by the Smart ED vehicle and the occupant in case of the frontal crash is presented in Figure 5.4.

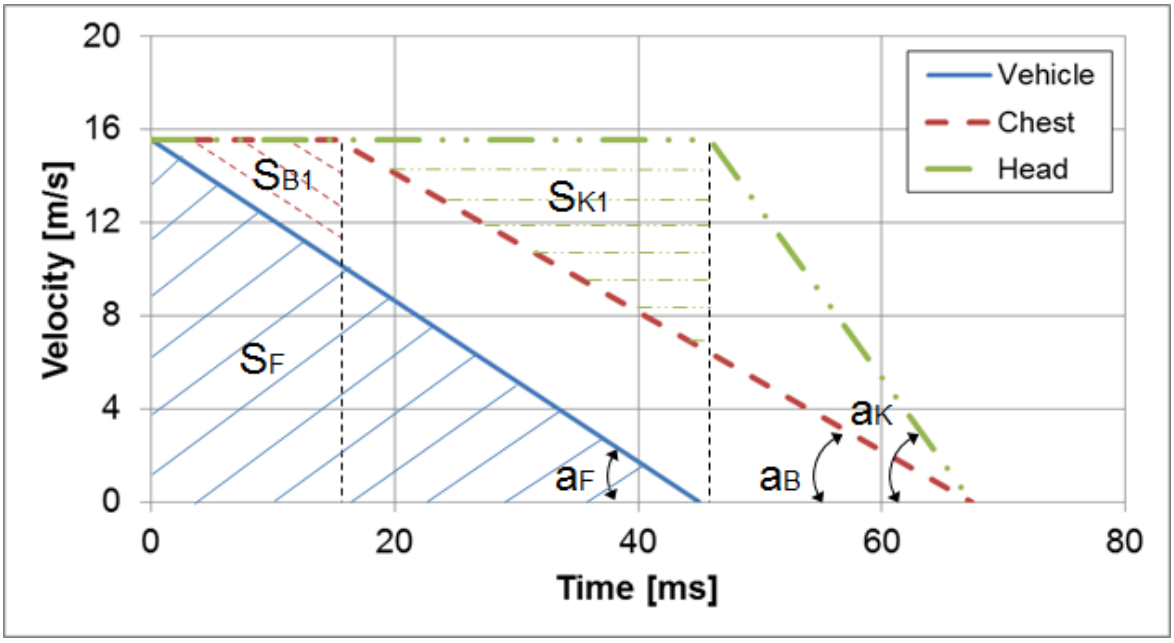

Figure 5.4: Velocity – time diagram of Smart in frontal crash against rigid wall [17]

In Figure 5.4:

S_F : Maximum deformation of front structure of the vehicle

a_F : Average deceleration of the vehicle during frontal crash

S_{B1} : Displacement of occupant's chest during belt slack

a_B : Average deceleration of the occupant's chest

S_{K1} : Free flight of the occupant's head

a_K : Average deceleration of occupant's head

Based on the above calculation for the frontal crash, the average target deceleration of the MiNIT is set at 32g. For this deceleration value of the vehicle, the average deceleration of the head remains below 73g, which approximately corresponds to an HIC value of 1000. Following the general trend, the maximum permissible deceleration of the MiNIT in the FMVSS 208 crash scenario is set to 50g.

5.1.2.5 Force deformation curve for frontal impact

Depending on the observations made from the benchmark simulations of the benchmark vehicles, the force deformation curve for a frontal crash can be divided in three regions according to the increasing force levels. Accordingly, the topology of the car body structure can also be divided into three groups, which deform under these force levels at different times during the impact.

As the next step, the components of the car body structure are divided into three groups using the basic topology created for the target vehicle. Each group may contain full or part of a certain car body component depending on its placement. For the MiNIT target car body structure the division of the components in three groups is done as follows. Subassembly A includes the bumper beam and the deformation elements. Subassembly B extends up to the firewall. Subassembly C represents the intrusion of the firewall in the passenger compartment. For each of these groups, permissible deformations can be defined as listed below, based on the global deformation value defined earlier for the front end.

- Subassembly A: 82.5 mm
- Subassembly B: 217.5 mm
- Subassembly C: 50 mm

Figure 5.5 schematically illustrates the allowable deformations in each of the three subassemblies.

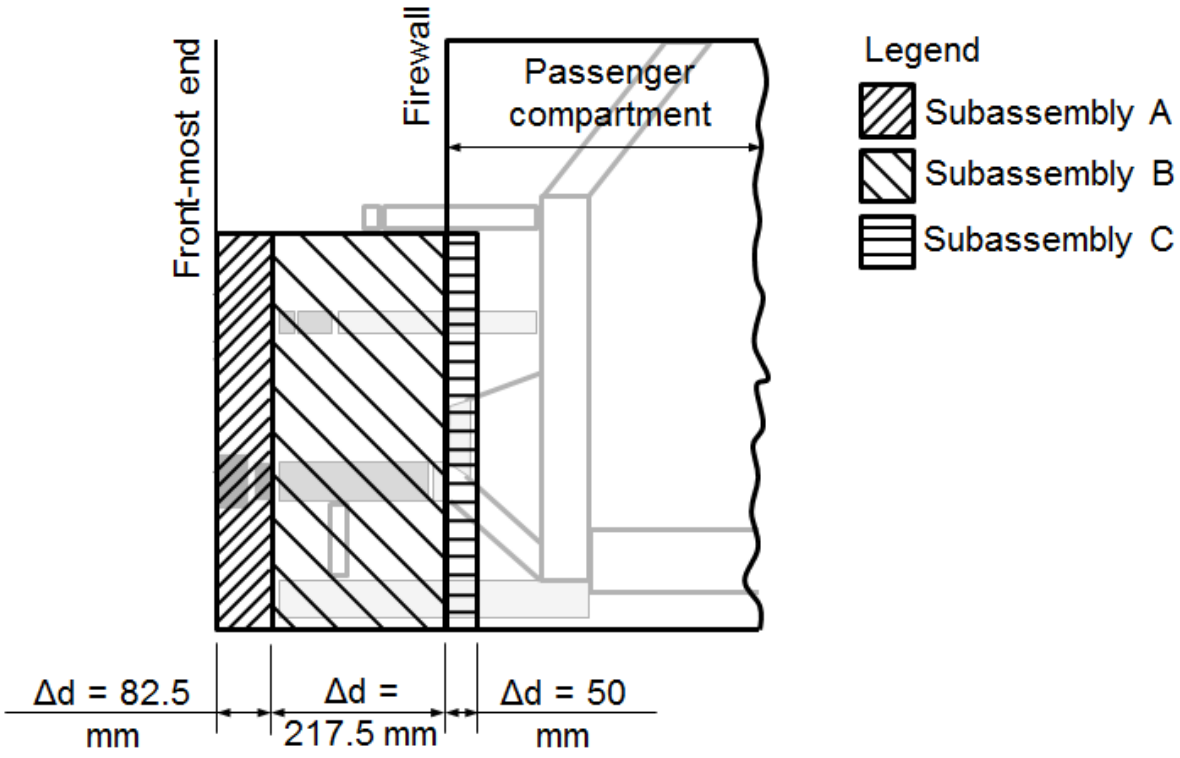

Figure 5.5: Division of MiNIT front structure topology into three subassemblies

Using the energy absorption targets and the allowable deformations defined, a target force deformation curve (hereafter called F-D curve) for frontal impact according to FMVSS 208 can be constructed. A similar trend as that observed in the benchmark simulations is followed while

constructing the F-D curve. Accordingly, the front structure should be soft at the start of the impact and should progressively become stiffer towards the passenger compartment. Thereby, safety can be ensured for a large range of speeds, including low speed impacts as well as high speed frontal crashes with rigid walls.

Using the targets defined for the deformation energy in the Section 5.1.2.2 by Eq. 5.2, and the allowable deformations defined in Figure 5.3 and Figure 5.5 for the vehicle and its different component groups during a frontal impact, the target F-D curve is defined for the target vehicle MiNIT. Additionally, the maximum and average deceleration targets set at 50g and 32g respectively for MiNIT in Section 5.1.2.4, are also used while determining the target F-D curve. This target curve is illustrated in Figure 5.6. Since pedestrian safety is achieved by a soft bumper shell and bumper foam in the MiNIT vehicle, the deformation of these components is not included in the target F-D curve shown in Figure 5.6.

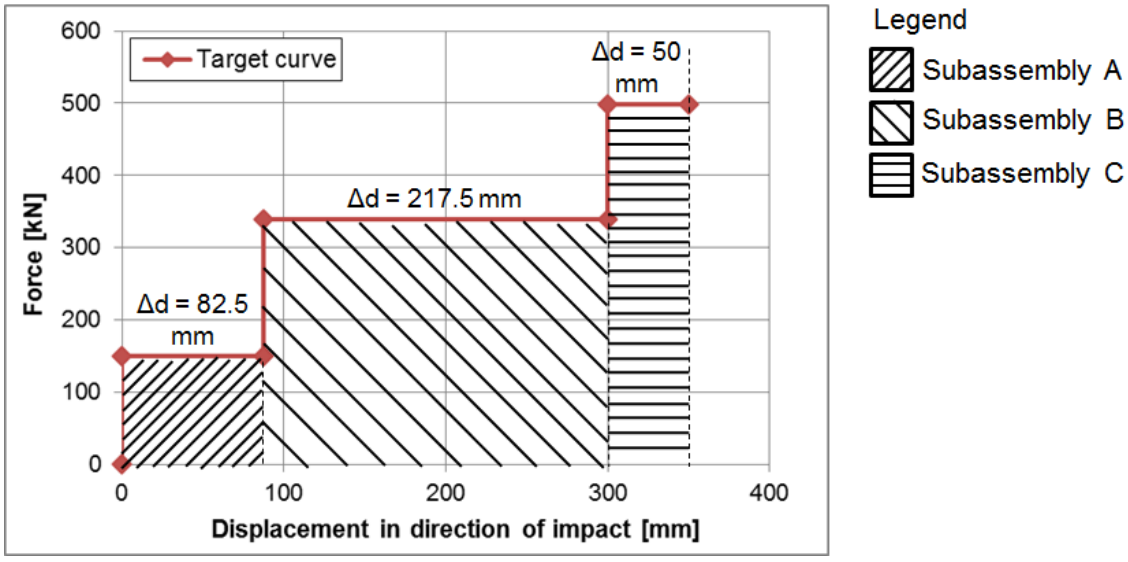

Figure 5.6: Target force – deformation curve for MiNIT front crash with rigid wall

5.2 Application of deformation configuration

5.2.1 Identification of active components in frontal crash

As explained in Section 4.2.2.1, the benchmark database provides basic guidelines for identifying the active components in a particular crash scenario. The engineering judgment of the design engineer is additionally necessary for this step. The observations made for the benchmark vehicles for the FMVSS 208 crash scenario are summarised in Figure 5.7 and Figure 5.8. The active components identified for the benchmark vehicles are coloured in a darker shade.

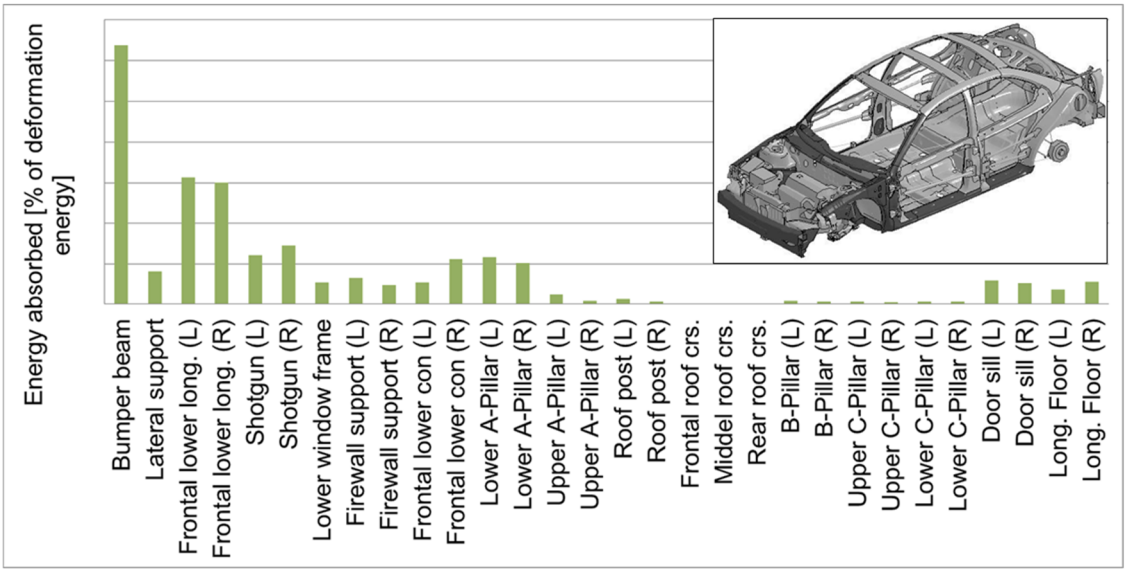

Figure 5.7: Active car body components of benchmark vehicle 1 in FMVSS 208 crash scenario

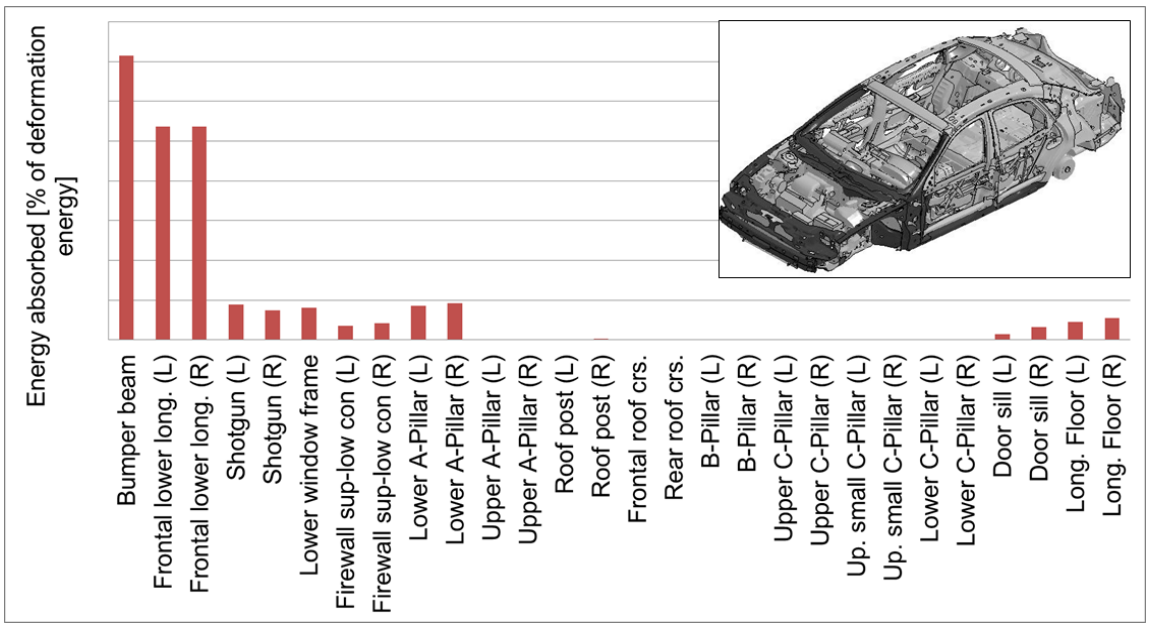

Figure 5.8: Active car body components of benchmark vehicle 2 in FMVSS 208 crash scenario

Considering the overall dimensions of the MiNIT car body and the allowable deformations defined for the frontal crash scenario in the attribute configuration in Section 5.1.2, the active components of the target MiNIT car body are identified, as listed in the Table 5.3. The components identified as active are then divided into three groups, each corresponding to the subassemblies A, B and C, as described in Section 5.1.2. Each component is also assigned a deformation type, elastic (E), elastic-plastic (E-P) and plastic (P). As according to FMVSS 208, whole width of the vehicle is overlapped by the rigid wall during the impact, both sides of the vehicle, left and right, will be symmetrically loaded and incur similar deformations.

Table 5.3: List of active components of MiNIT and their type of deformation during FMVSS 208

Part No.	Part name	Deformation type
Subassembly A		
3000021	Bumper beam	P
3000059	Frontal deformation element left	P
3000060	Frontal deformation element right	P
Subassembly B		
3000103	Upper cross member for bumper shell	P
3000101	Connecting member bet shotgun & upper cross member left	P
3000102	Connecting member bet shotgun & upper cross member right	P
3000001	Frontal lower longitudinal member left	P
3000002	Frontal lower longitudinal member right	P
Subassembly C		
3400002	Subframe	P
800015	Speer left	P
800016	Speer right	P
3010001	Joint 1 left	P / E-P
3010002	Joint 1 right	P / E-P
3000013	Lower A-Pillar left	E-P
3000014	Lower A-Pillar right	E-P
3000011	Door sill left	E-P
3000012	Door sill right	E-P
3000023	Frontal middle cross member	E-P
3000003	Frontal lower connecting member left	E-P
3000004	Frontal lower connecting member right	E-P
3000027	Frontal lower cross member	E-P
3000025	Frontal lower cross connecting member left	E-P
3000026	Frontal lower cross connecting member right	E-P
3000041	Upper A-Pillar left	E-P
3000042	Upper A-Pillar right	E-P

As discussed in Section 4.2.2.2, only those components, which are predicted to deform plastically, are required to be designed for optimum cross sections and materials. These components are hereafter called energy absorbing components.

5.2.2 Definition of deformation targets for components

The next tasks in the deformation configuration are defining the preferred mode of deformation and the actual deformation targets for the energy absorbing components, identified in the previous step. Depending on the direction of the load acting on the components, the preferred deformation mode is determined. For the frontal impact scenario, according to FMVSS 208, the preferred deformation modes of the individual energy absorbing components are listed in Table 5.4. In this table:

A1 : Regular folding

A2 : Irregular folding

B1 : Cantilever bending

B3 : Crumpling bending

Table 5.4: Deformation modes of energy absorbing components in MiNIT frontend

Part No.	Part name	Deformation mode
Subassembly A		
3000021	Bumper beam	B3
3000059	Frontal deformation element left	A1
3000060	Frontal deformation element right	A1
Subassembly B		
3000103	Upper cross member for bumper shell	B3
3000101	Connecting member bet shotgun & upper cross member left	B3
3000102	Connecting member bet shotgun & upper cross member right	B3
3000001	Frontal lower longitudinal member left	A1 & A2
3000002	Frontal lower longitudinal member right	A1 & A2
Subassembly C		
3400002	Subframe	B1
800015	Shotgun left	A1 & Local
800016	Shotgun right	A1 & Local
3010001	Joint 1 left	A2
3010002	Joint 1 right	A2

The components of the three subassemblies listed in Table 5.4 are schematically illustrated in Figure 5.9 with their part number and respective deformation mode. The figure 5.9 shows side

view of the front structure. Sequence of deformation of the subassemblies is represented by three stages in Figure 5.9. Although some areas of the components subframe and shotgun overlap with the components deforming in stage 2, i.e. with subassembly B, major deformation of these components is preferred during stage 3. Therefore, these components are grouped under subassembly C.

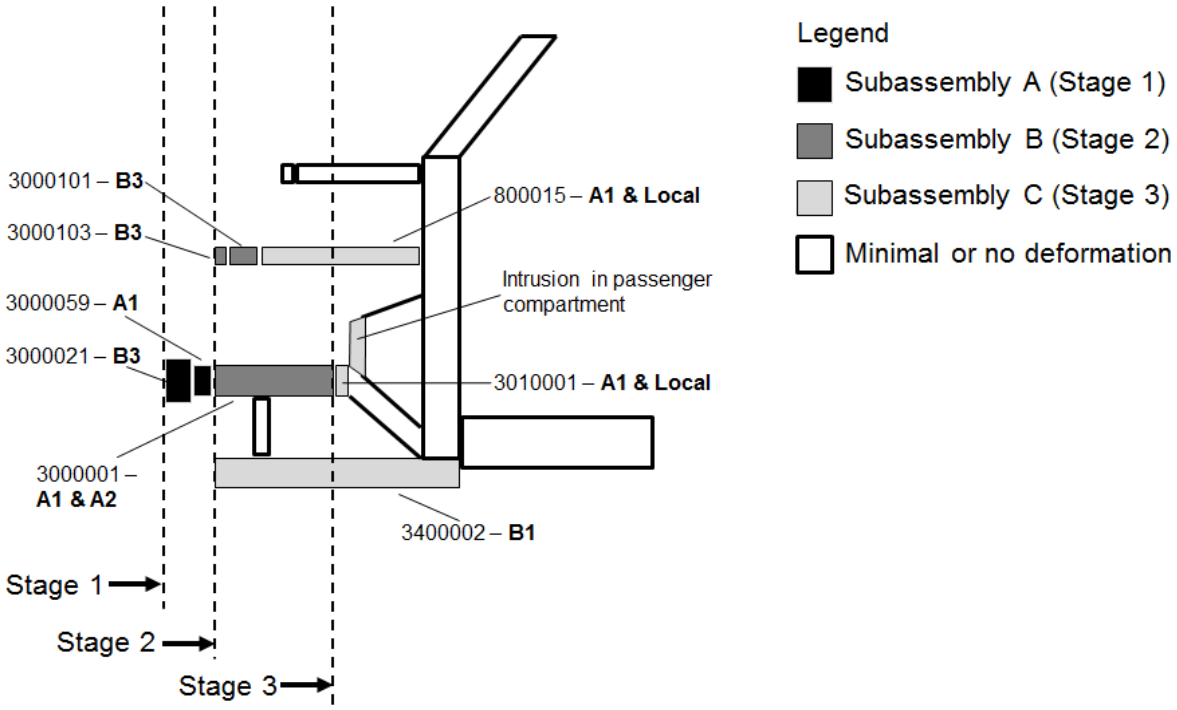

Figure 5.9: Components of subassemblies and their modes of deformation

In order to define the deformations of the energy absorbing components in frontal crash with a rigid wall, a spring model is constructed as explained in Section 4.2.2.3. The length and positioning of the individual components is obtained from the topology of the structure. The sequential deformation of each subassembly and its components, corresponding to the three regions in the target F-D curve from Figure 5.6, are illustrated schematically in Figures 5.10 – 5.13.

Legend for Figure 5.10 - Figure 5.13

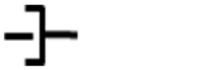
Plastically deforming components


Local deformations / Elastically deforming components


No deformation

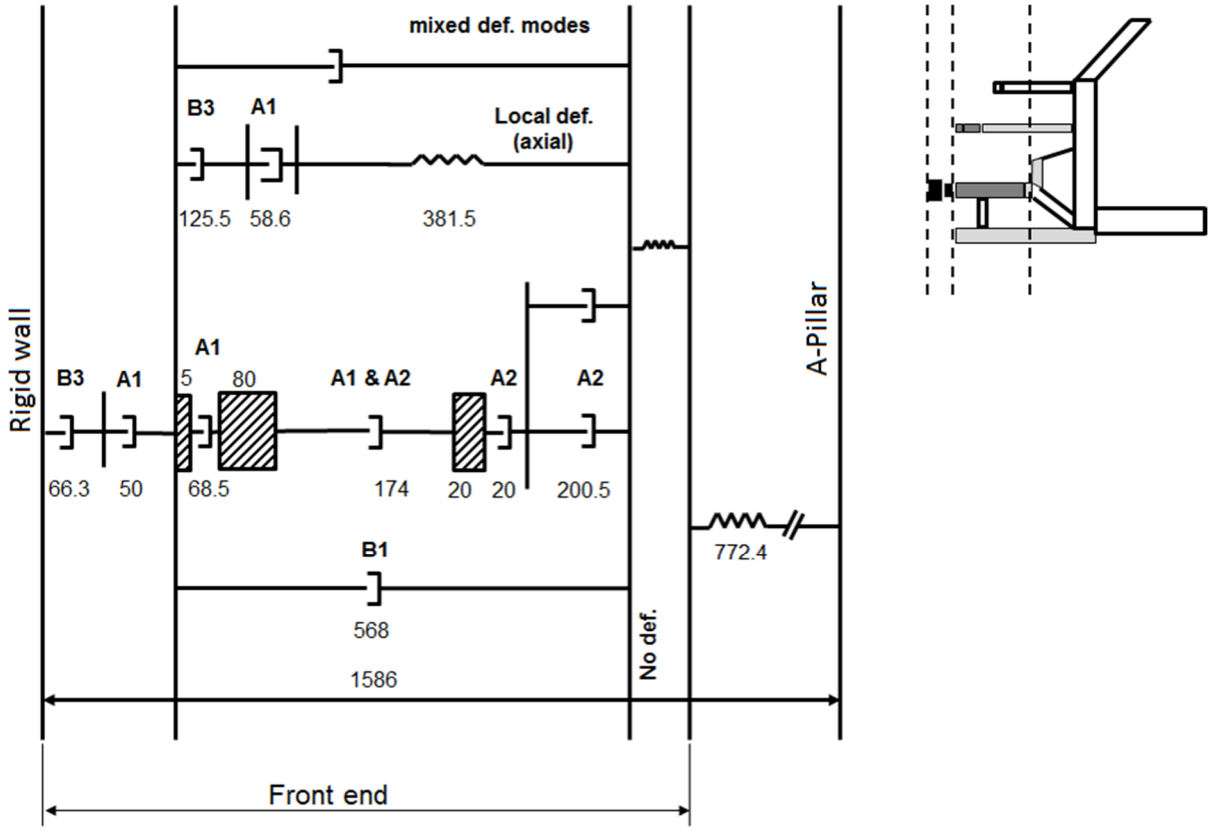

Figure 5.10: Undeformed state of MiNIT front end – Stage 0

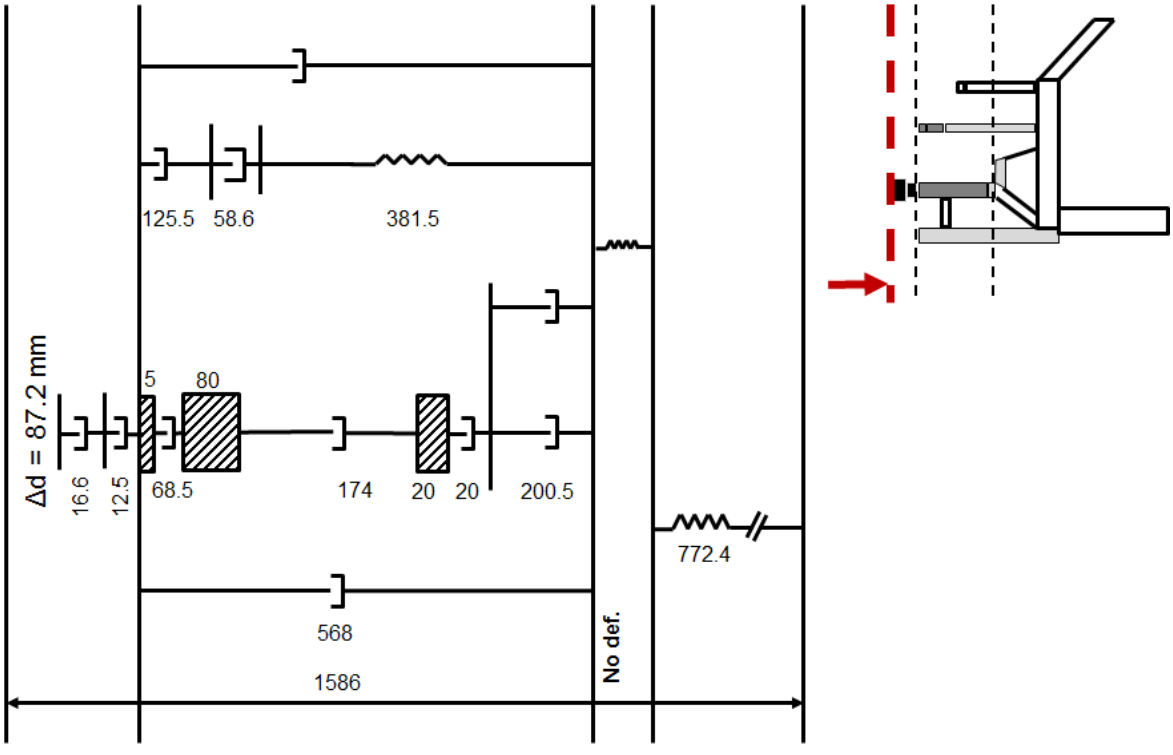

Figure 5.11: Deformation of MiNIT front end – Stage 1

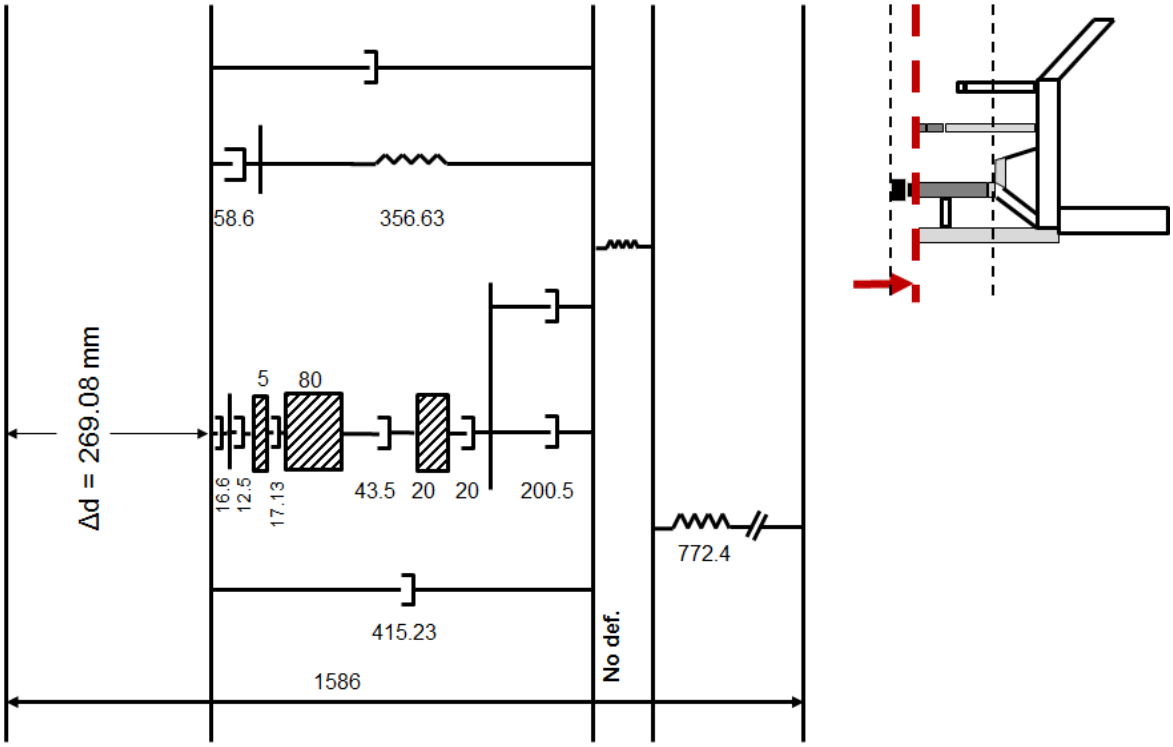

Figure 5.12: Deformation of MiNIT front end – Stage 2

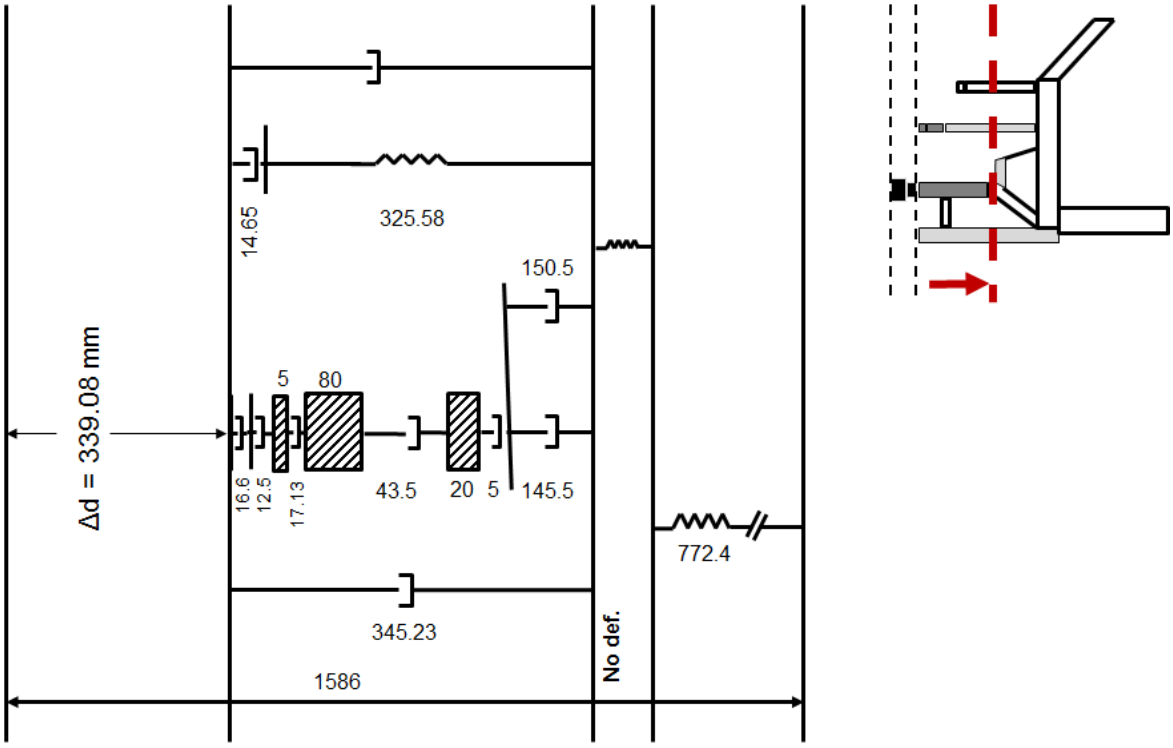

Figure 5.13: Deformation of MiNIT front end – Stage 3

It can be seen that the above spring model defines a total allowable deformation of about 340 mm during the front crash. However, the target defined in the F-D curve is 350 mm. As this is the initial prediction of deformations in the concept design phase, this discrepancy between the two values can be ignored at this stage. The global target can be achieved later by optimising the structure in further design phases.

5.2.3 Definition of energy absorption targets

As discussed in Section 4.1.3.3, the distribution of the deformation energy into various vehicle systems is observed from the benchmark vehicle simulations. The definition of this energy distribution in the micro-sized passenger vehicle MiNIT is based on these observations. The characteristic features of the profile based construction concept, the FlexBody concept, are also considered while defining the energy distribution. According to the FlexBody concept, the car body structure, consisting of profiles and joints, absorbs most of the energy in an impact scenario. The closing structures of the vehicle have a low contribution in the energy absorption, whereas the outer shell does not contribute at all. Therefore, assuming a reasonable percentage of energy absorption for the other vehicle systems, such as suspensions, tires, radiators etc., the target percentage of the energy absorbed by the FlexBody car body structure of MiNIT can be defined. For the MiNIT the energy distribution in the FMVSS 208 crash scenario, is defined as illustrated in Figure 5.14. Accordingly, for the FMVSS 208 crash scenario, the energy absorption target for the profile structures and joints of the MiNIT car body structure of is set at 64% of the total energy of deformation.

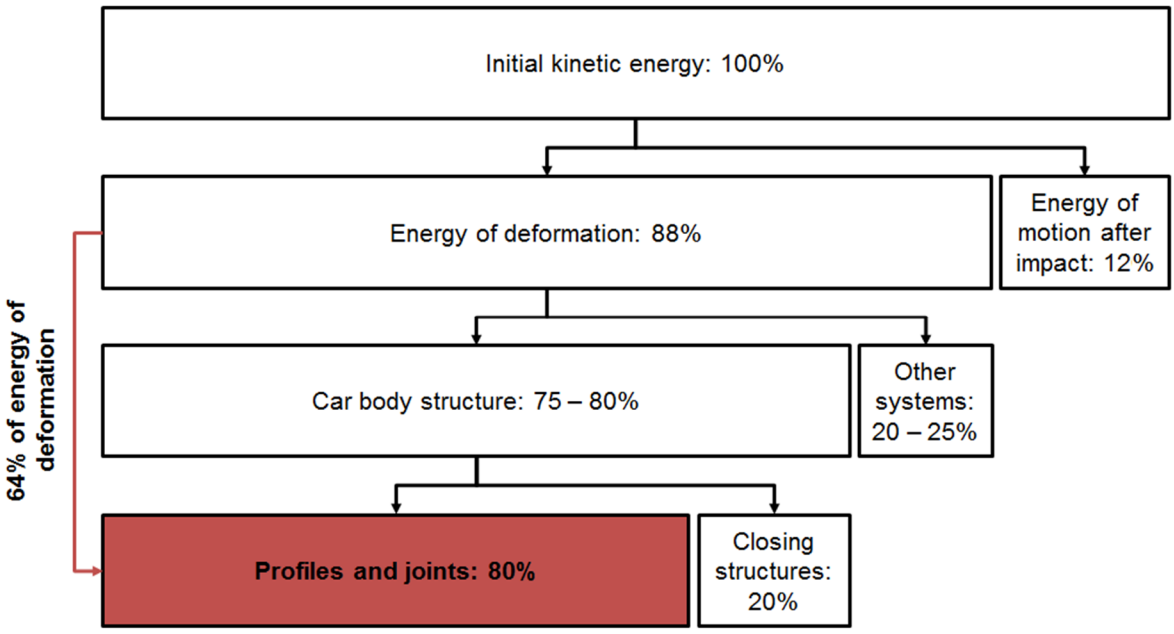

Figure 5.14: Energy distribution in MiNIT structure in FMVSS 208 crash scenario

The energy absorption targets for the individual profiles, listed in Table 5.4, are defined as the next step. For this purpose, inputs are taken from the benchmark data, the target F-D curve and the energy distribution defined earlier. However, one to one mapping of the energy targets on the basis of the benchmark data is not always possible. Therefore, lastly, the design engineer should decide if the benchmark guidelines are reasonable and define the final targets for each energy absorbing component. Following the above procedure, the energy absorption targets are defined for the MiNIT front end for the frontal crash scenario, as presented in Table 5.5.

Table 5.5: Targets for energy absorption for individual components for FMVSS 208 scenario

Part No.	**Part name**	**Energy absorption targets**					
		From F-D curve		**From bench.**	**Defined acc. to judgment**		
		kJ	**%**	**%**	**%**	**%**	**kJ**
Subassembly A							
3000021	Bumper beam	8.3	7.7	17.0	5.0	10.0	10.8
3000059	Frontal defo ele lft.			0.0	2.5		
3000060	Frontal defo ele rt.			0.0	2.5		
Subassembly B							
3000103	Up crs bumper shell	46.1	42.7	0.0	5.0	39.0	42.2
3000101	Conn shotgun-up crs lft.			0.0	2.5		
3000102	Conn shotgun-up crs rt.			0.0	2.5		
3000001	Frontal lower long lft.			10.0	11.0		
3000002	Frontal lower long rt.			10.0	11.0		
Subassembly C							
3400002	Subframe	15.9	14.7	0.0	10.0	15.0	16.2
800015	Shotgun lft.			3.0	4.0		
800016	Shotgun rt.			3.0	4.0		
3010001	Joint 1 lft.			0.0	2.0		
3010002	Joint 1 rt.			0.0	2.0		
Total		**70.4**	**65.1**		**64.0**	**64.0**	**69.2**

5.3 Application of section configuration

As discussed in Section 4.3.4.3, the regression method is chosen for analysing the profile structures in this work, as it gives the most satisfactory results for the range of profile structures analysed in the section configuration. The regression analysis of the numerical data gives regression equations for calculating the performance characteristics of the structures, such as F_{max}, M_m etc. These equations can be used to calculate these performance values for any cross section having dimensions in the selected geometrical range summarised in Table 4.4. Additionally, other materials with similar material properties as those analysed in this work can also be analysed using this approach.

Using the regression equations, suitable cross-sectional geometries are chosen for the energy absorbing profile structures in the MiNIT front end, such that they satisfy the deformation and energy targets defined in Section 5.2.2 and 5.2.3 as closely as possible. The materials for these profiles are chosen considering the performance targets as well as the desired deformation sequence defined for the front end. Due considerations are also given to include additional design features in the profiles, so that the desired deformation behaviour can be obtained. These features include, for example, positioning of triggering dents for the profiles to realise axial folding mode. Table 5.6 and Table 5.7 present the chosen profile geometries and materials for the energy absorbing structures in the front end of the MiNIT car body structure. The tables also give the values of the performance characteristics calculated using the regression equations. As stated in Section 4.3.4.3, the components deforming in the crumpling bending mode (B3) cannot be designed using the regression equations developed in this work. Therefore, the components in the MiNIT front end deforming in this mode (B3) are designed by performing conventional FE analysis. Due to the irregular shape of the axially deforming joint 1, mean forces are not evaluated for the joint 1 using the regression equations. The design is realised by trying different wall thickness values for this joint.

Table 5.6: Design of profile structures deforming in axial modes using section configuration

Part No.	Part name	Part design					Predictions by regression		Wrt. Target values
		b	d	l	t	Mat	Fm	Eabs	ΔEabs
		mm	mm	mm	mm		kN	kJ	kJ
Subassembly A									
3000021	Bumper beam	NA	NA	NA	NA	AW6082	NA	NA	NA
3000059	Frontal defo ele lft	80	80	50	2.5	AW6082	66.4	2.49	-0.21
3000060	Frontal defo ele rt	80	80	50	2.5	AW6082	66.4	2.49	-0.21
Subassembly B									
3000103	Up crs bumper shell	NA	NA	NA	NA	AW6060	NA	NA	NA
3000101	Conn shotgun-up crs lft	NA	NA	NA	NA	AW6060	NA	NA	NA
3000102	Conn shotgun-up crs rt	NA	NA	NA	NA	AW6060	NA	NA	NA
3000001	Frontal lower long lft	79.5	79.5	242.5	2.0	AW6082	44.3	8.02	-3.87
3000002	Frontal lower long rt	79.5	79.5	242.5	2.0	AW6082	44.3	8.02	-3.87
Subassembly C									
3400002	Subframe	Table 5.7							
800015	Shotgun lft	62	59	58.6	1.5	AW6060	20.6	1.94	-2.39
		99	59	381.5	1.5	AW6060	18.4		
800016	Shotgun rt	62	59	58.6	1.5	AW6060	20.6	1.94	-2.39
		99	59	381.5	1.5	AW6060	18.4		
3010001	Joint 1 lft	NA	NA	NA	NA	AW6082	NA	NA	NA
3010002	Joint 1 rt	NA	NA	NA	NA	AW6082	NA	NA	NA

Table 5.7: Design of profile structure deforming in cantilever bending modes using section configuration

Part No.	Part name	Part design					Predictions by regression		Wrt. Target values
		b	d	l	t	Mat	Mm	Eabs	ΔEabs
		mm	mm	mm	mm		kNm	kJ	kJ
3400002	Subframe	50	70	568	2.0	S235	1.62	7.54	-3.27

It can be observed from the above tables that the difference between the values calculated by regression method and the target values set is not very high. Therefore, the geometry and materials chosen for each component are used for constructing the front end of the MiNIT structure.

5.4 Validation of structural knowledge-base using FMVSS 208 scenario

The front end of the micro passenger vehicle MiNIT designed and dimensioned for frontal crash in the previous Sections 5.1, 5.2 and 5.3, is analysed using the FE simulation technique, in order to validate the simplified design approach developed in this work. The FE analysis is carried out using the software HyperWorks for pre- and post-processing and LS-Dyna explicit solver for simulating the structure. This section presents the results obtained from the simulation and compares them with the targets set in the previous sections.

The simulation is carried out on full vehicle model of the MiNIT. The front end of this model is constructed as per the design generated using structural knowledgebase. The remaining vehicle is not constructed as per the design generated using structural knowledge-base. Since the analysis is carried out for a frontal crash scenario according to FMVSS 208, only the front end of the MiNIT body structure is loaded, and is, therefore, of interest. The package layout of the vehicle is also constructed. Using the full model of MiNIT for this validation allowed the assessment of realistic behaviour of the front end in connection with the whole vehicle.

5.4.1 Comparison of component targets for FMVSS 208 scenario

The deformations in the direction of impact and the energy absorption behaviour of the components of the front end in the numerical simulation are compared with the target values, defined in the deformation configuration. Table 5.8 presents this comparison.

Table 5.8: Comparison between numerical results and performance targets for components of MiNIT front structure

Part No.	Part name	From simulation	Wrt. Target values	From simulation	Wrt. Target values
		dx	Δdx	Eabs	ΔEabs
		mm	mm	kJ	kJ
Subassembly A					
3000021	Bumper beam	75.0	25	3.29	-2.12
3000059	Frontal defo ele lft	29.1	-8.4	1.94	-0.77
3000060	Frontal defo ele rt	29.8	-7.7	1.94	-0.76
Subassembly B					
3000103	Up crs bumper shell	143.0	17.5	2.54	-2.86
3000101	Conn shotgun-up crs lft			1.02	-1.68
3000102	Conn shotgun-up crs rt			0.91	-1.79
3000001	Frontal lower long lft	185.4	3.5	8.78	-3.11
3000002	Frontal lower long rt	184.8	2.9	8.32	-3.58
Subassembly C					
3400002	Subframe	212.0	-10.8	23.85	13.04
800015	Shotgun lft	30.9	-68.9	0.85	-3.47
800016	Shotgun rt	50.5	-49.4	0.94	-3.39
3010001	Joint 1 lft	1.5	-13.5	0.17	-1.99
3010002	Joint 1 rt	1.5	-13.5	0.16	-2.01

The differences observed in the deformations of the components are nominal and can be considered acceptable for the concept design phase. The larger value of difference in deformation of the shotgun is obtained due to the restrictions imposed on its deformation by adjoining attachments. It can also be seen from Table 5.8 that the joints 1 incurred very low deformation in the FE simulation. As a larger deformation of these joints represents a larger amount of intrusion in the passenger compartment, the incurred difference is acceptable.

The energy absorption values of individual components obtained from simulations match the targets defined for almost all components with a nominal difference. However, the difference in case of the subframe is high. This difference can be attributed to the complex shape of the subframe and additional bending modes occurring in the structure.

The target deformation modes obtained in the FE simulation also match the defined desired modes for all components apart from the subframe. Figure 5.15 illustrates two such examples.

Defined mode	Observed in simulation
A1 & A2: Regular and irregular axial folding	
a) Frontal lower longitudinal member left	
B3: Crumpling bending	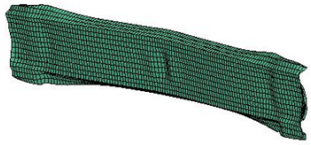
b) Bumper beam	

Figure 5.15: Comparison between defined and observed deformation modes

5.4.2 Comparison of global targets for FMVSS 208 scenario

The global performance targets defined for the MiNIT vehicle in frontal crash in 5.1.2 are also compared with the simulation results. Table 5.9 presents the comparison of these energy and deformation targets.

Table 5.9: Comparison between defined and observed global targets for FMVSS 208 scenario

	Target	**Observed in simulation**
Energy of deformation $E_{Def,2}$	108.11 kJ	109.53 kJ
Deformation of front end	300 mm	296 mm
Intrusion in passenger compartment	50 mm	29 mm
Maximum deceleration	50g	58g
Average deceleration	30g	32g

Comparison of the target and achieved force – deformation curves is illustrated in Figure 5.16.

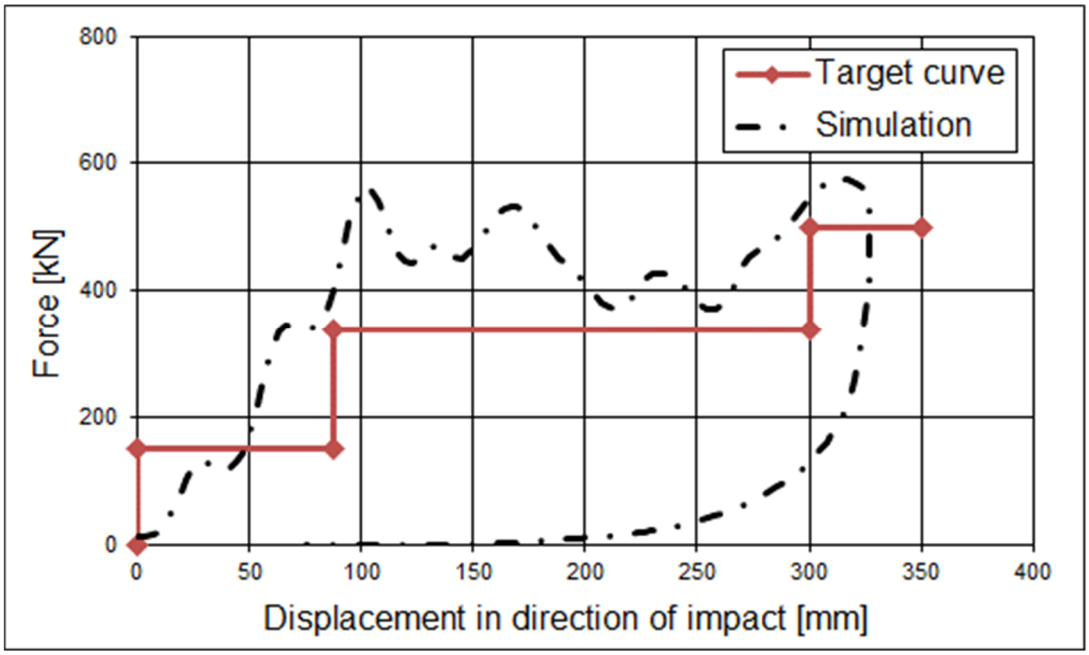

Figure 5.16: Force deformation curve of MiNIT front end obtained in simulation

As can be seen from the Table 5.9, and Figure 5.16, the target and observed values of the global performance criteria match to a large extent. Some differences that can be observed are acceptable for the concept design phase, and with fine tuning of the front-end structure, can be eliminated in further design stages.

6. Summary and Conclusions

Lack of detailed design information in beginning of the design process, requires lengthy optimisation cycles before arriving at optimum concept design of a car body structure. This increases the overall development time and costs of the vehicle. For the small series manufacturers, with restricted resources, these limitations pose a great challenge. As a solution to these problems, this work proposes a Multi Objective Knowledge-based design approach, the MOK approach. This work develops simplified methods for performing three steps in the MOK design approach, namely, attribute configuration, deformation configuration and section configuration, necessary for developing the structural concept of a crashworthy car body. This approach is developed for profile based car body structures.

The attribute configuration determines the global performance targets of a car body structure for various crash scenarios. The targets include the amount of energy to be absorbed by the car body structure and allowable deformations of the structure in a particular crash scenario. A benchmark developed by performing FE simulations of two vehicles is used as a basis for deducing the global performance targets. This work, thus, demonstrates the use of benchmark data for determining precise global design targets for a new car body structure.

On the basis of the global performance targets, the deformation configuration determines the performance targets for individual car body components. For a particular crash scenario, active car body components are identified and preferred modes of deformation are assigned to these components. Depending on the assigned deformation modes, the global performance targets for deformation and energy absorption are broken down to individual active components. The data obtained from the benchmark simulations performed in attribute configuration are also taken as guideline for this process. A logical method for deriving local design targets from the global targets is, thereby, presented in this work.

In the section configuration, simplified methods are developed for choosing appropriate initial cross-sectional geometry and materials for the active components to satisfy the defined targets. Regular and irregular axial folding and cantilever bending deformation modes of the car body components are focused in this work. Using the techniques of DoE, a set of profile structures in a definite spectrum, suitable for profile based car body structures, is analysed numerically. The same set of profile structures is also analysed by using available analytical methods. These methods are applied in their simplest form, without any computer programming.

The comparison of the results obtained from the numerical and analytical analysis showed considerable difference between both the results. The simplest forms of the analytical methods are therefore considered unsuitable for application in the section configuration for predicting the performance of profile structures in the chosen spectrum. Regression equations developed by performing regression analysis of the numerical data are, therefore, used for selecting the initial geometry and material of the active components.

The application of the methods developed in the three configurations is demonstrated for concept design of the front-end structure of the micro-sized compact passenger vehicle, MiNIT. The concept design is generated considering the crash scenario of frontal impact with a rigid wall. This concept design is validated using FE simulation techniques. It is observed from the simulation results that the front end of MiNIT satisfied all the defined targets with acceptable deviations.

Future Work

This work builds the benchmark for defining the crash performance targets of the profile based car body structures based on FE analysis of two vehicles. This benchmark can be extended further by analysing other vehicles of different sizes, such as mini, compact etc. and types, such as hatch back, convertible etc, with a focus on vehicles constructed using profile based construction concept. Such a benchmark will enable assessing the difference in distribution of the loads and the deformation behaviour of different types of vehicles. This information can then be applied for designing different types of vehicles constructed as profile based structures.

In this work the regression analysis is essentially performed for two collapse modes namely, axial collapse and cantilever bending. Due to different boundary conditions and deformation patterns, this analysis cannot be used for assessing other bending modes such as crumpling under bending load. A similar analysis can be conducted for such bending modes. This will permit designing the components deforming in these modes using the regression method.

The main aim of this work was to develop and demonstrate a simplified design approach for profile based car body structures considering crash loads. Therefore, the approach developed is demonstrated only for a frontal crash scenario. This approach should also be applied to other crash scenarios, where other considerations for deformation behaviour of the vehicle need to be made.

The types of cross sections analysed in this work are restricted to square and rectangular sections. Similar analysis can be performed for structures with other cross sections, such as hexagonal and octagonal sections. Similarly, structures made of a wider range of materials can be analysed using a similar approach. This will enlarge the spectrum of cross sections and materials that can be analysed using the structural knowledgebase. Considering the material strain rate sensitivity as an additional parameter in this approach will enable assessing the profile based car body structures under crash loads more accurately in the concept design phase itself.

Lastly, an interactive tool based on simple computer programs can be developed for synthesising the whole approach. This tool can be used by design engineers who have the basic understanding of design for crashworthiness. Moreover, such a tool will prove to be especially useful for small series manufacturers who have stringent restrictions on the time and costs available for the design and the available resources.

7 Appendix

7.1 Fundamentals of regression analysis

Regression analysis is widely used in statistics to find the influence of number of independent parameters on a single or multiple response variables. For example, if there are k parameters, X_1, X_2, X_3,….., X_k and one response variable Y, then based on the data obtained from the experiments carried out using DoE, regression analysis formulates a mathematical model to describe the relationship of the X parameters with Y. Different statistical quantities are used to assess the quality of the regression model [67]. A regression analysis carried out for finding influence of a single independent parameter on one response parameter is called as linear regression, whereas that carried for more than one independent parameters and one or more response parameters is termed as multiple regression. The basics of linear regression are presented in Section 7.1.1. The basics of multiple regression lie in the concept of linear regression. The basics of multiple regression and the statistical values used for assessing the regression model are presented in Section 7.1.2.

7.1.1 Linear regression

Let us consider a number of experiments are performed by varying the value of an independent variable X in a fixed design space for analysing its influence on the response parameter Y. If there exists a perfect linear relationship between X and Y variables, then the relationship can be depicted using an equation of line as:

$$Y = a + bX \qquad \textit{Eq. 7.1}$$

Where,

b : Slope of the line

a : Y-intercept

When the results of the experiments are plotted as Y against X, it is generally observed that the points do not lie on a straight line, although the trend of plotted points may seem to be linear. The linear regression method then selects one straight line from all possible straight lines depicting the trend of the points such that a best fit to the experimental data is obtained. This selected straight line thus explains the relationship between X and Y in the best possible manner. This line is termed as *regression line* of Y on X. The equation of the line is called the *regression equation*.

When the values of Y are calculated using the regression equation for the values of X, they will normally not be the same as those observed from the experiments. The predicted values of the response parameter can, therefore, be depicted by Y'. Thereby, the regression equation can be written as:

$$Y' = a + bX \qquad \textit{Eq. 7.2}$$

In Eq. 7.2 *b* is called a *regression coefficient.*

The values of *a* and *b* can be calculated using the method of least squares and the values of X and Y from the experimental data. Figure 7.1 shows an exemplary plot of Y verses X and corresponding regression line Y'. The mean values of Y and X are represented by $\overline{Y}$ and $\overline{X}$.

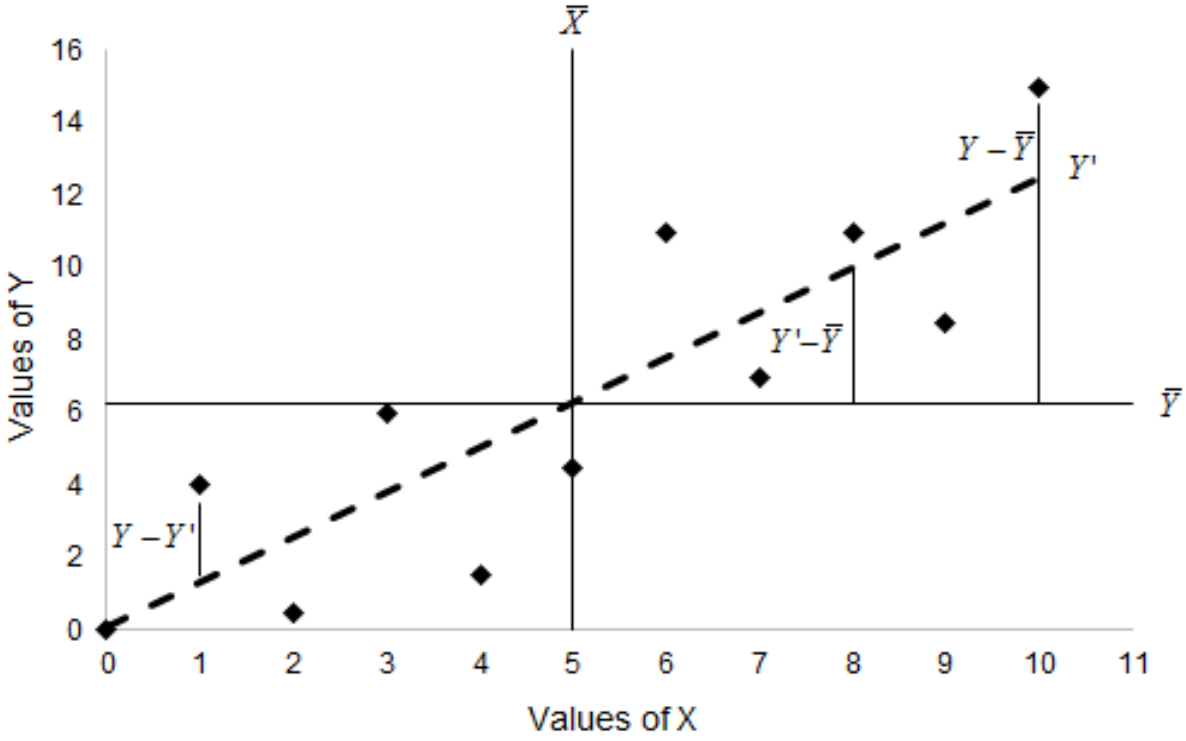

Figure 7.1: Regression line of Y on X [67]

The difference between the observed values Y from the experiments and the predicted value Y' from the regression is called as *residual* and for a particular experimental run is given by:

$$e = Y - Y' \qquad \textit{Eq. 7.3}$$

The values of a and b in the regression equation are determined using the method of least squares such that the residual sum of squares represented by Eq. 7.4 is minimum.

$$\sum e^2 = \sum (Y - Y')^2 \qquad \textit{Eq. 7.4}$$

Accordingly, the values of a and b can be found using Eq. 7.5 and Eq. 7.6.

$$b = \frac{\sum XY - (\sum X)(\sum Y)/n}{\sum X^2 - (\sum X)^2/n} \qquad \textit{Eq. 7.5}$$

$$a = \bar{Y} - b\bar{X} \qquad \textit{Eq. 7.6}$$

Where,

n : Number of experimental runs

The deviation of the observed values of Y from their mean can be expressed as sum of two components, as shown by Eq. 7.7.

$$Y - \bar{Y} = (Y' - \bar{Y}) + (Y - Y') \qquad \textit{Eq. 7.7}$$

Squaring and summing over n:

$$\sum_{i=1}^{n} (Y_i - \bar{Y})^2 = \sum_{i=1}^{n} (Y_i' - \bar{Y})^2 + \sum_{i=1}^{n} (Y_i - Y_i')^2 \qquad \textit{Eq. 7.8}$$

The second term on the right hand side is called the *residual sum of squares* (SS_{res}). The first term on the right hand side is called the *regression sum of squares* (SS_{reg}). Sum of both the terms is called as the *total sum of squares* (SS_{tot}). The Eq. 7.8 can also be written as:

$$SS_{tot} = SS_{reg} + SS_{res} \qquad \textit{Eq. 7.9}$$

For a perfect linear relationship between Y and X, SS_{res} will be zero and SS_{reg} will equal to SS_{tot}. On the other hand, when there is not a slightest linear relationship between Y and X, the coefficient of regression b and SS_{reg} will be zero and SS_{res} will equal to SS_{tot}. These sums of squares are used to find the degree to which the Y and X values are linearly related to each other. Dividing Eq. 7.9 by SS_{tot},

$$1 = \frac{SS_{reg}}{SS_{tot}} + \frac{SS_{res}}{SS_{tot}} \qquad \textit{Eq. 7.10}$$

$$1 = r^2 + \left(1 - r^2\right) \qquad \textit{Eq. 7.11}$$

In Eq. 7.11 *r* is called the *correlation coefficient* between Y and X. In Eq. 7.11 r^2 is the part of total sum of squares that can be accounted for by the linear regression of Y on X and $(1 - r^2)$ is that part of total sum of squares that cannot be accounted for by the linear regression of Y on X. Therefore r^2 is a measure for degree to which the set of experimental points cluster about the regression line [67].

7.1.2 Multiple regression

Multiple regression uses the same principles as that of linear regression to analyse the effect of multiple X parameters on one or more response parameters. A multiple regression equation can be written as below.

$$Y' = a + b_1 X_1 + b_2 X_2 + ... + b_k X_k \qquad \textit{Eq. 7.12}$$

The unknown values a, b1, b2, …… bk in Eq. 7.12 are determined using the principles of linear regression in such a way that there is the highest possible correlation between the response parameters and the independent variables. Here, the correlation coefficient is depicted by R. The regression coefficients b1, b2, … bk represent the contribution of each X variable to the dependent (or response) variable.

Nonlinear factors can be considered by adding a quadratic or cubic term in the regression equation as depicted in Eq. 7.13.

$$Y' = a + b_1 X_1 + b_2 X_1^2 + b_3 X_2 + b_4 X_2^3 + ... \qquad \textit{Eq. 7.13 [75]}$$

The interactions between two or more X parameters can be modelled as below.

$$Y' = a + b_1 X_1 + b_2 X_2 + b_3 X_1 X_2 + ... \qquad \textit{Eq. 7.14 [75]}$$

A response parameter can also be transformed. For example, if the response is transformed to lnY' then the regression equation can be represented as:

$$Y' = e^{(a+b_1X_1+b_2X_2+b_3X_1X_2+b_4X_2^2+.....)} \qquad \textit{Eq. 7.15 [75]}$$

Various statistical values are used to assess the quality of the multiple regression model fitted to the given experimental data. These values are briefly explained below.

7.1.2.1 R^2 and R^2_{adj}

These parameters are termed as coefficient of determination and adjusted coefficient of determination respectively. The value R^2, as mentioned before, indicates how well the regression model fits the experimental data. When the regression is carried out using the least square method, R^2 increases with increase in number of variables in the model. Thus, R^2 can sometimes overestimate the quality of the regression model. The parameter adjusted R^2 is, therefore, calculated, which also indicates how well the model fits the data, but unlike R^2, increases only if the new term in the model improves the model. Therefore, great difference in the values of R^2 and R^2_{adj} indicates presence of unnecessary terms in the regression model. Closer the values of R^2 and R^2_{adj} are to 1, better the model fits the experimental data. Generally values above 0.90 are considered acceptable [67], [68].

7.1.2.2 Prediction measure Q^2

The prediction measure depicts the prediction ability of the generated regression model. Certain response values $\hat{Y}$ are calculated for some points which are not measured in the experiments and Q^2 is calculated using Eq. 7.16. Closer the value of Q^2 is to 1, better is the ability of prediction of the model. If for a particular regression model R^2 is larger and Q^2 is smaller, then it can be concluded that the model is properly fitted but contains unnecessary terms. The regression model can be reduced in such scenarios [68].

$$Q^2 = 1 - \frac{\sum\left(Y - \hat{Y}\right)^2}{\sum\left(Y - \bar{Y}\right)^2} \qquad \textit{Eq. 7.16 [75]}$$

7.1.2.3 p-value

A p-value is a parameter for depicting the statistical significance of a parameter in a regression model. It uses the concept of null hypothesis. First, it is assumed that a particular independent parameter does not have any influence on the response variable in the population. Then, from the sample or the results of the experiments, the value indicating the influence of

that particular parameter is checked and determined if it is the sort of value indicating no effect in the population. If the value from the sample is unlikely for having no influence, then it is decided that there is an influence and therefore the parameter is significant. Small p-value indicates that the parameter is significant. Generally the p-values less than 5% are considered to be statistically significant [68].

8 Literature Cited

[1] Karthik Shankaran, “Corporate Internal Training: Structural Design of Vehicles.” Detroit Engineered Products.

[2] Srinivasa Babu, “Corporate Internal Training: CAE Design Methodology.” Detroit Engineered Products.

[3] Srinivasa Babu, “Corporate Internal Training: Design Methodology.” Detroit Engineered Products.

[4] Karthik Shankaran, “Corporate Internal Training: Automotive BIW Structural Concepts.” Detroit Engineered Products.

[5] Karthik Shankaran, “Corporate Internal Training: BIW Lightweight Body – Concepts, Materials, Manufacturing,” Detroit Engineered Products.

[6] T. Roeth, A. Kampker, U. Reisgen, K. Hameyer, R. W. De Doncker, T. Stolze, A. Vetter, J. Hagedorn, D. U. Sauer, and D. Mueller, “Entwicklung von elektrofahrzeugspezifichen Systemen,” in *Elektromobilitaet - Grundlagen einer Zukunftstechnologie*, Springer Vieweg, 2013, pp. 235 – 334.

[7] J. Hillmann, “The new Golf VII - Lightweight Design in Large Scale Production,” in *Aachen Body Engineering Days*, 2012.

[8] M. Heer and R. Schmerberg, “AUDI Q7 – SUV der 3. Generation: Karosserieauslegung im Spannungsfeld zwischen Funktion und Design,” in *Karosseriebautage Hamburg*, 2006, pp. 83 – 105.

[9] L. Trender and M. Schromm, “Gesamtfahrzeugkonzept und CFK-Anwendungen in Rolling Chassis und Karosserie des Porsche 918 Spyder,” in *Aachener Karosserietage*, 2013.

[10] Audi AG, “Audi Space Frame ASF.” 2012.

[11] Imperia GmbH, “FlexBody® | Lightweight Engineering.” [Online]. Available: http://flexbody.net/.

[12] L.-E. Elend and K. Koglin, “Die Karosserie als Initiator für den Fahrzeugleichtbau,” in *1. VDI-Fachkonferenz Leichtbaustrategien für den Automobilbau*, 2011.

[13] M. Dukat, T. Christiansen, and L. P. Heinisch, “Porsche: So geht intelligenter Karosserieleichtbau,” in *1. VDI-Tagung: Gießen von Fahrwerks- und Karosseriekomponenten*, 2014.

[14] T. Roeth and G. Müller, “Intelligent body construction kit for the world-wide first electric car sharing vehicle,’” in *ACI-Tagung, Strategies in Car Body Engineering – 2011*, 2011.

[15] T. Roeth, A. Nagle, and G. Müller, “Leichtbau-Karosseriebaukasten mit hochfunktionaler Absicherung am Beispiel des Micro-Cars 'ec2go',” in *Werkstoffe im Automobilbau 2013, 4. ATZ-Fachtagung*, 2013.

[16] Imperia GmbH, “Imperia Automotive Engineering.” [Online]. Available: http://www.imperia.info/.

[17] Smart, “Electric Drive (ED)” [Online]. Available http://www.smartusa.com/

[18] Protoscar, “Protoscar.” [Online]. Available: www.protoscar.com.

[19] Karthik Shankaran, “Corporate Internal Training: Automotive Structural Design Concepts.” Detroit Engineered Products.

[20] Karthik Shankaran, “Corporate Internal Training: Vehicle Engineering - FEM and Application.” Detroit Engineered Products.

[21] H. F. Mahmood and B. B. Fileta, “Design of Vehicle Structures for Crash Energy Management,” in *Vehicle Crashworthiness And Occupant Protection*, American Iron and Steel Institute, 2004, pp. 11–110.

[22] Karthik Shankaran, “Corporate Internal Training: Automotive Benchmarking Concepts.” Detroit Engineered Products.

[23] Vimal Adithan, “Corporate Internal Training: Foundations of Finite Element Methods.” Detroit Engineered Products.

[24] T. Chandrupatla and A. Belegundu, *Introduction to Finite Elements in Engineering*, Second Edi. Prentice Hall of India Private Limited, 2000.

[25] T. Wierzbicki, L. Recke, W. Abramowicz, and T. Gholami, “Stress profiles in thin-walled prismatic columns subjected to crush loading-I. Compression,” *Comput. Struct.*, vol. 51, no. 6, pp. 611–623, 1994.

[26] T. Wierzbicki, L. Recke, W. Abramowicz, T. Gholami, and J. Huang, “Stress profiles in thin-walled prismatic columns subjected to crush loading-II. Bending,” *Comput. Struct.*, vol. 51, no. 6, pp. 625–641, 1994.

[27] H. F. Mahmood and A. Paluszny, “Stability of plate type box columns under crush loading,” *Comput. Methods Gr. Transp. Veh.*, vol. 50, pp. 17–33, 1982.

[28] W. Abramowicz and N. Jones, “Transition from initial global bending to progressive buckling of tubes loaded statically and dynamically,” *Int. J. Impact Eng.*, vol. 19, no. 5–6, pp. 415–437, 1997.

[29] H. F. Mahmood and A. Paluszny, “Design of Thin Walled Columns for Crash Energy Management - Their Strength and Mode of Collapse,” in *International Conference on Vehicle Structural Mechanics*, 1981.

[30] S. Ramamrutham and R. Narayan, *Strength of materials*, 12th ed. Dhanpat Rai Publishing Company (P) Ltd., 1998.

[31] W. Abramowicz and N. Jones, “Dynamic progressive buckling of circular and sqaure tubes,” *Int. J. Impact Eng.*, vol. 4, no. 4, pp. 243–270, 1986.

[32] T. Wierzbicki and W. Abramowicz, “On the crushing mechanics of thin walled structures,” *J. Appl. Mech.*, vol. 50, pp. 727–734, 1983.

[33] R. J. Hayduk and T. Wierzbicki, “Extensional collapse modes of structural members,” *Comput. Struct.*, vol. 18, no. 3, pp. 447–458, 1984.

[34] W. Abramowicz and N. Jones, “Dynamic axial crushing of square tubes,” *Int. J. Impact Eng.*, vol. 2, no. 2, pp. 179–208, 1984.

[35] N. Jones, *Structural Impact*. Cambridge University Press, 1997.

[36] W. Abramowicz and T. Wierzbicki, “Axial crushing of multi-corner sheet metal columns,” *J. Appl. Mech.*, vol. 56, pp. 113–120, 1989.

[37] D. Kecman, “Bending collapse of rectangular and square section tubes,” *Int. J. Mech. Sci.*, vol. 25, no. 9–10, pp. 623–636, 1983.

[38] D. Kecman, “Bending collapse of rectangular section tubes in relation to the bus roll over problems,” Cranfield Institute of Technology, 1979.

[39] FORCEFIVE, “Manual - Fast Concept Modeller.” 2009.

[40] Contact Software, “Fast Concept Modelling.” [Online]. Available: http://www.contact-software.com/en/products/fast-concept-modelling.html.

[41] SFE GmbH, “SFE Concept.” [Online]. Available: http://www.homepage.sfe-group.org/en/products/sfe-concept/.

[42] H. F. Mahmood and A. Paluszny, “Axial Collapse of Thin Wall Cylindrical Column,” in *Vehicle Structural Mechanics Conference and Exposition*, 1984.

[43] H. F. Mahmood, A. Paluszny, and Y. S. Lin, “Bending collapse of automotive type components,” 1988.

[44] H. F. Mahmood, A. Paluszny, and X. D. Tang, “A 3D Computer Program for Crashworthiness Analysis of Vehicle Structures Composed of Thin-Wall Beam Components,” in *(ASME)*, 1986, vol. 79.

[45] H. F. Mahmood and A. Paluszny, “Analytical Technique for Simulating Crash Response of Vehicle Structures Composed of Beam Elements,” in *Proceedings of the Sixth International Conference on Vehicle Structural Mechanics (SAE)*, 1986, pp. 277–287.

[46] Impact Design Europe, “Visual Crash Studio.” [Online]. Available: http://www.impactdesign.pl/vcs.html.

[47] W. Abramowicz, “Macro element method in crashworthiness of vehicles,” in *Crashworthiness, Energy management and occupant protection*, J. A. C. Ambrosia, Ed. Springer-Verlag Wien New York, 2001.

[48] W. Abramowicz, “Thin-walled structures as impact energy absorbers,” *Thin-Walled Struct.*, vol. 41, no. 2–3, pp. 91–107, 2003.

[49] VDI Standard: *VDI 2221 Systematic approach to the development and design of technical systems and products*, 1993.

[50] UN/ECE, “UN/ECE Regelungen.” [Online]. Available: http://www.bmvbs.de/SharedDocs/DE/Artikel/LA/un-ece-regelungen.html.

[51] NHTSA, “National Highway Traffic Safety Administration Website.” [Online]. Available: http://www.nhtsa.gov/.

[52] EuroNCAP, “EuroNCAP regulations.” [Online]. Available: www.euroncap.com.

[53] carhs.training, *Safety Companion 2014*. carhs gmbh, Germany, 2014.

[54] European Parliament Council, *2007/46/EC*. European Union: EUR-Lex, 2007.

[55] ECE, *ECE-R12: Lenkanlage bei Unfallstoessen*. European Union, 2008, pp. 11–40.

[56] European Parliament Council, *2007/46/EC (with Amendments)*. European Union, 2014.

[57] NHTSA, *FMVSS 305: Spillage and Electrical Shock Protection*. USA: http://www.nhtsa.gov/, 2008.

[58] NHTSA, *FMVSS 208: Occupant Crash Protection*, no. 208. USA: http://www.nhtsa.gov/, 2008.

[59] NCAC, “Finite Element Model Archive.” [Online]. Available: http://www.ncac.gwu.edu/vml/models.html.

[60] E.Sridhar, “Corporate Internal Training: Structural Design.” Bechtel India Pvt. Ltd.

[61] N. Jones, “Energy-absorbing effectiveness factor,” *Int. J. Impact Eng.*, vol. 37, no. 6, pp. 754–765, 2010.

[62] W. Abramowicz, “The effective crushing distance in axially compressed thin walled metal columns,” *Int. J. Impact Eng.*, vol. 1, no. 3, pp. 309–317, 1983.

[63] N. Jones and S. S. Hsu, “Quasi-static and dynamic axial crushing of thin-walled circular stainless steel, mild steel and aluminium alloy tubes,” *Int. J. Crashworthiness*, vol. 9, no. 2, pp. 195–217, 2004.

[64] CRGRAPH, “Homepage CRGRAPH.” [Online]. Available: http://www.crgraph.de/.

[65] DIN Deutsches Institut für Normung e.V., *DIN 50125: Testing of metallic materials — Tensile test pieces*. Berlin, 2009.

[66] LSTC (Livermore Software Technology Corporation), LS-DYNA® KEYWORD USER'S MANUAL, VOLUME I, LS-DYNA R8.0. LSTC, 2015.

[67] A. L. Edwards, *Multiple Regression and Analysis of Variance and Covariance*, First. W.H.Freeman & Co Ltd, 1979.

[68] CRGRAPH and C. Ronniger, “VisualXSel 12.0 - Help Documentation.” 2012.

Publications by the candidate

International Journals

1. Kiran Kumar Dama, V Suresh Babu, R N Rao and Sridhar Emmadi "*Multi Objective Knowledgebase Concept Design Methodology of Automotive Space Frame Structures for Crashworthiness by Numerical Methods*", Materials Today: Proceedings, Volume 4, Issue 2, Part A, 2017, pp 1837–1842, DOI: 10.1016/j.matpr.2017.02.027. (SCOPUS)

2. Kiran Kumar Dama, V Suresh Babu, R N Rao, IsmailJani Shaik and Sridhar Emmadi "*Structural Performance Assessment of a Chrysler Neon Compact Passenger Vehicle by Numerical Methods*", Materials Today: Proceedings, Volume 4, Issue 2, Part A, 2017, pp 1820–1828, DOI: 10.1016/j.matpr.2017.02.025. (SCOPUS)

3. Kiran Kumar Dama, V Suresh Babu, R N Rao and Ismail Jani Shaik "*Development of Automotive FlexBody Chassis Structure in Conceptual Design Phase using Additive Manufacturing*", Materials Today: Proceedings. (Accepted). (SCOPUS)

4. Kiran Kumar Dama, V Suresh Babu, R N Rao and Ismail Jani Shaik "*State of the Art on Basic Methodologies for Crashworthy Design of Automotive Body Components Considering Axial Collapse Mode*", Materials Today: Proceedings. (Accepted). (SCOPUS)

5. Kiran Kumar Dama, V Suresh Babu, R N Rao and Ismail Jani Shaik "*State of the Art on Basic Methodologies for Crashworthy Design of Automotive Body Components Considering Bending Collapse Mode*", Materials Today: Proceedings. (Accepted). (SCOPUS)

6. Kiran Kumar Dama, V Suresh Babu and R N Rao "*State of the Art on Automotive Lightweight Body-in-White Design*", Materials Today: Proceedings (Accepted). (SCOPUS)

7. Kiran Kumar Dama, V Suresh Babu and R N Rao "*State of the Art on Constructional Concepts of Automotive Body Structures*", Materials Today: Proceedings (Accepted). (SCOPUS)

8. Kiran Kumar Dama, V Suresh Babu and R N Rao "*Development of Benchmark Database to Define the Performance Targets of a Passenger Car by Computer Aided Engineering*", Journal of Mechanical Science and Technology (Under review). (SCI)

9. Kiran Kumar Dama, V Suresh Babu and R N Rao "*Defining the Target Structural Deformation Concert for Crashworthiness of a Passenger Car by Computer Aided Engineering*", The Proceedings of the Institution of Mechanical Engineers, Part D: Journal of Automobile Engineering (Communicated). (SCI)

10. Kiran Kumar Dama, V Suresh Babu and R N Rao "*Nonlinear Finite Element Analysis Validation of an Automotive Body-In-White(BIW) Structures by Static Physical Tests*", The Proceedings of the Institution of Mechanical Engineers, Part D: Journal of Automobile Engineering (Communicated). (SCI)

International Conferences

11. Kiran Kumar Dama, V Suresh Babu and R N Rao, "*A Study: Automotive Sustainable Design for GHG Emission Reduction in the Environment by Down-weighting*", Proceedings, International Conference on New Frontiers in Chemical, Energy and Environmental Engineering (INCEEE,2015), NIT Warangal, INDIA, March 20-21, 2015, pp. 21-22.

12. Kiran Kumar Dama, V Suresh Babu and R N Rao "*Crashworthiness Assessment of a Ford Taurus Passenger Sedan by CAE Tools*", Proceedings, International Conference on Computer Aided Engineering (CAE 2015), GITAM University, INDIA, December 10-12, 2015, pp. 401-407.

13. Kiran Kumar Dama, V Suresh Babu, R N Rao and Madhava Rao Y "*A Study on Existing Multi Material FlexBody Constructional Concepts of Light-Duty Passenger Vehicle Body-in-White Structures*", Proceedings, First International and Eighteenth National ISME Conference on Enabling Sustainable Development in Mechanical Engineering (ISME 2017), NIT Warangal, INDIA, February 23-25, 2017, pp. 80.

14. Kiran Kumar Dama, V Suresh Babu, R N Rao and Vijaya Ramaraju M "*A Study on Existing Tools for Hastening the Automotive Concept Design*", Proceedings, First International and Eighteenth National ISME Conference on Enabling Sustainable Development in Mechanical Engineering (ISME 2017), NIT Warangal, INDIA, February 23-25, 2017, pp. 89.

National Conferences

15. Kiran Kumar Dama, V Suresh Babu and R N Rao "*State of the Art on Regression Analysis for Assessing the Regression Model in Automotive Conceptual Design Phase*", Proceedings, National Symposium of Mechanical Engineering Research Scholars (NSMERS 2016), NIT Warangal, INDIA, October 07, 2016.